Relaxation of Reactor Coolant Pump Flywheel Inspection Requirements

Prepared for:

Consumers Power Company
Florida Power & Light Company
Entergy Operations
Northeast Utilities Service Company

Prepared by:

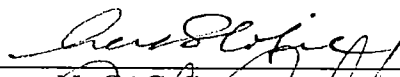Structural Integrity Associates, Inc.

Prepared by: _____   Date: 3/22/95
C. C. Markovits

_____   Date: 3/22/95
A. J. Giannuzzi

_____   Date: 3/22/95
N. G. Cofie

Reviewed &
Approved by: _____   Date: 3/22/95
P. C. Riccardella

9504100151 137pp.

Structural Integrity Associates, Inc.

REVISION CONTROL SHEET

Document Number: SIR-94-080, Rev. 1

Title: Relaxation of Reactor Coolant Pump
Flywheel Inspection Requirements

Client: Consumers Power Company
Florida Power & Light Company
Entergy Operations
Northeast Utilities Service Company

SI Project Number: CEOG-01Q-401

Section	Pages	Revision	Date	Comments
6.0	6-6	1	3/22/95	Addressed LOCA overspeed
8.0	8-1	1	3/22/95	Revised Reference 5

Structural Integrity Associates, Inc.

EXECUTIVE SUMMARY

The inspection requirements for reactor coolant pump (RCP) flywheels are specified in Regulatory Guide 1.14 (RG 1.14), Revision 1 issued by the U.S. Nuclear Regulatory Commission. In addition to mandated preservice inspections, RG 1.14 requires the following inservice inspection plan:

a) An in-place ultrasonic volumetric examination is to be performed on the areas of higher stress concentration at the bore and keyway. This should occur at approximately 3-year intervals, during the refueling or maintenance shutdown, coinciding with the ISI schedule, as required by Section XI of the ASME Code.

b) A surface examination of all exposed surfaces and complete ultrasonic volumetric examination shall be performed at approximately 10-year intervals, during the plant shutdown, coinciding with the ISI schedule, as required by Section XI of the ASME Code.

To date, plants that are committed to RG 1.14, have complied with its in-service inspection requirements, while most plants that are not committed to RG 1.14 have taken guidance from its inspection requirements. This has resulted in many examinations of the flywheel as part of the normal ISI program. The inspections have never revealed a condition which could lead to the failure of the flywheel. While several instances have been recorded in the literature where the reactor coolant pump shaft has been subjected to cracking, no reported instance of flywheel service-induced degradation or cracking has been reported.

The flywheel inspections, both at 3-year and 10-year intervals, result in significant outage time, man-rem exposure and cost to utilities which may be minimized by use of a more carefully designed inspection program. This program should account for the failure history of the flywheels, potential in-service degradation mechanisms and applicable locations, prior inspection results, and an evaluation of the failure propensity of the entire coolant pump motor to determine if failure of a flywheel between inspections is a credible event.

This report presents analyses of flywheel integrity performed by Structural Integrity Associates (SI) for four utilities in the Combustion Engineering (CE) Owners Group to justify relaxation of the RG 1.14 in-service inspection requirements. The four utilities are Consumers Power (Palisades), Entergy Operations (Arkansas Nuclear Units 1/2 and Waterford Unit 3), Florida Power & Light (St. Lucie Units 1/2) and Northeast Utilities (Millstone Unit 2). ANO-1 is not covered by RG 1.14 but is included in this study to determine if their current inspection plan can also be relaxed. Flywheels at these plants have been used in a study to determine alternate inspection requirements for the RCP flywheels. This evaluation includes a detailed review of past ultrasonic data of the affected plants, an industry-wide survey of other plants, the determination of degradation mechanisms which may affect the flywheel, stress analyses and fracture mechanics evaluations.

Structural Integrity Associates, Inc.

The evaluations have demonstrated that for the plants considered in this study, the inspection of the RCP flywheels as mandated by Regulatory Guide 1.14 and incorporated in the Plants' Technical Specifications can be eliminated without compromising safety. This conclusion is supported by several observations made during the evaluations presented in this report and summarized below.

- Inspections that have been performed to date at all seven plants have never revealed the presence of any service induced flaws. The inspections have spanned several years and have been performed using both ultrasonic and surface examination methods.

- A survey of several other plants was also performed to determine if any flaws have been reported during flywheel inspections. The survey revealed that to date, no flaws have been reported in any of the plants that were contacted.

- Various mechanisms that could potentially degrade the flywheel materials during service were evaluated. It was concluded that other than fatigue crack growth, there are no other mechanisms that can affect the service performance of the flywheel. Fatigue crack growth analyses were performed to show that crack growth, assuming a conservative initial flaw at the worst location, is negligibly small.

- Flaw tolerance evaluations performed using conservative linear elastic fracture mechanics principles and considering the critical location of the flywheel indicated that the flywheels do not present a safety concern for current plant life and life extension. These evaluations were performed using lower bound fracture toughness values at the most highly stressed locations. A conservative flaw size of 0.25 inch was assumed to be present, due to UT detection uncertainty. Fatigue crack growth analyses using the ASME Section XI crack growth law showed that this initial flaw propagated to less than 0.3 inch following 4000 startup/shutdown cycles (about eight times those estimated for the plant life). This final flaw size is significantly below the ASME Code allowable flaw size for any of the flywheels examined in this study.

Structural Integrity Associates, Inc.

Table of Contents

Structural Integrity *Associates, Inc.*

List of Tables

Structural Integrity Associates, Inc.

List of Figures

Structural Integrity Associates, Inc.

Structural Integrity Associates, Inc.

Structural Integrity Associates, Inc.

Structural Integrity Associates, Inc.

Structural Integrity Associates, Inc.

1.0   INTRODUCTION

1.1   Background

Reactor coolant pump (RCP) flywheels operate at speeds such that in the very unlikely event of a failure during operation, they present a potential safety concern to the reactor coolant system, the containment and other equipment of systems important to safety as a result of the effects of missile impact. Regulatory Guide 1.14 (RG 1.14), Revision 1, issued by the U.S. Nuclear Regulatory Commission (NRC), presents a methodology for minimizing the potential for failure of RCP flywheels in light-water-cooled reactors [1]. Included within the requirements of RG 1.14 are the material, fabrication, design, testing and inspection requirements necessary to assure the flywheel is placed into service in compliance with the Guide, and the ASME Boiler and Pressure Vessel Code, providing a high quality component for plant operation.

Most utilities added surveillance requirements to conduct flywheel inspection according to RG 1.14 in order to resolve Systematic Evaluation Program (SEP) Topic III-10.B, "Pump Flywheel Integrity." This requirement was subsequently incorporated into the Technical Specifications of the plants as a result of Standard Review Plan (SRP) Section 5.4.1.1 [2] which was identified under NRC Staff SEP Topic V-7, "Reactor Coolant Pump Overspeed." It was expected that a generic review on SEP Topic V-7 would be conducted by the NRC. However, the issuance of NUREG-0933 [3], made this review unnecessary since it was concluded from this NUREG that there is a very low risk associated with flywheel failure. In spite of this, utilities still continue to spend considerable resources on the inspection of the flywheels per the requirements of RG 1.14.

Subsequent to initial plant operation, RG 1.14 mandates in-service inspection (ISI) to be performed at specific intervals to assure that the structural integrity of the flywheel is maintained. The inspection requirements, as specified within RG 1.14, require that a spin test be performed prior to initial operation at the design speed of the flywheel. Then, the

Structural Integrity Associates, Inc.

finished flywheel is subjected to a check of critical dimensions and a nondestructive examination (NDE) which includes the following:

1. Inspection of areas of higher stress concentration for surface defects in accordance with Section III of the ASME Code with acceptance criteria in accordance with paragraph NB-2500 of the Code.

2. Ultrasonic volumetric examination of 100% of each finished flywheel as specified in paragraph NB-2500 of the Code.

Following introduction into service, the ISI program for the flywheel is to be performed for each flywheel in accordance with the following paragraphs:

a) An in-place ultrasonic volumetric examination is to be performed on the areas of higher stress concentration at the bore and keyway. This should occur at approximately 3-year intervals, during the refueling or maintenance shutdown, coinciding with the ISI schedule, as required by Section XI of the ASME Code.

b) A surface examination of all exposed surfaces and complete ultrasonic volumetric examination shall be performed at approximately 10-year intervals, during the plant shutdown, coinciding with the ISI schedule, as required by Section XI of the ASME Code.

To date, plants that are committed to RG 1.14, have complied with its in-service inspection requirements, while most plants that are not committed to RG 1.14 have taken guidance from its inspection requirements. This has resulted in many examinations of the flywheel as part of the normal ISI program. The inspections have never revealed a condition which could lead to the failure of the flywheel. While several instances have been recorded in the

Structural Integrity Associates, Inc.

literature where the reactor coolant pump shaft has been subjected to cracking, no reported instance of flywheel service-induced degradation or cracking has been reported.

The flywheel inspections, both at 3-year and 10-year intervals, result in significant outage time, man-rem exposure and cost to utilities which may be minimized by use of a more carefully designed inspection program. This program should account for the failure history of the flywheels, potential in-service degradation mechanisms and applicable locations, prior inspection results, and an evaluation of the failure propensity of the entire coolant pump motor to determine if failure of a flywheel between inspections is a credible event.

Evaluations have been performed by the utilities participating in this study to demonstrate flaw tolerance of the flywheels in the six plants in conformance with RG 1.14 requirements. The evaluations are documented in References 4 through 9. It was shown in these evaluations that the flywheel materials have adequate toughness and that the critical speeds of the flywheels are significantly greater than their normal operating speeds, such that the probability of missiles resulting from the failure of a flywheel is extremely small. As part of this study, these evaluations were reviewed. In all cases, it was found that there is adequate safety margin against brittle and ductile fracture of the flywheel. Supplemental stress analyses and fracture mechanics evaluations were performed to demonstrate that at the most critical location of the flywheels, fracture is not a concern for the balance of plant life, such that current inspection requirements can be relaxed without compromising safety.

This report documents the independent review and analyses of flywheel integrity performed by Structural Integrity Associates (SI) for four utilities in the Combustion Engineering (CE) Owners Group to justify relaxation of the RG 1.14 in-service inspection requirements. The four utilities are Consumers Power (Palisades), Entergy Operations (Arkansas Nuclear Units 1/2 and Waterford Unit 3), Florida Power & Light (St. Lucie Units 1/2) and Northeast Utilities (Millstone Unit 2). ANO-1 is not covered by RG 1.14 but is included in this study to determine if their current inspection plan can also be relaxed. Flywheels at these plants have been used in a study to determine alternate inspection requirements for the RCP

Structural Integrity Associates, Inc.

flywheels. This evaluation includes a detailed review of past ultrasonic data of the affected plants, an industry-wide survey of other plants, the determination of degradation mechanisms which may affect the flywheel, stress analyses and fracture mechanics evaluations.

1.2 Objective and Organization

The objective of this study is to perform a comprehensive evaluation of the flywheel to justify the relaxation of the inspection requirements of RG 1.14. This investigation examines the flywheel material properties, fabrication processes and design, reviews past operating history and inspection results for the flywheel throughout the industry. The study then postulates an initial flaw and performs a crack growth and stability analysis for the flywheels under the most severe environmental and loading conditions for the component. In addition, all other failure mechanisms which can affect low alloy steels under the flywheel conditions are examined. This information can be utilized to develop a new recommended inspection schedule which will maintain safe performance of the RCP while reducing inspection costs and exposure.

Section 2 of this report examines the flywheel geometry and material properties for each of the plants in the evaluation. Section 3 discusses previous inspection results of the plants analyzed in this study, as well as from the industry in general, where information is available. Section 4 discusses the potential service degradation mechanisms which may undermine the serviceability of the flywheel. Section 5 provides a finite element stress analysis of the flywheel, examining locations of stress intensification under bounding loading conditions. Section 6 provides fracture mechanics analyses, postulating the maximum flaw that could be present, yet undetected during ultrasonic examination (UT), and propagating it using bounding crack growth rates for the flywheel operating conditions. ASME Section XI allowable flaw sizes are also calculated in this section and compared to the final flaw sizes, considering potential crack growth. Recommendations are provided along with a summary and conclusions in Section 7. Section 8 lists the references used to support this study.

Structural Integrity Associates, Inc.

2.0 DESCRIPTION OF FLYWHEELS

RCP flywheels are large steel discs which are attached to the shafts of RCP motors. The function of the flywheels is to maintain the rotational inertia of the RCP motor, providing coast-down and assuring a more gradual loss of main coolant flow to the core in the event that pump power is lost. In most cases, the flywheels consist of two or more discs bolted together either at the top and/or at the bottom of the motor.

Two basic types of flywheels are encountered in the plants under evaluation in this study. The first type is a "solid" flywheel in which the flywheel is directly attached to the shaft. These flywheels have relatively small bores; typically between 11 and 14 inches. They are shrunk-fit to the shafts such that contact is maintained between the flywheels and the shafts, even at maximum postulated overspeed conditions. There is at least one vertical keyway which key the flywheel to the shaft to provide continuity of the rotating assembly. Figure 2-1 shows a photograph of this type of flywheel in the RCP motor assembly with details shown in Figure 2-2.

The second type is a "hollow" flywheel in which the flywheel is shrunk fit unto a spoke or spider arm arrangement. These spokes are welded to the shaft, extending about 10 to 12 inches radially from the shaft and also extend from the top to the bottom flywheels in the axial direction. A typical RCP motor assembly for this configuration is shown in Figure 2-3. In addition to the vertical keyway, these flywheels also have a continuous circumferential groove which helps to prevent axial movement of the flywheels.

The flywheels in most cases are fabricated from ferritic steel plates. As required by RG 1.14, the flywheel materials are processed by vacuum-melt and degassing processes. All flame-cut surfaces are removed by machining to a depth of at least 1/2-inch below the flame-cut surface. No welding is permitted in the finished flywheel.

The normal operating temperature of the flywheels is ambient containment temperature (100°F to 110°F) since they are not in contact with the reactor coolant. Normal operating speeds for the flywheels range between 900 and 1200 rpm with design overspeed being 25% greater than the normal operating speed.

Structural Integrity Associates, Inc.

Table 2-1 provides specific information about the flywheels of the six plants considered in this evaluation, including materials, operating conditions and critical dimensions. The flywheels under consideration can be categorized into two types discussed above, with either a small or large bore. Flywheels at ANO-1, Palisades and St. Lucie are "hollow" and therefore have a large-bore diameter (measuring approximately 30 inches). Flywheels at ANO-2, Millstone-2, and Waterford-3 are "solid" and therefore have a smaller bore diameter (measuring approximately 14 inches). The following provides a brief description of the flywheels at each of the plants.

2.1 Arkansas Nuclear One Unit 1 (ANO-1)

Each of the existing reactor coolant pump motors has two flywheel assemblies, a large assembly at the upper end of the motor and a small assembly at the lower end. The flywheels are "hollow". Since the top assembly is much larger in diameter than the bottom assembly, ultrasonic testing is performed on the top assembly only. This top configuration is judged to be critical and therefore, the only flywheel evaluated in this report. It has a bore of 30.4 inches with an outside diameter of 72 inches. The keyway measures 0.75 inches in width, by 0.39 inches in depth.

The material of the flywheel is ASTM-A-516, Grade 65 (rolled plate). The minimum yield strength specified for this material is 35,000 psi. The nil-ductility transition (NDT), as determined by the Charpy V-Notch tests, is less than $+10°F$. The minimum fracture toughness of the flywheel material was calculated in Reference 4 as 109.6 ksi$\sqrt{in}$

The normal operating speed of the pump is 1,200 rpm. The motor is designed for a maximum overspeed of 125%. In the event that a double-ended rupture (a reactor coolant piping break in either the suction or discharge side of the pump) of the 28-inch pump discharge piping occurs at the same time as a loss of power to the pump motor, a speed of 1,800 rpm is predicted.

It is anticipated that the RCP motor at ANO-1 will be replaced at a future date. The flywheel dimensions and material of the new motor are different from the existing flywheel, as shown in Table 2-1. The new replacement flywheel is "solid" and therefore has a smaller outside diameter and smaller bore than the existing flywheel. The keyway dimensions of the

Structural Integrity Associates, Inc.

new replacement flywheel are, however, larger than the existing one. The new flywheel is fabricated from SA 533, Grade B while the existing flywheel is fabricated from ASTM-A-516, Grade 65. Operating speeds and overspeeds are the same for both flywheels.

A comparative analysis performed between the existing and the new replacement flywheel using equations presented in Section 5 indicates that the stresses are lower in the replacement flywheel for the same speed. Also the fracture toughness of the new flywheel is judged to be better in the new flywheel than the existing one. In this report, a bounding evaluation will be performed for ANO-1 by considering only the existing flywheel. The results of this evaluation can be conservatively applied to the replacement flywheel.

2.2   Arkansas Nuclear One Unit 2 (ANO-2)

The flywheel assembly at ANO-2 consists of two discs (6 inches thick each) of the solid disc type. Each disc is shrunk-on and keyed to the motor shaft at a location between the upper motor bearing bracket and the rotor punchings.

The material used for the flywheels is pressure vessel quality vacuum improved steel plate produced to ASTM-A-533, Grade B, Class 1 specification. The minimum fracture toughness calculated in Reference 5 is 100 ksi$\sqrt{\text{in}}$. A replacement RCP motor has been installed at one motor location at ANO-2. The flywheel material for the replacement motor is ASTM-A-508, Class 5. The fracture toughness of this flywheel material is 112 ksi$\sqrt{\text{in}}$ which is bounded by that of the existing ASTM-A-533 Grade B, Class 1 material.

The normal operating speed is 900 rpm and the overspeed is 1125 rpm. The LOCA overspeed for the motor is 2359 rpm.

2.3   Millstone Unit 2

Each flywheel assembly consists of two solid discs bolted together, shrunk onto, and keyed to the shaft above the motor. The dimensions of each disc include an outer bore diameter of 75 inches, an inner bore diameter of 13.74 inches and thickness of 12 inches (two, 6-inch slabs). The keyway measures 2.5 inches in width, by 1.062 inches in depth.

Structural Integrity Associates, Inc.

The flywheel is made of ASTM-A-516, Grade 65 material, which is pressure vessel quality, vacuum-improved steel plate. To improve the fracture toughness properties of the material, the flame-cut discs, with a 1/2 inch allowance for machining, were heat treated as follows:

- heated to 1650°F $\pm$ 25°F and held for a minimum of 3.5 hours;
- water quenched to below 400°F;
- tempered at 1140°F for 3 hours.

This material exceeds the requirements of ASTM-A-516, Grade 70. The nil-ductility transition (NDT) is lower than the value of +10°F as specified in Reference 1. A conservative value of fracture toughness was estimated in Reference 6 to be 90 ksi$\sqrt{in}$ at the operating temperature of 100°F. Considering the fact that a much lower NDT value was observed in Reference 6 than required in Reference 1, a higher fracture toughness value can be justified for the material of this flywheel.

During Refueling Outage 12, the original General Electric motor on Pump B was replaced with a motor also manufactured by General Electric. The flywheel for the replacement motor has the same dimensions as the original one except that it is one solid flywheel compared to the two discs bolted together for the original flywheel. The material of the replacement flywheel is SA-508, Class 5 which is estimated to have fracture toughness which is at least equal to that of the original SA-516, Grade 70 material.

The normal operating speed of the flywheel is 900 rpm; the design overspeed (125% of operating speed) is 1125 rpm.

2.4   Palisades

Each of the four flywheels at Palisades has a 72-inch outer diameter, 34-inch inner bore diameter and are 7 inches thick. They are of the "hollow" type fitted over a spoked center section and bolted down to a separate bore lower flywheel of a smaller diameter. Near the outer periphery is a row of 24 equally-spaced threaded blind holes for the purpose of adding balancing weights, although these have not been used. Four larger diameter (3-inch) counterbored holes, 11-inch from the outer periphery of the flywheel, allow for bolting to

Structural Integrity Associates, Inc.

the lower flywheel section. The keyway is relatively small, measuring 0.5 inch in width, by 0.25 inch in depth.

The flywheel is made from ASTM-A-108 (1017), low carbon steel with a minimum yield strength of 27,000 psi and tensile strength of 50,000 psi. The pump flywheels are machined from cross rolled blanks.

The NDT of the flywheel material is no higher than 40°F with an average Charpy V-notch (CVN) energy of 100 ft-lb observed at 70°F. Therefore, this material does not meet the NDT requirement of Reference 1 although the CVN requirement is met. The NDT was determined to be 40°F, 30°F greater than 10°F specified per the requirements of RG 1.14. However, the operating temperature of 100°F is 60°F above NDT. This margin coupled with a CVN energy at 70°F exceeds the required energy of 50 ft-lbs, demonstrating adequate fracture toughness for this material. The fracture toughness was determined to be 100 ksi$\sqrt{in}$ in Reference 7.

The normal operating speed is 900 rpm with design overspeed of 1125 rpm.

2.5   St. Lucie Units 1 and 2

The flywheels at St. Lucie 1 and 2 are of the "hollow" type with the flywheels shrunk-fit unto a spoke arrangement. The top flywheel which is the critical one has an outside diameter of 72 inches, bore diameter of 32.5 inches and thickness of 7.785 inches. The vertical keyway has a width of 1 inch and 1/2 inch into the flywheel and 1/2 inch into the spider arm.

The flywheel material for Unit 1 meets the requirement of SA-516 Grade 70, while the material for Unit 2 is ASTM A-543 Class 1 Type B. The minimum fracture toughness (K_{Ic}) for the Unit 1 flywheel is 90 ksi$\sqrt{in}$ at 100°F; K_{Ic} for Unit 2 is 100 ksi$\sqrt{in}$ at normal operating temperature [8].

The normal operating speed is 900 rpm with design overspeed of 1125 rpm. LOCA accident speed is specified as 265% of normal speed. However the LOCA overspeed is limited by speed for electrical breaking effects of the motor which is specified as 105% of normal speed.

Structural Integrity Associates, Inc.

2.6 Waterford Unit 3

The flywheel at Waterford-3 is of the solid type and has an outer diameter of 78 inches, an inner bore diameter of 13.75 inches and a thickness of 8.5 inches. The keyway measures 1.0 inch in length, by 0.531 inch in depth.

The material used to manufacture the flywheel is pressure vessel quality, prepared by the vacuum melt and degassing process, ASTM-A-543, Grade B, Class 1 steel plate. The lower bound fracture toughness is 100 ksi$\sqrt{in}$, as determined in Reference 9.

The normal operating speed is 1200 rpm. The design overspeed is defined as 125% of normal operating speed (1500 rpm). A maximum speed of 1585 rpm is predicted during a pump discharge accident event.

Table 2-1

Flywheel Specifications

Plant Name	Pump Motor Manufacturer	No. of Motors	No. of Flywheels per Motor	Flywheel Material	Design Overspeed (rpm)	Design Operating Speed (rpm)	Bore Diam. (in.)	Outer Diam. (in.)	Thickness (in.)	Keyway Width (in.)	Keyway Depth (in.)	No. of Keyways
ANO-1	Allis-Chalmers	4	2[1]	ASTM-A-516, Gr. 65	1500	1200	30.4	72.0	8.0	0.75	0.39	1
ANO-1	Jeumont Shneider	1	1	ASTM-A-533, Grade B, Cl. 1	1500	1200	11.61 and 11.55	67.87	6.496	2.165	0.8346	3
ANO-2	General Electric	4	1[2]	ASTM-A-533, Gr. B, Cl. 1	1125	900	13.74	81.5	11.75	2.5	1.062	1
ANO-2	General Electric	1	1	ASTM-A-508 Cl. 5	1125	900	13.74	81.5	11.75	2.5	1.062	1
Millstone-2	General Electric	4	1[2]	ASTM-A-516, Gr. 70	1125	900	13.74	75.0	12.0	2.5	1.062	1
Millstone-2	General Electric	1	1	ASTM-A-508 Cl. 5	1125	900	13.74	75.0	12.0	2.5	1.062	1
Palisades	Allis-Chalmers	4	2[3]	ASTM-A-108	1125	900	33.0	72.0	7.0	0.5	0.25	1
St. Lucie-1	Allis-Chalmers	4	2[4]	ASTM-A-516 Gr. 70	1125	900	32.5	72.0	7.785	1.0	0.50	1
St. Lucie-2	Allis-Chalmers	4	2[4]	ASTM-A-543, Gr. B, Cl. 1	1125	900	32.5	72.0	7.785	1.0	0.50	1
Waterford-3	General Electric	4	1[2]	ASTM-A-543, Gr. B, Cl. 1	1500	1200	13.75	78.0	8.5	1.0	0.531	1

Notes

1) Top flywheel consists of three plates bolted together. Bottom flywheel consists of one plate.
2) Consists of two plates bolted together.
3) Top flywheel consists of two plates bolted together. Bottom flywheel consists of one plate.
4) Top and bottom flywheels consist of one plate each.
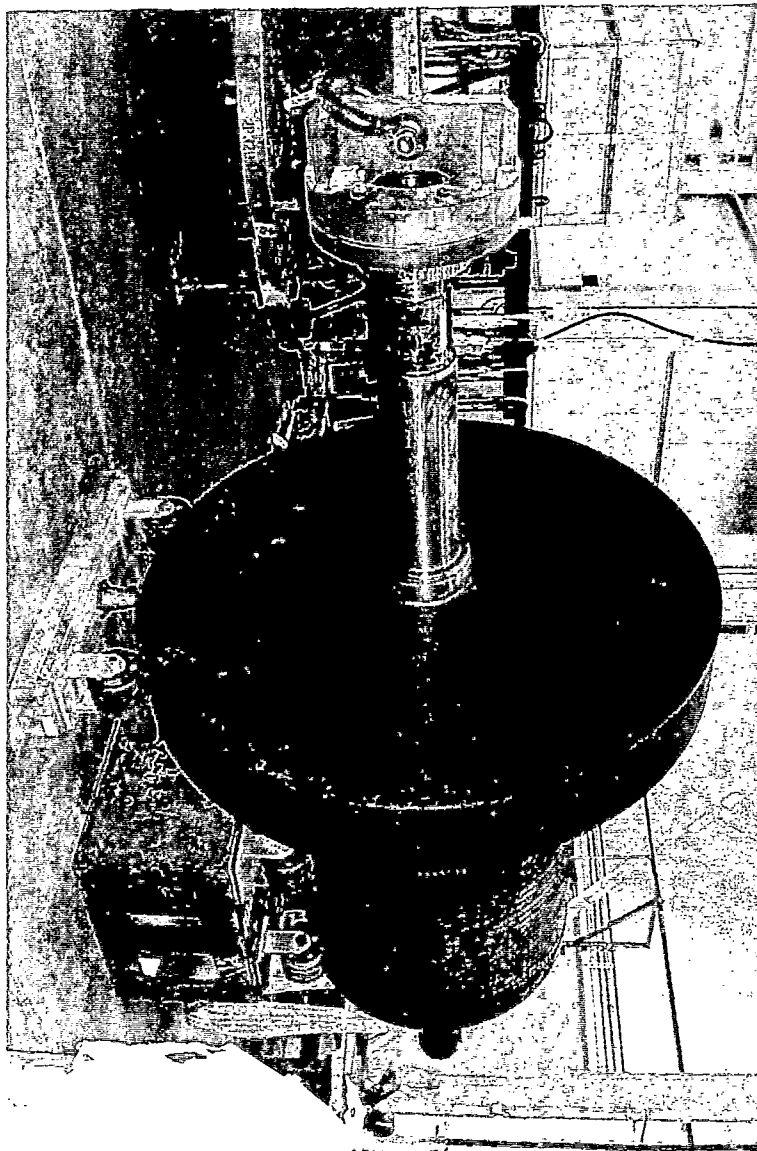
Figure 2-1. Photograph of Solid Flywheel

Pawl Region

Bolt Holes
(typical)

Keyway

Hub

Inner Bore
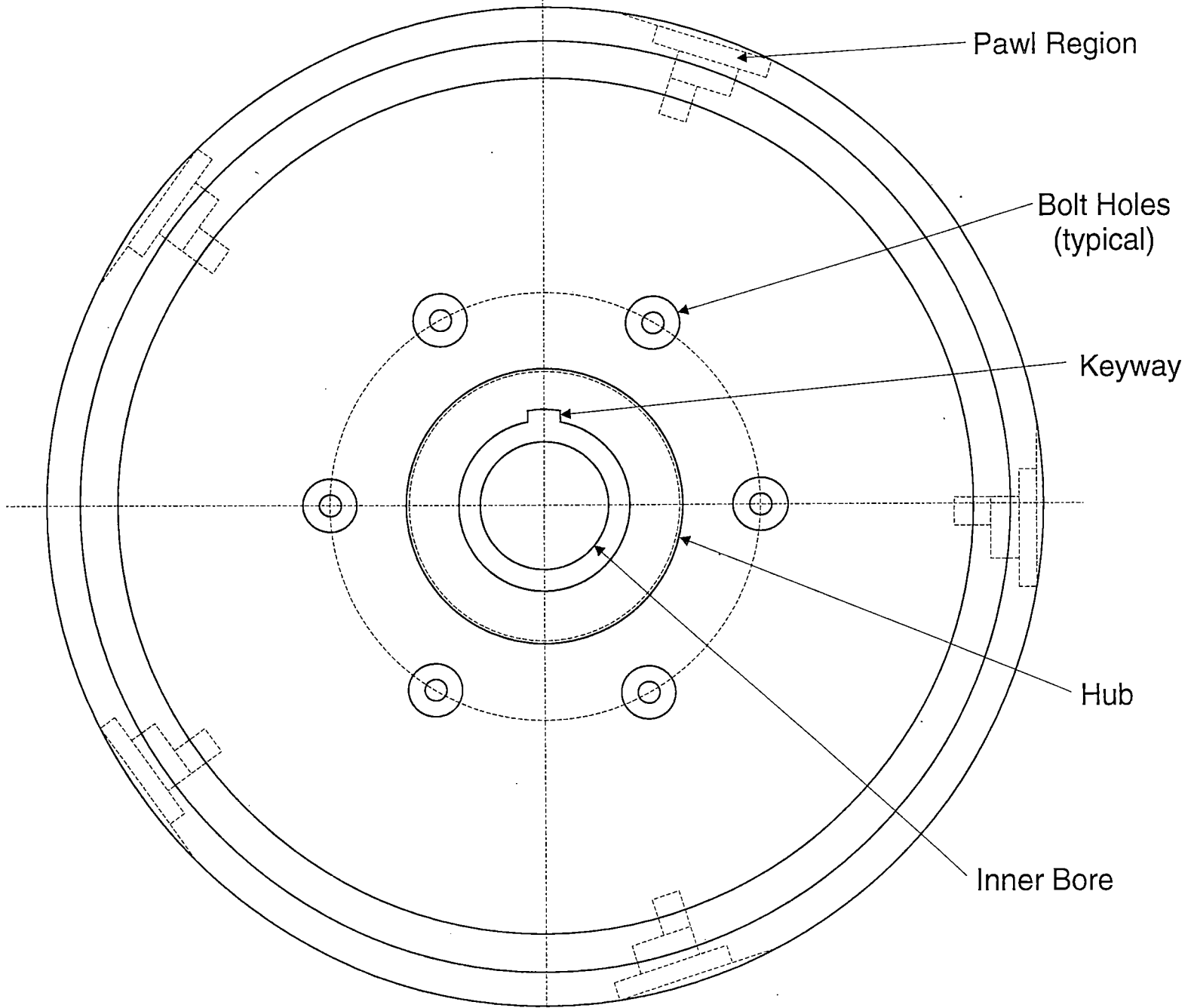
Figure 2-2. Critical Area of Flywheel

94688r0
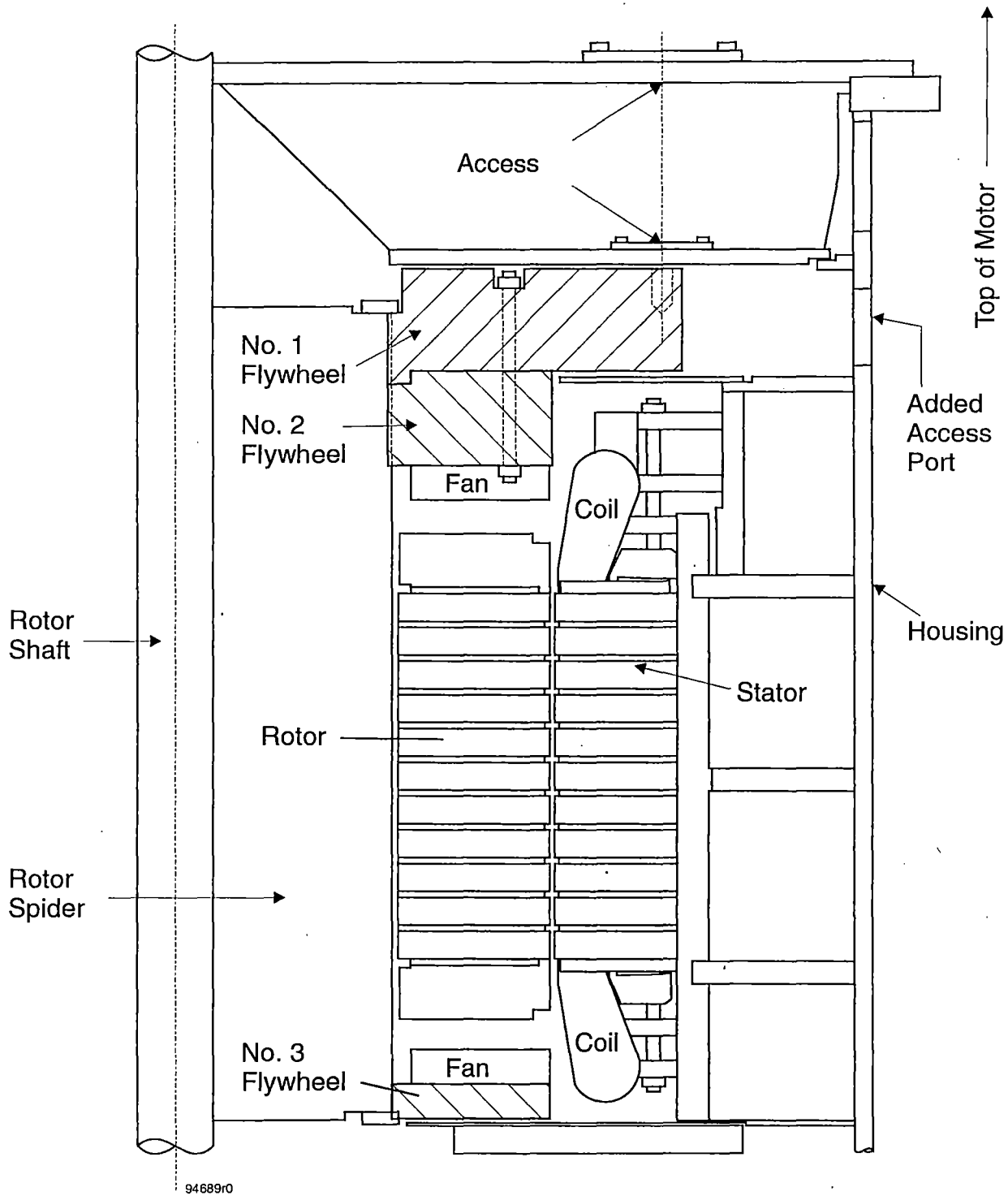
Figure 2-3. Typical Assembly for Hollow Flywheel

3.0 PREVIOUS INSPECTION RESULTS FOR RCP FLYWHEELS

Since the issuance of RG 1.14, most utilities have performed inspections of the RCP flywheels per the requirements of the document. Many plants have performed both the 3-year interval UT examination and surface examinations as well as complete UT examinations during the 10-year interval using procedures recommended in RG 1.14.

UT procedures require the use of a couplant for sound transmission between the search unit (which transmits and receives ultrasound) and the surface of the flywheel. Straight-beam examination (longitudinal) is used to detect laminar-type discontinuities which interfere with the angle-beam examination. Angle-beam examination (shear wave) is used to detect discontinuities and cracking which are detrimental to the service life or operation of the flywheel.

Lamellar discontinuities frequently occur in rolled plate and are revealed during ultrasonic inspections. They are usually elongated non-metallic inclusions (such as sulfides and silicates) and their distribution is seldom uniform because it depends on factors such as rolling practice and impurity segregation in the ingot. When their orientation is parallel to the design tensile stresses and their existence is not evidenced by lamellar tearing during fabrication, their existence is ignored during ultrasonic examinations. Laminar indications are also revealed during ultrasonic inspections. These discontinuities are caused during manufacturing, where air is trapped in the steel and rolled out. Typically they lie within a $10°$ band parallel to the top and bottom surface of the flywheel and are in a plane parallel to the top and bottom surfaces. These laminations do not pose any structural integrity concerns for the flywheel since they are not oriented in the plane of the stresses.

Inspection results considered in this study from plant operation were examined to determine if any flaws have been identified during the RG 1.14 mandated inspections. In addition, a survey of other plants was performed to determine if there are any plants that have identified flaws during the inspections.

Structural Integrity Associates, Inc.

3.1 Plant-Specific Results

The inspection results for the plants under evaluation are presented in Tables 3-1 through 3-6. As can be seen from these tables, the flywheels have been inspected on numerous occasions. As explained previously, ANO-1 is not covered specifically by the requirements of RG 1.14, therefore, the flywheel inspection program is conducted every ten years. From Tables 3-1 through 3-6, it can be seen that no cracks have ever been reported during these inspections. Only geometric reflectors and laminar indications which typically occur during fabrication have been identified. As explained earlier, these indications do not present any structural integrity concerns for the flywheels since they are not oriented in the plane of the stresses.

3.2 Industry-wide Survey

Personnel from over 30 plants were contacted to assess their inspection history and inspection results associated with the performance of their RCP flywheels. A detailed set of questions were presented. Highlights of the survey are as follows:

- All plants conduct ISI of the flywheel component using manual ultrasonic inspection techniques.

- A wide range of costs are associated with in-situ ultrasonic examination of the flywheels, dependant upon a variety of factors including the presence of qualified on-site personnel and access to the flywheel.

- Some plants have incorporated inspection requirements into their plant-specific technical specification document or final safety analysis report (FSAR). Some plants have coordinated the 10-year (complete) inspection to coincide with motor overhaul, reducing the amount of maintenance effort.

Structural Integrity Associates, Inc.

-   Most plants have reported that obtaining access for inspection is difficult and, in most cases, very costly.

-   In some cases plant personnel are subjected to some level of radiation exposure during the inspections.

-   Industry experience related to RCP flywheel performance has identified no reportable indications from ISI of flywheels (other than laminations and other non-structurally significant fabrication defects). No service induced cracking or other defects which would increase the probability of flywheel failure have been identified as a result of this investigation.

Structural Integrity Associates, Inc.

Table 3-1

Inspection Summary for ANO-1 RCP Flywheels

RCP Flywheel No.	Year Examined	Inspection Volume or Area	Examination Methods Used	Areas of Flaws/Cracks Identified
A B C D	1983	100% Examination of each flywheel	Acoustic Emission	None
D	1992	100%	UT & MT	None

The ANO-1 flywheels for each RCP motor consist of two assemblies, one at the top of the motor and one at the bottom. Since the top assembly is larger in diameter than the bottom assembly, the plant Technical Specifications (4.2.6) only address the top assembly. The results above refer to the top flywheel assembly only.

No cracks have ever been identified on any of the RCP flywheels.

Structural Integrity Associates, Inc.

Table 3-2

Inspection Summary for ANO-2 RCP Flywheels

RCP Flywheel No.	Refueling Outage & Year Examined	Inspection Volume or Area	Examination Methods Used	Indications Detected
2P32A	2R2 - 1982	Bore & Keyway	Volumetric - UT 10°	Geometric
	2R4 - 1985	Bore & Keyway	Volumetric - UT 10°	Geometric
	2R5 - 1986	Bore & Keyway	Volumetric - UT 10°	None
		Accessible Surfaces	Volumetric - UT 0°	None
	2R7 - 1989	Bore & Keyway	Volumetric - UT 10°	None
		Accessible Surfaces	Volumetric - UT 0°	None
	2R8 - 1991	Bore & Keyway	Volumetric - UT 45°	None
		Accessible Surfaces	Volumetric - UT 0°, 45° & Surface-ECT	None
	Post 2R9 - 1993	Bore & Keyway	Volumetric - UT 45°	None
		Accessible Surfaces	Volumetric - UT 0°, 45° & Surface-MT	Laminations
2P32B	2R2 - 1982	Bore & Keyway	Volumetric - UT 10°	Geometric
	2R4 - 1985	Bore & Keyway	Volumetric - UT 10°	Geometric
	2R5 - 1986	Bore & Keyway	Volumetric - UT 10°	None
		Accessible Surfaces	Volumetric - UT 0°	Lamination
	2R7 - 1989	Bore & Keyway	Volumetric - UT 10°	None
		Accessible Surfaces	Volumetric - UT 0°	None
	2R8 - 1991	Bore & Keyway	Volumetric - UT 45°	None
		Accessible Surfaces	Volumetric - UT 0°, 45° & Surface-ECT	None
	Post 2R10 - 1994	Bore & Keyway	Volumetric - UT 45°	None
		Accessible Surfaces	Volumetric - UT 0°, 45° & Surface-MT	Laminations
2P32C	2R2 - 1982	Bore & Keyway	Volumetric - UT 10°	Geometric
	2R4 - 1985	Bore & Keyway	Volumetric - UT 10°	Geometric
	2R5 - 1986	Bore & Keyway	Volumetric - UT 10°	None
		Accessible Surfaces	Volumetric - UT 0°	None
	2R7 - 1989	Bore & Keyway	Volumetric - UT 10°	None
		Accessible Surfaces	Volumetric - UT 0°	None
	2R8 - 1991	Bore & Keyway	Volumetric - UT 45°	None
		Accessible Surfaces	Volumetric - UT 0°, 45° & Surface-ECT	None
	2R10 - 1994	Bore & Keyway	Volumetric - UT 45°	None

Structural Integrity Associates, Inc.

Table 3-2
(concluded)

RCP Flywheel No.	Refueling Outage & Year Examined	Inspection Volume or Area	Examination Methods Used	Indications Detected
2P32D	2R2 - 1982	Bore & Keyway	Volumetric - UT 10°	Geometric
	2R4 - 1985	Bore & Keyway	Volumetric - UT 10°	Geometric
	2R5 - 1986	Bore & Keyway	Volumetric - UT 10°	None
		Accessible Surfaces	Volumetric - UT 0°	None
	2R7 - 1989	Bore & Keyway	Volumetric - UT 10°	None
		Accessible Surfaces	Volumetric - UT 0°	None
	2R8 - 1991	Bore & Keyway	Volumetric - UT 45°	None
		Accessible Surfaces	Volumetric - UT 0°, 45° & Surface-ECT	None
	2R10-1994	Bore & Keyway	Volumetric - UT 45°	None

Structural Integrity Associates, Inc.

Table 3-3

Inspection Summary for Millstone Unit 2 RCP Flywheels

RCP Flywheel No.	Year Examined	Inspection Volume or Area	Examination Methods Used	Indications Detected
RP-40-A	1978	Bore & Keyway	Volumetric - UT 10° L	No
	1982	Bore & Keyway	Volumetric - UT 10° L	Geometric
	1985	Bore & Keyway	Volumetric - UT 10° L	Geometric
	1985	Surface Limited Scan	Eddy Current	Surface Scratches
	1992	Bore & Keyway	Volumetric - UT 10° L	No
RP-40-B	1978	Bore & Keyway	Volumetric - UT 10° L	No
	1980	Bore & Keyway	Volumetric - UT 10° L	No
	1985	Bore & Keyway	Volumetric - UT 10° L	Geometric
	1985	Surface Limited Scan	Eddy Current	No
	1989	Bore & Keyway	Volumetric - UT 10° L	No
	1992	Bore & Keyway	Volumetric - UT 10° L	No
RP-40-C	1978	Bore & Keyway	Volumetric - UT 10° L	No
	1982	Bore & Keyway	Volumetric - UT 10° L	Geometric
	1985	Bore & Keyway	Volumetric - UT 10° L	Geometric
	1985	Surface Limited Scan	Eddy Current	No
	1989	Bore & Keyway	Volumetric - UT 10° L	No
	1992	Bore & Keyway	Volumetric - UT 10° L	No
RP-40-D	1978	Bore & Keyway	Volumetric - UT 10° L	No
	1980	Bore & Keyway	Volumetric - UT 10° L	No
	1985	Bore & Keyway	Volumetric - UT 10° L	Geometric
	1985	Surface Limited Scan	Eddy Current	No
	1989	Bore & Keyway	Volumetric - UT 10° L	No
	1992	Bore & Keyway	Volumetric - UT 10° L	No

Structural Integrity Associates, Inc.

Table 3-4
Inspection Summary for Palisades Flywheels

RCP Flywheel No.	Year Examined	Inspection Volume or Area	Examination* Methods Used	Indications Detected
PCS-72-RCL-1A	1970	Upper Surface	Volumetric - UT 100%	None
	1973	Upper Surface	Volumetric - UT 100%	None
	1976	Upper Surface	Volumetric - UT 100%	None
	1978	Upper Surface	Volumetric - UT 100%	Geometric
	1979	Upper Surface	Volumetric - UT 100%	None
	1981	Upper Surface	Volumetric - UT 100%	None
	1983	Upper Surface	Volumetric - UT 100%	Lamination
	1986	Upper Surface	Volumetric - UT 100%	Geometric
	1991	Upper Surface	Volumetric - UT 100%	Lamination
	1992	Upper Surface	Volumetric - UT 100%	Lamination
	1993	Upper Surface	Volumetric - UT 100%	Lamination
PCS-72-RCL-1B	1970	Upper Surface	Volumetric - UT 100%	Lamination
	1973	Upper Surface	Volumetric - UT 100%	None
	1976	Upper Surface	Volumetric - UT 100%	None
	1978	Upper Surface	Volumetric - UT 100%	Geometric
	1979	Upper Surface	Volumetric - UT 100%	Geometric
	1981	Upper Surface	Volumetric - UT 100%	None
	1983	Upper Surface	Volumetric - UT 100%	Lamination
	1986	Upper Surface	Volumetric - UT 100%	Geometric
	1991	Upper Surface	Volumetric - UT 100%	Lamination
	1992	Upper Surface	Volumetric - UT 100%	Lamination
	1993	Upper Surface	Volumetric - UT 100%	Lamination
PCS-72-RCL-2A	1970	Upper Surface	Volumetric - UT 100%	Lamination
	1973	Upper Surface	Volumetric - UT 100%	None
	1976	Upper Surface	Volumetric - UT 100%	None
	1978	Upper Surface	Volumetric - UT 100%	Lamination
	1979	Upper Surface	Volumetric - UT 100%	Lamination
	1981	Upper Surface	Volumetric - UT 100%	None
	1983	Upper Surface	Volumetric - UT 100%	Lamination
	1986	Upper Surface .	Volumetric - UT 100%	None
	1991	Upper Surface	Volumetric - UT 100%	Lamination
	1992	Upper Surface	Volumetric - UT 100%	Lamination
	1993	Upper Surface	Volumetric - UT 100%	Lamination

Table 3-4
(concluded)

RCP Flywheel No.	Year Examined	Inspection Volume or Area	Examination* Methods Used	Indications Detected
PCS-72-RCL-2B	1970	Upper Surface	Volumetric - UT 100%	Lamination
	1973	Upper Surface	Volumetric - UT 100%	None
	1976	Upper Surface	Volumetric - UT 100%	None
	1978	Upper Surface	Volumetric - UT 100%	Lamination
	1979	Upper Surface	Volumetric - UT 100%	None
	1981	Upper Surface	Volumetric - UT 100%	Geometric
	1983	Upper Surface	Volumetric - UT 100%	Lamination
	1986	Upper Surface	Volumetric - UT 100%	Geometric
	1991	Upper Surface	Volumetric - UT 100%	Lamination
	1992	Upper Surface	Volumetric - UT 100%	Lamination
	1993	Upper Surface	Volumetric - UT 100%	Lamination

* All examinations are straight beam examinations.

Table 3-5

Inspection Summary for St. Lucie Units 1 and 2

RCP Flywheel No.[1]	Year Examined	Inspection Volume or Area[2]	Examination Methods Used[3]	Indications Detected*
1A1	1983	B	UT	None
1A2		B	UT	None
1B1		B	UT	None
1B2		B	UT	None
2A1	1986	A	UT	None
2A2		A	UT	None
2B1		A	UT	None
2B2		A	UT	None
1A1	1987	B	UT	None
1A2		B	UT	None
1B1		B	UT	None
1B2		B	UT	None
2A1	1989	A	UT	None
2A2		A	UT	None
2B1		A	UT	None
2B2		A	UT	None
1A1	1990	A	UT	None
1A2		A	UT	None
1B1		A	UT	None
1B2		A	UT	None
2A1	1992	B	UT	None
		C	PE	None
2A2		B	UT	None
		C	PE	None
2B1		B	UT	None
		C	PE	None
2B2		B	UT	None
		C	PE	None

Table 3-5
(concluded)

RCP Flywheel No.[1]	Year Examined	Inspection Volume or Area[2]	Examination Methods Used[3]	Indications Detected*
1A1	1993	A	UT	None
1A2		A	UT	None
1B1		A	UT	None
1B2		A	UT	None
2A1	1994	A	UT	None
2A2		A	UT	None
2B1		A	UT	None
2B2		A	UT	None

Notes:

1) RCP Pump Flywheel identification per unit:

St. Lucie Unit 1   St. Lucie Unit 2
        1A1   2A1
        1A2   2A2
        1B1   2B1
        1B2   2B2

2) Inspection Method/Area Requirements:

A = 100% Volumetric of Bore and Keyway Areas
B = 100% Volumetric of Flywheel
C = Partial Volumetric of Flywheel Surface

3) Examination Methods Used:

UT = Volumetric (Ultrasonic Examination)
PE = Surface (Partial Ultrasonic Surface Wave)

Structural Integrity Associates, Inc.

Table 3-6

Inspection Summary for Waterford-3 Flywheels

RCP Flywheel No.	Refueling Outage & Date Examined	Inspection Volume or Area	Examination Methods Used	Indication Detected
RCP 1A	RF01 - 04/28/88	Bore & Keyway	Volumetric - UT 10°	None
	RF04 - 03/27/91	Bore & Keyway	Volumetric - UT 9°	None
RCP 1B	RF02 - 05/04/88	Bore & Keyway	Volumetric - UT 10°	None
	RF04 - 03/27-91	Bore & Keyway	Volumetric - UT 9°	None
RCP 2A	RF02 - 05/04/88	Bore & Keyway	Volumetric - UT 10°	None
	RF04 - 05/06/91	Bore & Keyway	Volumetric - UT 9°	None
RCP 2B	RF02 - 05/04/88	Bore & Keyway	Volumetric - UT 10°	None
	RF04 - 05/06/91	Bore & Keyway	Volumetric - UT 10°	None

Structural Integrity *Associates, Inc.*

4.0 POTENTIAL FLYWHEEL DEGRADATION MECHANISMS

The typical RCP flywheel is exposed to a dry air environment at a nominal operating temperature of approximately 100-110°F. Consequently, under normal operating conditions, no water-related degradation mechanisms would be expected to be operative. However, a potential seal leak in the RCP housing could produce the potential for a water spray, injecting a mist of primary PWR water in the flywheel vicinity. As a result of this potential event, environmentally-related degradation mechanisms are addressed as potentially active for the RCP flywheel.

A comprehensive review of the material degradation mechanisms potentially affecting low alloy steel components in light water reactor environments is presented in Reference 10. They are classified under the following general categories:

- Corrosion
- Fabrication Defects
- Embrittlement
- Mechanical/Thermal
- Fatigue

The mechanisms are reviewed for their relevance to RCP flywheels in the following paragraphs.

Corrosion

At low temperatures, (below 200°F), the environmentally-related degradation mechanisms are typically not as prominent as at higher temperatures for most materials. However, some corrosion mechanisms are active for low alloy steels, such as pitting and hydrogen embrittlement which are prominent low temperature degradation mechanisms. Examining

Structural Integrity Associates, Inc.

the corrosion mechanisms in Reference 10, one observes that because of the temperature, the active mechanisms which must be considered are the following:

- General Corrosion or Wastage
- Crevice Corrosion
- Pitting
- Hydrogen Embrittlement
- Microbiologically Influenced Corrosion (MIC)

General Corrosion or Wastage

Although the flywheel environment is normally dry air, potential seal leaks in the RCP can produce conditions where primary PWR water may be directed at the flywheel. Under this condition, boric acid corrosion is possible. Particularly since the flywheel is open to air (an oxidizing environment), it is possible that the boric acid could concentrate thereby producing a condition in which accelerated general corrosion or wastage is possible. However, the flywheel operating temperature is so low that no concentrating mechanism is readily apparent. Therefore, it is believed that boric acid wastage is not a likely degradation mechanism for the flywheel.

On the other hand, general corrosion or impingement corrosion is possible if sufficient coolant were to leak from a faulty seal. Under these circumstances, it is likely that the leakage would be readily detected prior to significant corrosion occurring as a result of normal plant operation. In addition, the flywheels are typically painted with corrosion resistant paints to mitigate any general corrosion concerns.

Crevice Corrosion

Depending upon the design of the flywheel assembly, it is possible for crevices to be present which may give rise to the possibility of crevice corrosion. However, since this component

Structural Integrity Associates, Inc.

is in a low temperature region of the system and there are no obvious concentrating mechanisms for crevice corrosion, it is expected that crevice corrosion will not be a likely degradation mechanism for the RCP flywheel.

Pitting and MIC

Pitting and MIC can be combined as potentially operative degradation mechanisms for the flywheel, but only during extended downtime, particularly when stagnant, low temperature water is present. This is not a normal condition for the flywheel. However, it is possible that this may occur and should be addressed in an appropriate maintenance/inspection plan. Clearly, without a specific operating event which exposes the low temperature primary PWR water to the flywheel, and since the flywheel is nominally in dry air during operation and downtime, pitting and/or MIC should not be problems for the RCP flywheel.

Hydrogen Embrittlement

One mechanism which can produce significant deterioration to a flywheel is hydrogen embrittlement. This mechanism requires that the component be exposed to an aqueous environment, at or near room temperature and the component must have been heat treated (or mis-heat treated) so that the material is in an untempered, very hard condition. For this class of alloys, the fabrication specifications require that suitable post weld heat treatment be performed following any thermal operations so that the likelihood for hydrogen embrittlement is minimized. Additionally, this phenomenon is likely to occur early in plant life, or even before plant operation if the component is exposed to ambient moist air. Consequently, if prior inspections have not revealed evidence of hydrogen embrittlement damage, and if no further thermal treatments are performed, e.g., weld repair, or severe grinding; hydrogen embrittlement should not be a concern.

Structural Integrity Associates, Inc.

Fabrication Defects

Among the fabrication defects which may affect structural material components, the principal defects potentially affecting the flywheel are casting and forming defects [10]. The flywheel is most often produced from plate formed material, and as such is a high quality component, with few fabrication defects. Appropriate volumetric inspections on the finished component assure that fabrication defects are not present which can have a deleterious effect on the performance of the flywheel. Overspeed testing of the component provides additional confidence in the quality and structural reliability of the flywheel. Consequently, for a flywheel which has undergone proof testing and has been in service, fabrication defects should have a minimal effect on future performance.

Embrittlement

Embrittlement is an inactive mechanism for low alloy steel components at low temperatures [10].

Mechanical/Thermal Processes

Among the mechanical or thermal processes affecting low alloy steel performance at low temperatures, only fretting and mechanical wear are potentially active mechanisms. These mechanisms are potentially active for the flywheel. However, normal operational procedures checking flywheel balance and flywheel operational monitoring will detect evidence of significant fretting and wear. This mechanism need not be addressed since it will be addressed as part of the normal operational procedures and monitoring, for example, vibrational analysis and motor current monitoring.

Fatigue

Fatigue is a potentially significant degradation mechanism for the low alloy steel RCP flywheel in PWRs. In general, the degradation is the result of mechanical fatigue, generally high cycle. This mechanism and its potential effect on the operation and inspection of the flywheel is addressed analytically in later sections of this report.

Structural Integrity Associates, Inc.

5.0 STRESS ANALYSIS

Stress analyses have been performed for the flywheels under consideration to determine stresses to be used in the fracture mechanics analyses in the next section. Potential loadings for the flywheels include the following:

- centrifugal loads due to pump speed
- shrink-fit loads
- seismic loads
- vibrational loads
- key loading due to shaft torque

Of these loads, the most significant are centrifugal and shrink-fit loads. The other loads are considered small enough that they will not contribute significantly to flaw growth or fracture during the life of the flywheel.

5.1 Centrifugal Loads Due to Pump Speed

Without consideration of geometric discontinuities such as the keyway and bolt holes in the flywheel, the flywheel can be considered to be an annular rotating disc. The radial and tangential stresses in such a case can be calculated using the following equations from References 11 and 12:

$$\sigma_r = \frac{3 + \mu}{8} \cdot \frac{\rho \omega^2}{g} \cdot \left[a^2 + b^2 - \frac{a^2 b^2}{r^2} - r^2 \right] \tag{5-1}$$

$$\sigma_t = \frac{3 + \mu}{8} \cdot \frac{\rho \omega^2}{g} \cdot \left[a^2 + b^2 + \frac{a^2 b^2}{r^2} - \frac{1 + 3\mu}{3 + \mu} r^2 \right] \tag{5-2}$$

Structural Integrity Associates, Inc.

where:

σ_r = radial stress (psi)

σ_t = tangential stress (psi)

a = bore radius (in)

b = outer radius (in)

ρ = mass density (lb-sec^2/in^4), for steel = 0.283/386 = 0.00073 lb-sec^2/in^4

ω = rotational speed rad/sec, (rad $\cdot$ 2π)/60

μ = Poisson's ratio (in/in), for mild steel = 0.3 in/in

These equations have generally been used by most utilities to determine the flywheel centrifugal stresses for the RG 1.14 evaluation. The stress distribution from the inner bore to the outer bore, using Equations 5-1 and 5-2, is shown in Figure 5-1. Although the magnitude of the stresses will vary with angular velocity and specific flywheel dimensions, the overall shape of the stress distribution remains essentially the same at all speeds. For a radial crack emanating from the inner bore, the tangential stress will be the component contributing to crack growth. It can be noted from Figure 5-1 that the tangential stress is essentially linear over 90% of the flywheel with a sharp peaking effect due to the stress concentration at the bore. This peaking effect will be even more significant if the keyway is considered in the analysis.

To account for geometric discontinuities introduced by the keyway, finite element models were developed for the flywheels considered in this study. The bolt holes were not modeled because the stress concentration introduced by the keyway is more significant than that caused by the bolt holes. Moreover, the maximum tangential stress, responsible for propagating cracks, occurs near the inner bore where the keyway is located. The bolt holes are remote from this critical region. For the hollow flywheel, the circumferential keyway was also not modeled since it is parallel to the tangential stresses and therefore the stress concentration effect is not critical compared to the vertical keyways.

Structural Integrity Associates, Inc.

The ANSYS computer program [13] was used to develop the models. Each flywheel was modeled using the geometric and material information provided in Table 2-1. Two-dimensional isoparametric elements were used to develop a plane strain model for the flywheels. A plane strain model is justified for these analyses since the flywheels are relatively thick. The keyway for each of the flywheels was explicitly modeled in order to determine the stress concentration effect in this region, with adequate refinement of the finite element models in the keyway region in order to determine the peak stress. A typical finite element model for the large-bore flywheels is shown in Figure 5-2 while a typical smaller bore flywheel finite element model is shown in Figure 5-3. A total number of 2472 elements were used for the large diameter models, while 2944 elements were used for the smaller diameter models.

The analyses were performed under normal operating speeds of the motor for each plant. Results for other speeds can be determined by factoring the results obtained for the normal operating speeds by the square of the speed ratio. The ANSYS computer program allows for a rotational centrifugal force to be applied to the model, using the speed as input. To prevent rigid body motion, the nodal points on the outer bore, 180° from the keyway location, were restrained. Local stresses at these restrained locations are therefore fictitious and should be ignored.

Figures 5-4 through 5-27 present the tangential and radial stress distributions under centrifugal loading for all six flywheels considered in the evaluation. Four figures are presented for the flywheel of each plant. The first two figures for each plant depict the overall stress distribution and detailed keyway region stresses in the tangential direction. The third and fourth figures provide the overall stress distribution and detailed keyway stresses in the radial direction.

The stress distributions from the inner to the outer bore in the tangential and radial directions due to the centrifugal force are presented in Figures 5-28 through 5-33 for the six flywheels. In these figures, the stresses are plotted separately for the keyway region and

Structural Integrity Associates, Inc.

locations remote from the keyway region. As can be seen from these figures, there is a significant difference between the stress distribution in the vicinity of the keyway and remote from the keyway region. There is a very significant increase in stresses in the keyway region relative to the remote locations. However, these peak stresses are localized and after a short distance from the keyway, the stress distributions become identical.

Figures 5-34 through 5-39 provide a comparison between the results of the finite element analyses stress distributions (remote locations away from keyway) and the distributions determined using Equations 5-1 and 5-2. It can be seen that the comparisons are very good for all flywheels analyzed, thus providing added assurance of the validity of the finite element results.

5.2 Stresses Due to Shrink-Fit

The flywheels are shrunk-fit onto the RCP pump rotor assemblies to prevent the flywheel from rotating relative to the shaft. Even though it could not be verified that shrink-fit was applied to all the plants considered in this evaluation, the stresses associated with shrink-fit were analyzed for all the flywheels. The physical effect of shrink-fit is to increase the size of the inner bore of the flywheel by a very small amount. This effect was modeled in the ANSYS finite element model developed for the flywheels and described above. A unit displacement of 0.001 inches was applied radially to all nodes on the inner bore to simulate the shrink-fit. The stresses associated with this displacement have been scaled by the actual shrink-fit for the various flywheels. Although actual shrink-fit values were not available for all the flywheels considered in this evaluation, a value of 0.0052 inches was obtained for the flywheel at two of the plants for the small-bore flywheels and was used for these flywheels. Hence, the analysis results for these plants should be scaled by 5.2. A value of 0.0125 inches was reported for one of the larger bore flywheels. This value, even though it was judged to be conservative but was used for the evaluation of these flywheels. Results of this analysis for the larger bore flywheels should be scaled by 12.5 to obtain actual shrink-fit stresses.

The results of the 1 mil shrink-fit analysis are shown in Figures 5-40 through 5-63 for the five flywheels. As before, plots are presented for the tangential and radial stresses for both the overall flywheel stress distributions and for the detailed stress distributions in the keyway region. As can be seen from these figures, especially in the detailed keyway region, both the tangential and radial stresses are tensile in the keyway region.

5.3 Seismic Loads

Because the stresses from the dead weight of the flywheel are very small, the stresses resulting from seismic loads on the flywheel are also small. Furthermore, seismic loads on the RCP motor, RCP pump or the attached piping are not transmitted to the flywheel.

5.4 Vibrational Loads

Flywheels are continuously monitored to limit the amount of vibration. As such, vibrational loads are relatively small and for the purpose of this evaluation will not be considered.

5.5 Key Loading Due to Shaft Torque

Key loading becomes important when the shrink-fit between the flywheel and the shaft is lost. This occurs at relatively high speeds. However, at normal operating speeds and design overspeeds, there is adequate shrink-fit such that key loading is not a concern. This loading scenario will therefore not be considered in this evaluation.

Structural Integrity Associates, Inc.
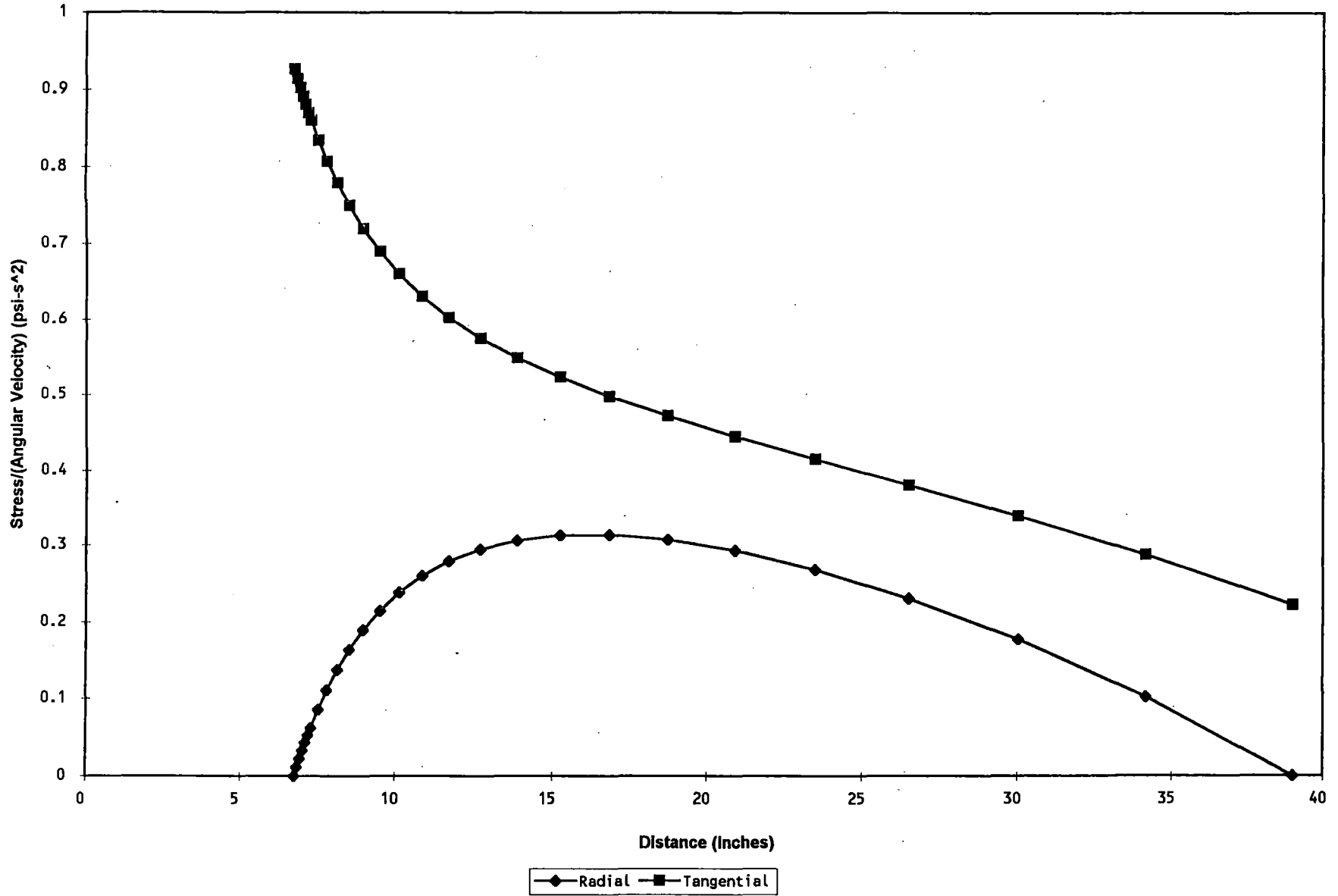
Figure 5-1. Flywheel Stress Distribution Due to Centrifugal Force
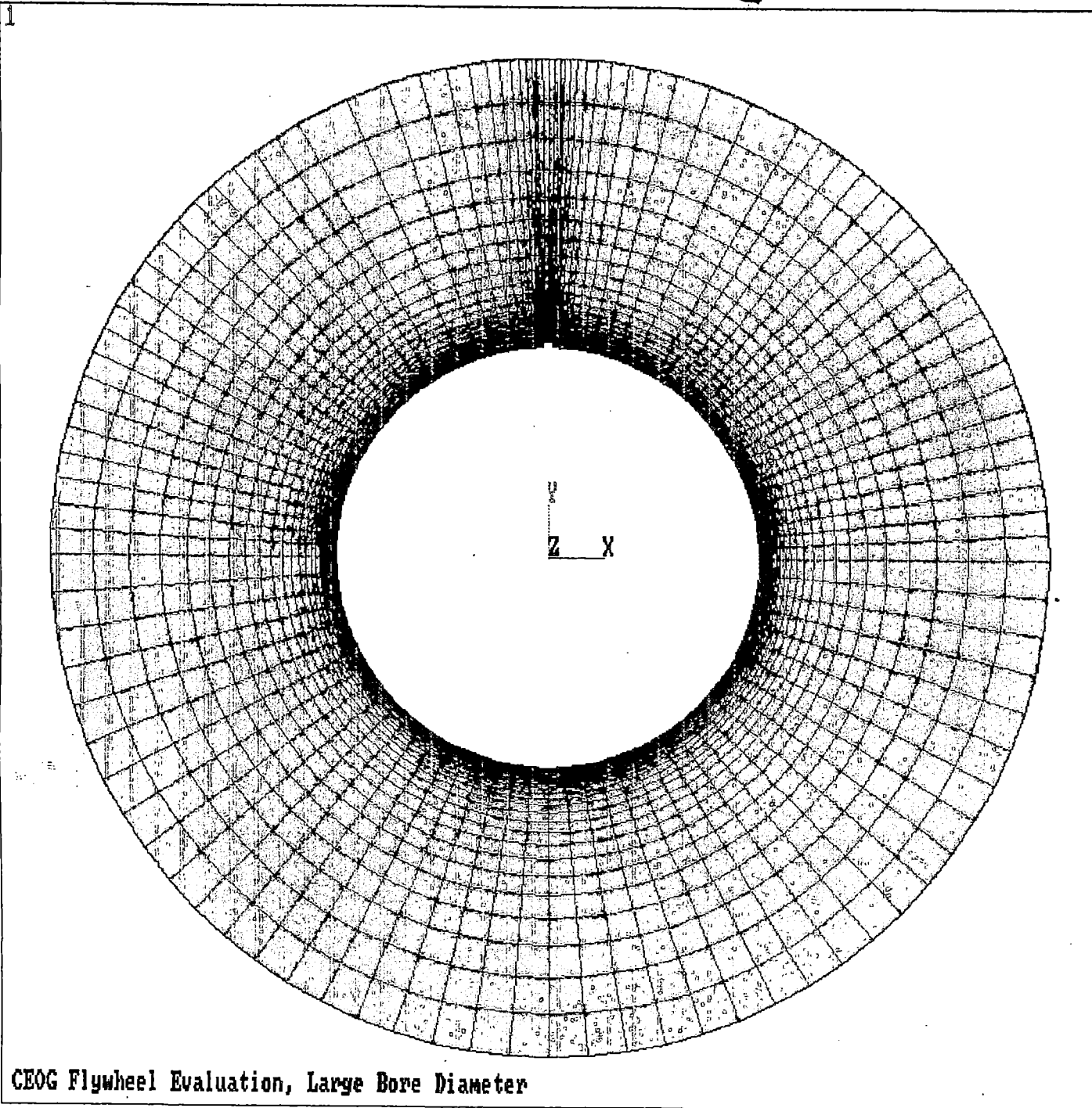
ANSYS-PC 4.4A1
AUG 30 1994
20:21:00
PREP7 ELEMENTS
TYPE NUM

ZV =1
DIST=39.6

Z   X

CEOG Flywheel Evaluation, Large Bore Diameter

Figure 5-2. Finite Element Model for Large Bore Flywheel
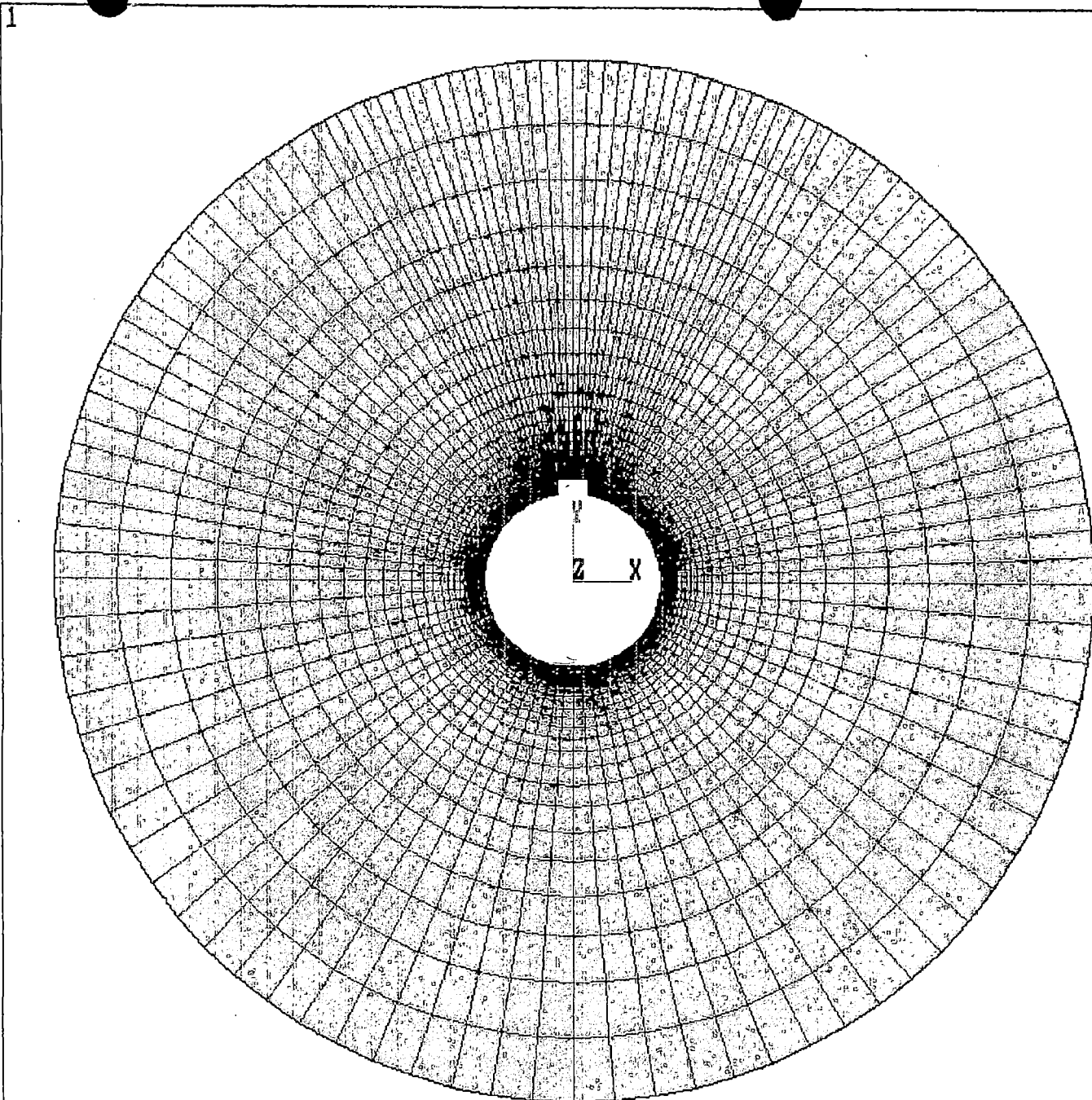
ANSYS-PC 4.4A1
AUG 30 1994
20:27:25
PREP7 ELEMENTS
TYPE NUM

ZV =1
DIST=44.825

CEOG Flywheel Evaluation, Small Bore Diameter

Figure 5-3. Finite Element Model for Small Bore Flywheel
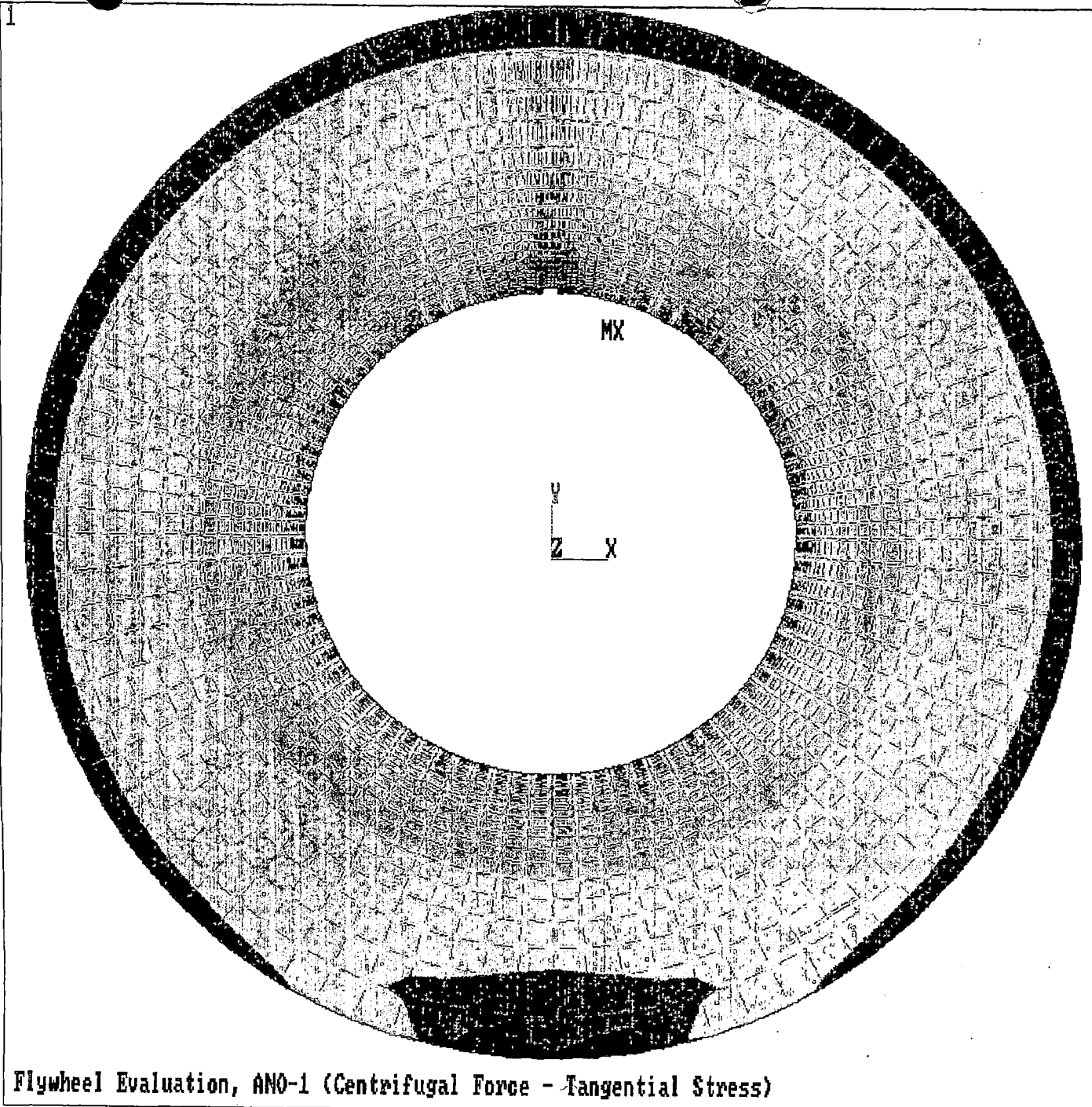
```
ANSYS-PC 4.4A1
OCT 25 1994
 7:24:16
POST1 STRESS
STEP=1
ITER=1
SY   (AVG)
CSYS=1
DMX =0.010646
SMN =-1102
SMNB=-5588
SMX =27396
SMXB=34857

ZV  =1
DIST=39.6
        -1102
         2065
         5231
         8398
        11564
        14731
        17897
        21064
        24230
        27396
```

Flywheel Evaluation, ANO-1 (Centrifugal Force - Tangential Stress)

Figure 5-4. Overall Tangential Stress Distribution Due to Centrifugal Force (ANO-1)
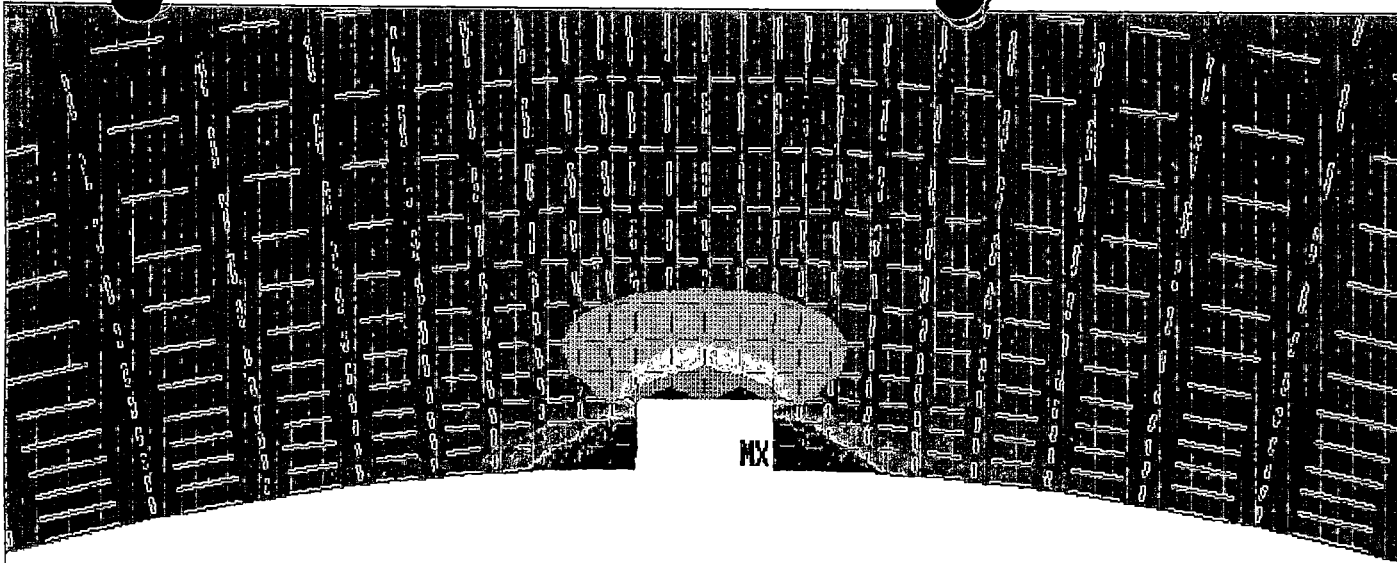
```
ANSYS-PC 4.4A1
OCT 25 1994
 5:56:29
POST1 STRESS
STEP=1
ITER=1
SY    (AVG)
CSYS=1
DMX =0.010646
SMN =-1102
SMNB=-5588
SMX =27396
SMXB=34857

ZV  =1
*DIST=4.023
*XF =0.004251
*YF =14.189
       -1102
        2065
        5231
        8398
        11564
        14731
        17897
        21064
        24230
        27396
```

Flywheel Evaluation, ANO-1 (Centrifugal Force - Tangential Stress)

Figure 5-5. Details of Tangential Stress Distribution in Keyway Region Due to Centrifugal Force (ANO-1)

ANSYS-PC 4.4A1
OCT 25 1994
7:21:38
POST1 STRESS
STEP=1
ITER=1
SX   (AVG)
CSYS=1
DMX =0.010646
SMN =-992.375
SMNB=-7605
SMX =7485
SMXB=14309

ZU =1
DIST=39.6
-992.375
-50.493
891.389
1833
2775
3717
4659
5601
6543
7485

Flywheel Evaluation, ANO-1 (Centrifugal Force - Radial Stress)

Figure 5-6. Overall Radial Stress Distribution Due to Centrifugal Force (ANO-1)

ANSYS-PC 4.4A1
OCT 25 1994
5:48:52
POST1 STRESS
STEP=1
ITER=1
SX   (AVG)
CSYS=1
DMX =0.010646
SMN =-992.375
SMNB=-7605
SMX =7485
SMXB=14309

ZV =1
*DIST=5.588
*XF =0.066362
*YF =14.762
            -992.375
            -50.493
            891.389
            1833
            2775
            3717
            4659
            5601
            6543
            7485

Flywheel Evaluation, ANO-1 (Centrifugal Force - Radial Stress)

Figure 5-7. Details of Radial Stress Distribution in Keyway Region Due to Centrifugal Force (ANO-1)

```
ANSYS-PC 4.4A1
OCT 25 1994
 6:12:39
POST1 STRESS
STEP=1
ITER=1
SY    (AVG)
CSYS=1
DMX =0.004488
SMN =-415.094
SMNB=-4125
SMX =20957
SMXB=26942

ZV   =1
DIST=44.825
        -415.094
        1960
        4334
        6709
        9084
        11458
        13833
        16208
        18582
        20957
```

Flywheel Evaluation, ANO-2 (Centrifugal Force - Tangential Stress)

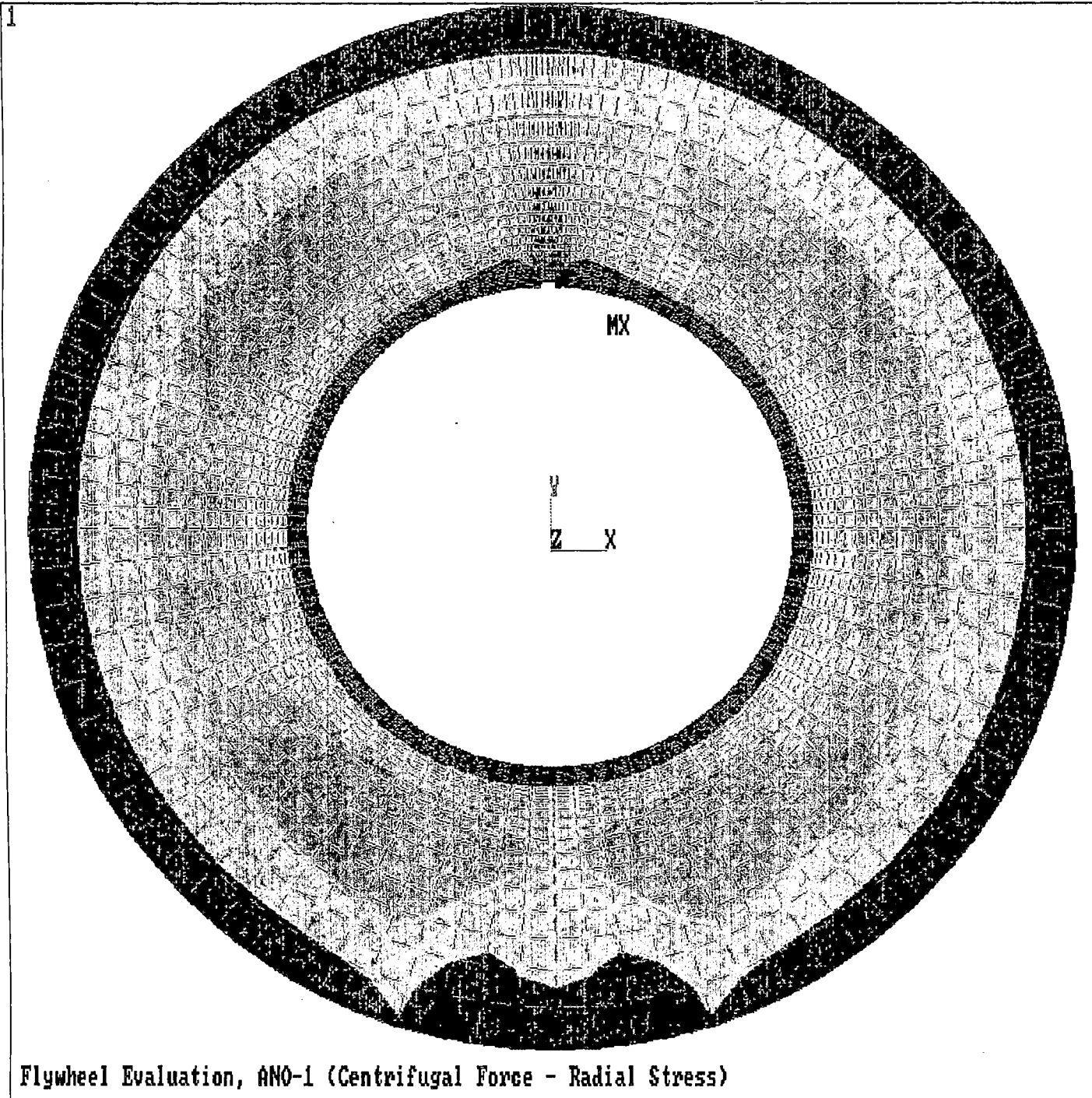Figure 5-8. Overall Tangential Stress Distribution Due to Centrifugal Force (ANO-2)

ANSYS-PC 4.4A1
OCT 25 1994
 7:14:51
POST1 STRESS
STEP=1
ITER=1
SY   (AVG)
CSYS=1
DMX =0.004488
SMN =-415.094
SMNB=-4125
SMX =20957
SMXB=26942

ZV =1
*DIST=5.318
*XF =-0.091287
*YF =6.826
-415.094
1960
4334
6709
9084
11458
13833
16208
18582
20957

MX

MN

Flywheel Evaluation, ANO-2 (Centrifugal Force - Tangential Stress)

Figure 5-9. Details of Tangential Stress Distribution in Keyway Region Due to Centrifugal Force (ANO-2)

```
                                          ANSYS-PC 4.4A1
                                          OCT 25 1994
                                           6:00:53
                                          POST1 STRESS
                                          STEP=1
                                          ITER=1
                                          SX   (AVG)
                                          CSYS=1
                                          DMX =0.004488
                                          SMN =-611.222
                                          SMNB=-5784
                                          SMX =8321
                                          SMXB=13801

                                          ZV  =1
                                          DIST=44.825
                                               -611.222
                                               381.206
                                               1374
                                               2366
                                               3358
                                               4351
                                               5343
                                               6336
                                               7328
                                               8321
```
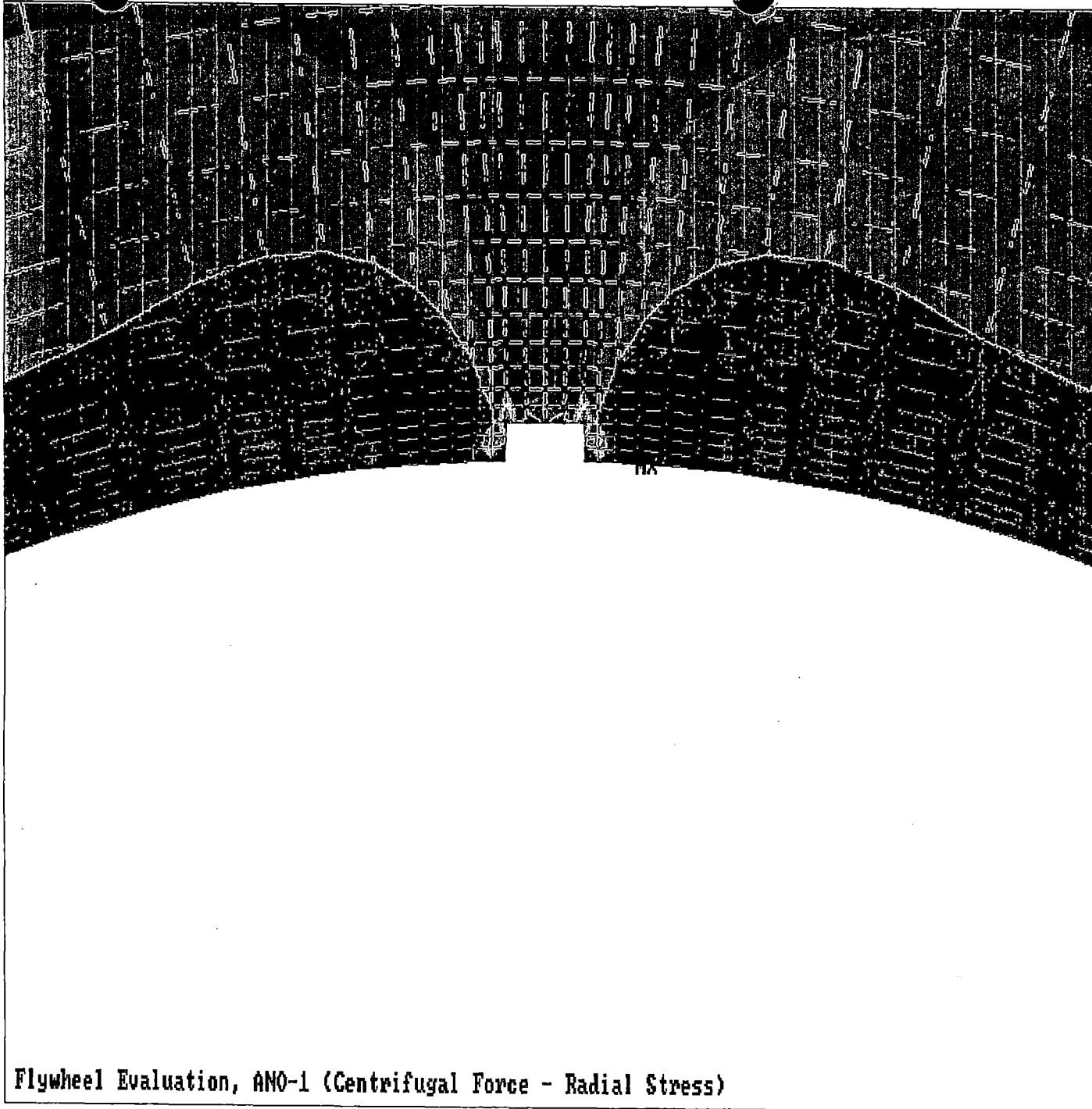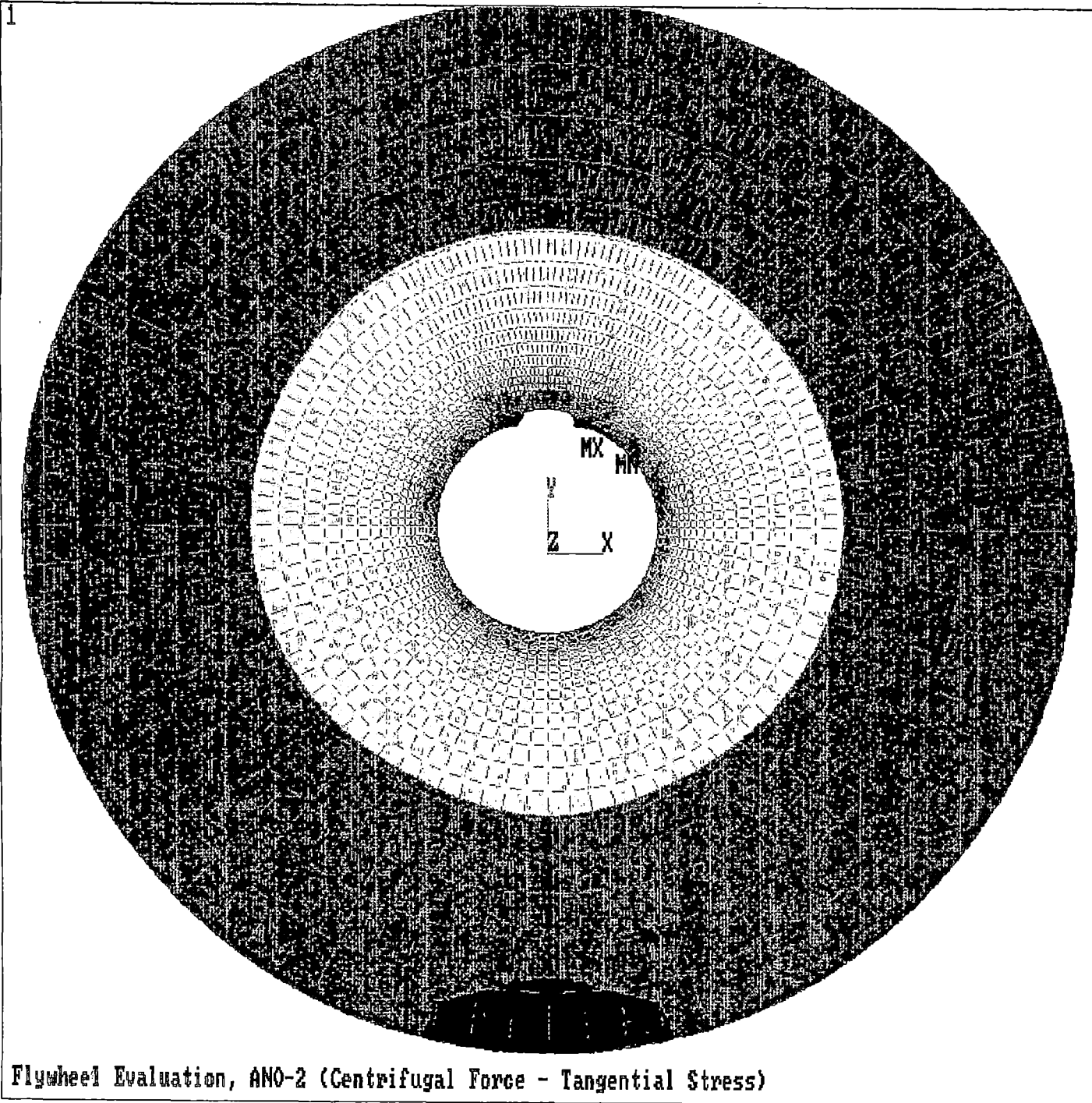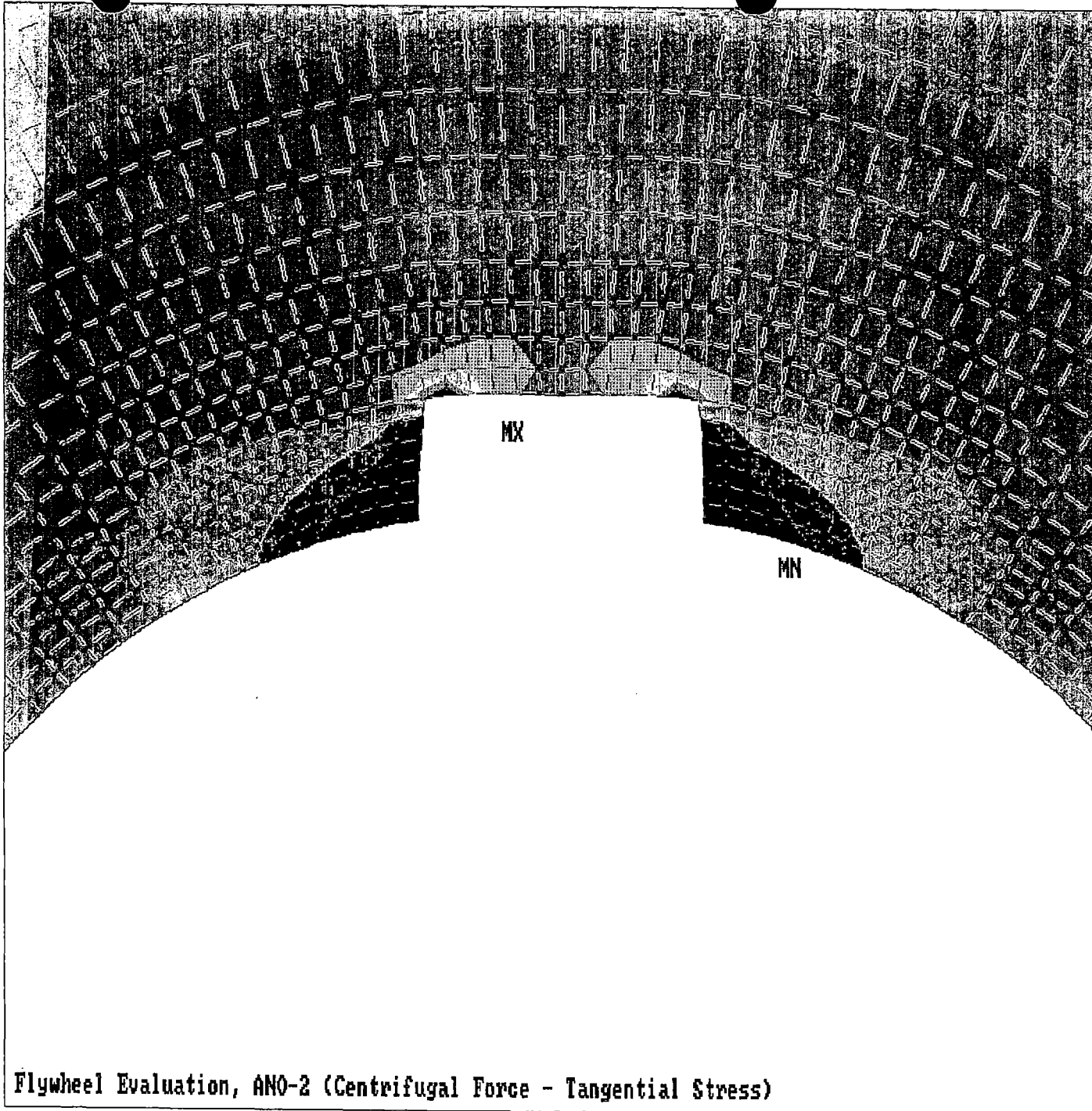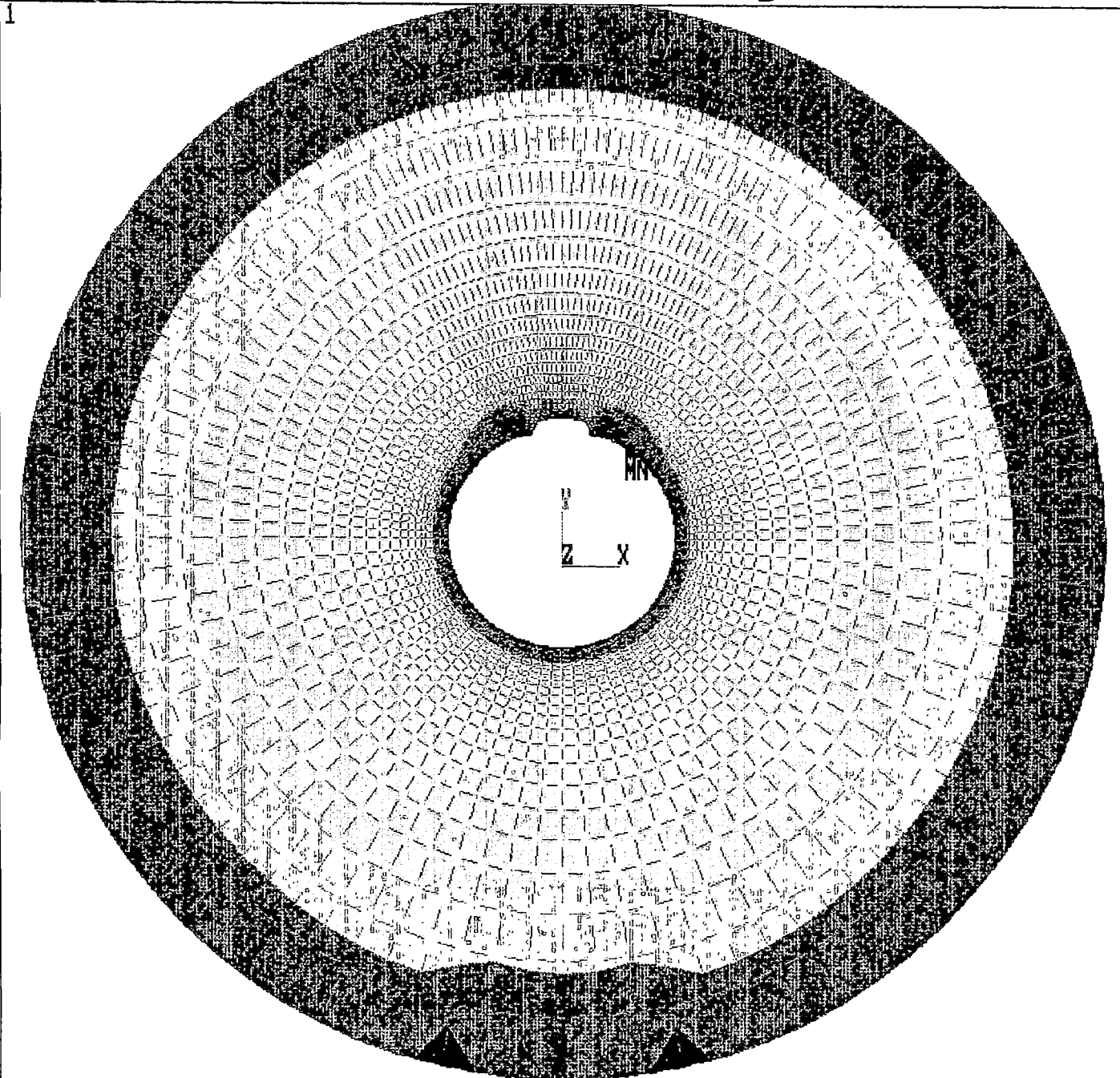
Flywheel Evaluation, ANO-2 (Centrifugal Force - Radial Stress)

Figure 5-10. Overall Radial Stress Distribution Due to Centrifugal Force (ANO-2)
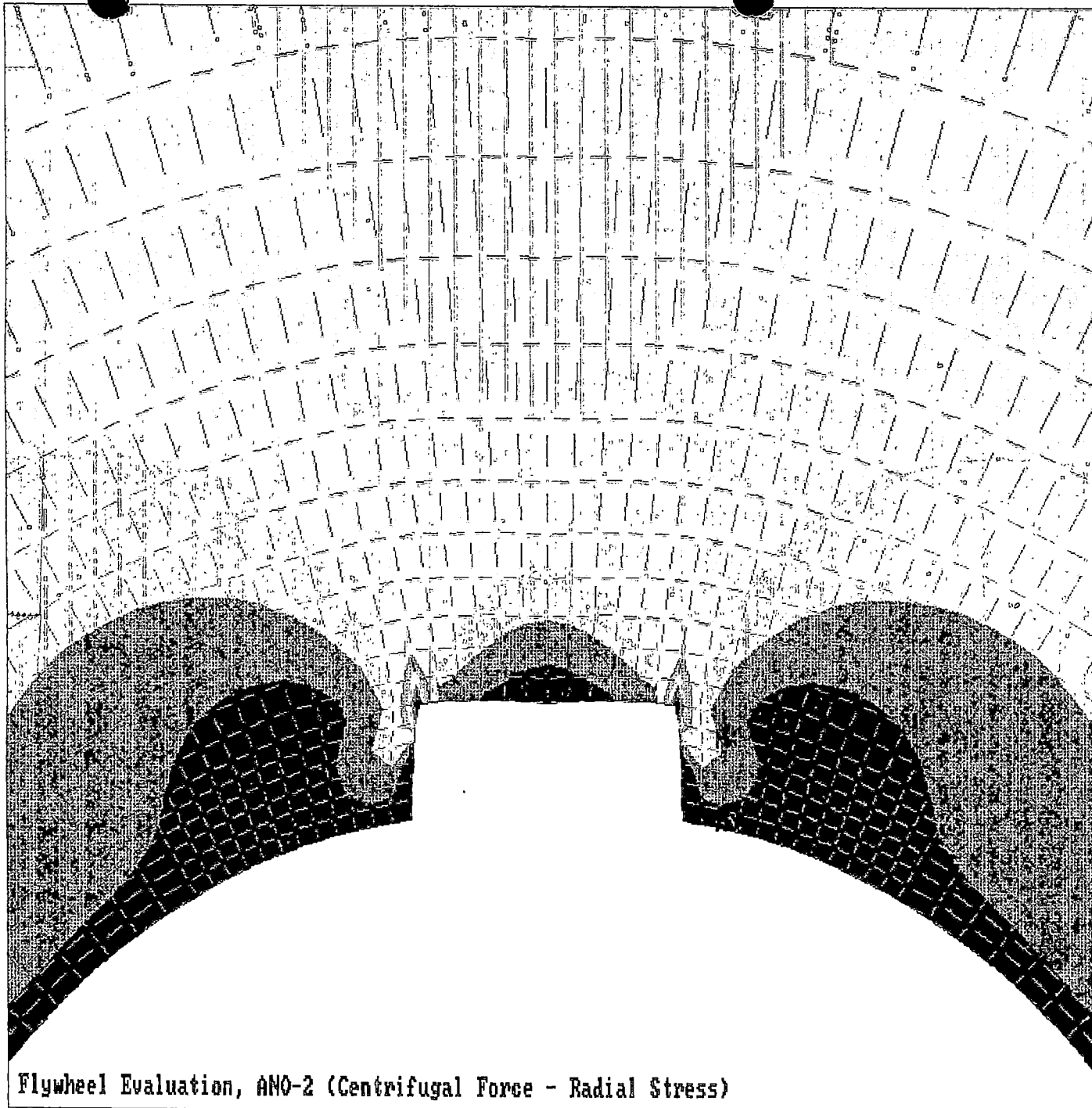
```
ANSYS-PC 4.4A1
OCT 25 1994
 6:07:12
POST1 STRESS
STEP=1
ITER=1
SX    (AVG)
CSYS=1
DMX =0.004488
SMN =-611.222
SMNB=-5784
SMX =8321
SMXB=13801

ZV  =1
*DIST=5.657
*XF =0.074057
*YF =9.925
      -611.222
      381.206
      1374
      2366
      3358
      4351
      5343
      6336
      7328
      8321
```

Flywheel Evaluation, ANO-2 (Centrifugal Force - Radial Stress)

Figure 5-11. Details of Radial Stress Distribution in Keyway Region Due to Centrifugal Force (ANO-2)

```
ANSYS-PC 4.4A1
OCT 25 1994
10:20:40
POST1 STRESS
STEP=1
ITER=1
SY   (AVG)
CSYS=1
DMX =0.00353
SMN =-352.992
SMNB=-3481
SMX =17939
SMXB=23369

ZV  =1
DIST=41.25
        -352.992
        1679
        3712
        5744
        7777
        9809
        11842
        13874
        15907
        17939
```

Flywheel Evaluation, Millstone (Centrifugal Force - Tangential Stress)

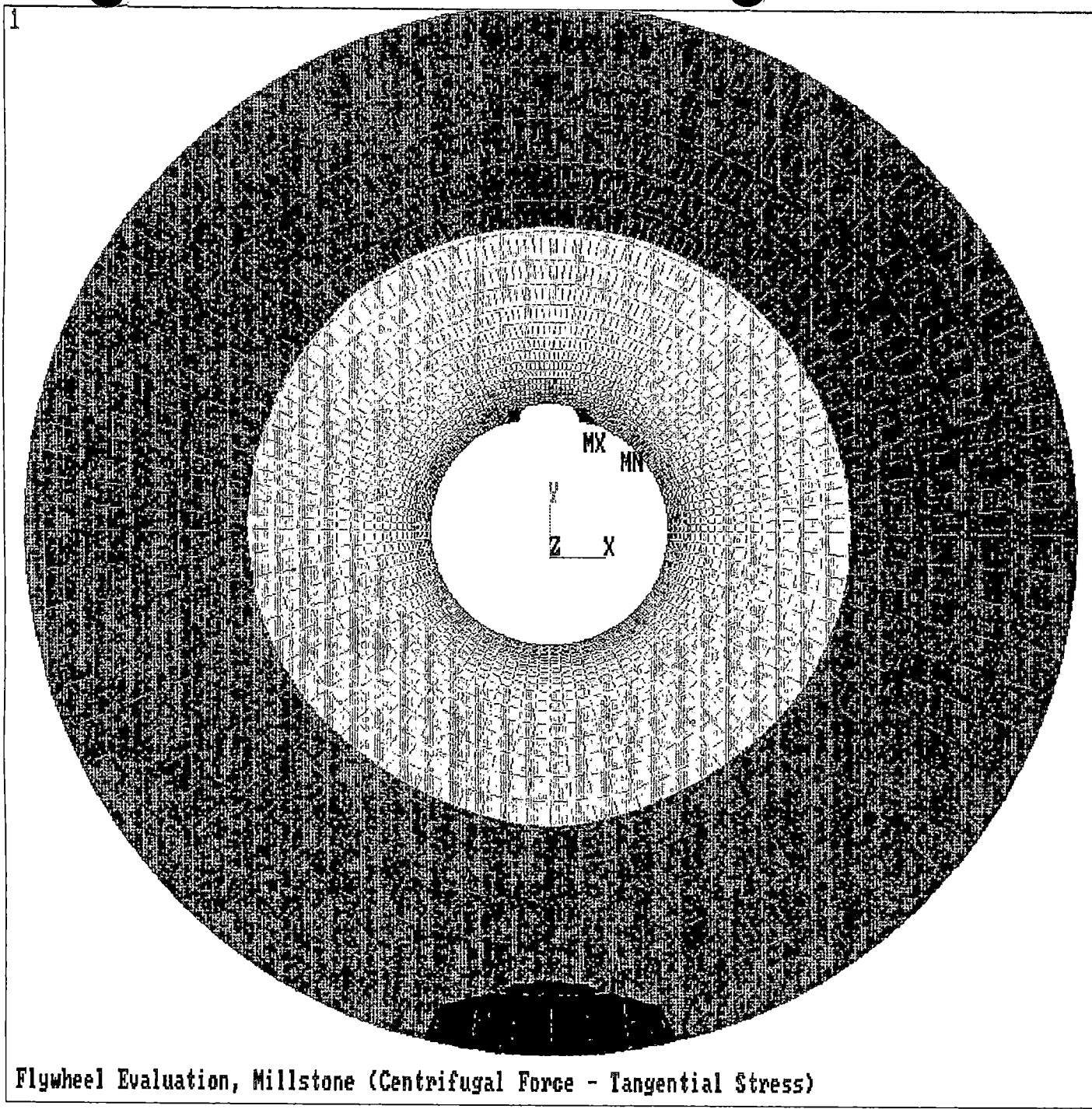Figure 5-12. Overall Tangential Stress Distribution Due to Centrifugal Force (Millstone-2)

```
ANSYS-PC 4.4A1
OCT 25 1994
10:15:00
POST1 STRESS
STEP=1
ITER=1
SY   (AVG)
CSYS=1
DMX =0.00353
SMN =-352.992
SMNB=-3481
SMX =17939
SMXB=23369

ZV   =1
*DIST=5.583
*XF  =0.109989
*YF  =6.025
        -352.992
        1679
        3712
        5744
        7777
        9809
        11842
        13874
        15907
        17939
```

MX

MN

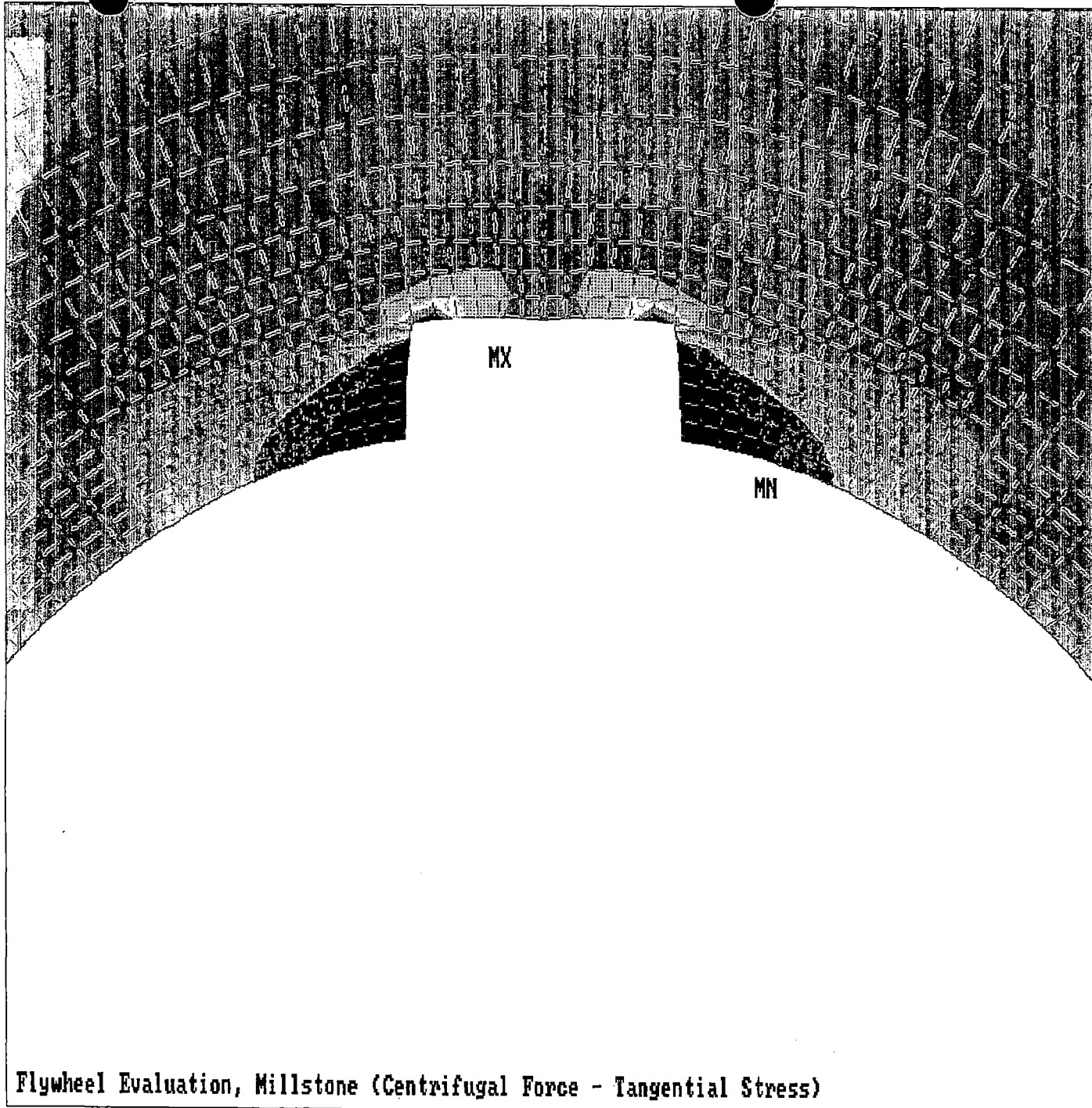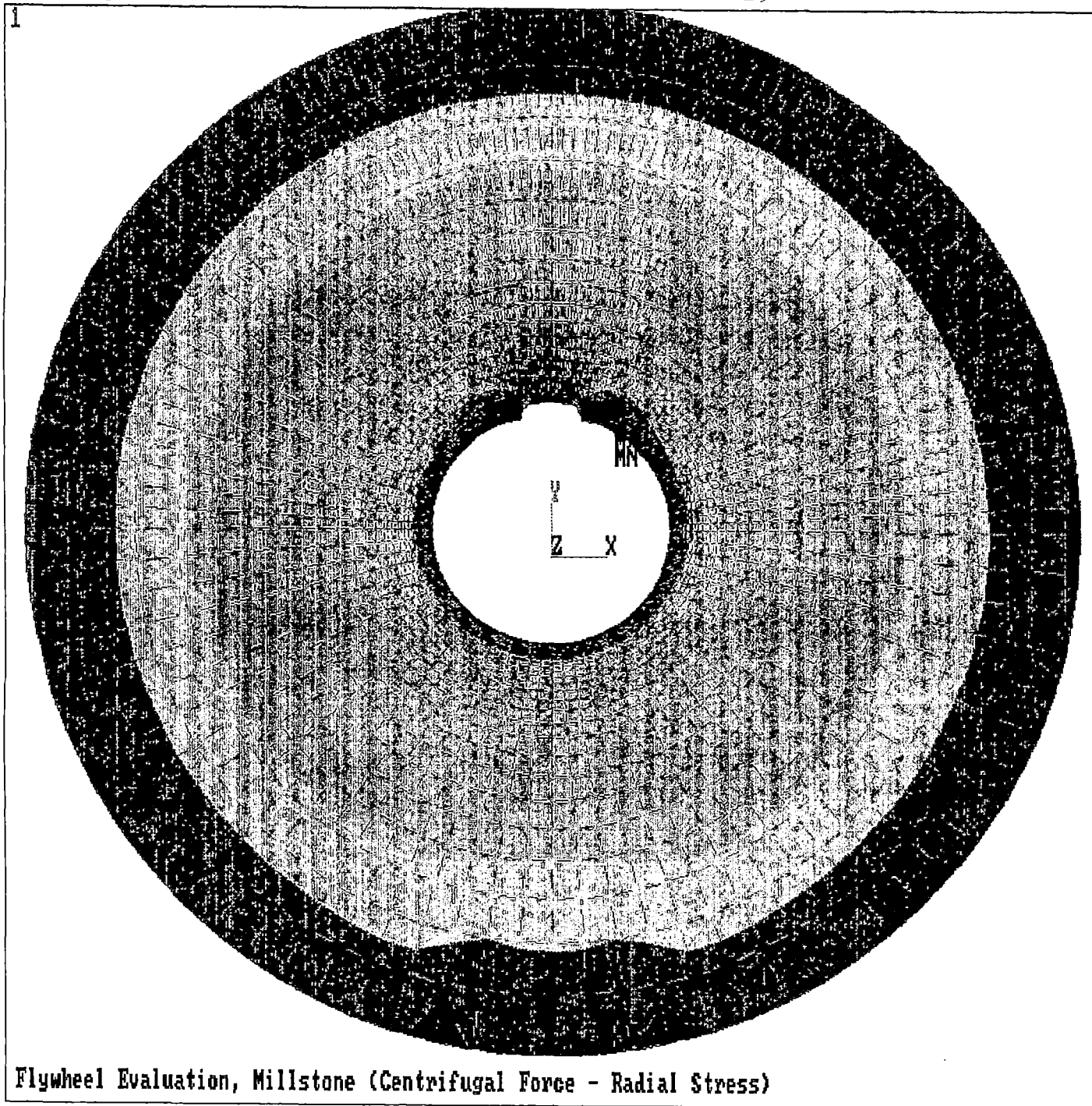Flywheel Evaluation, Millstone (Centrifugal Force – Tangential Stress)

Figure 5-13. Details of Tangential Stress Distribution in Keyway Region Due to Centrifugal Force (Millstone-2)

```
ANSYS-PC 4.4A1
OCT 25 1994
 9:48:31
POST1 STRESS
STEP=1
ITER=1
SX   (AVG)
CSYS=1
DMX =0.00353
SMN =-521.061
SMNB=-5386
SMX =7105
SMXB=11964

ZU  =1
DIST=41.25
      -521.061
       326.309
       1174
       2021
       2868
       3716
       4563
       5411
       6258
       7105
```

Flywheel Evaluation, Millstone (Centrifugal Force - Radial Stress)

Figure 5-14. Overall Radial Stress Distribution Due to Centrifugal Force (Millstone-2)
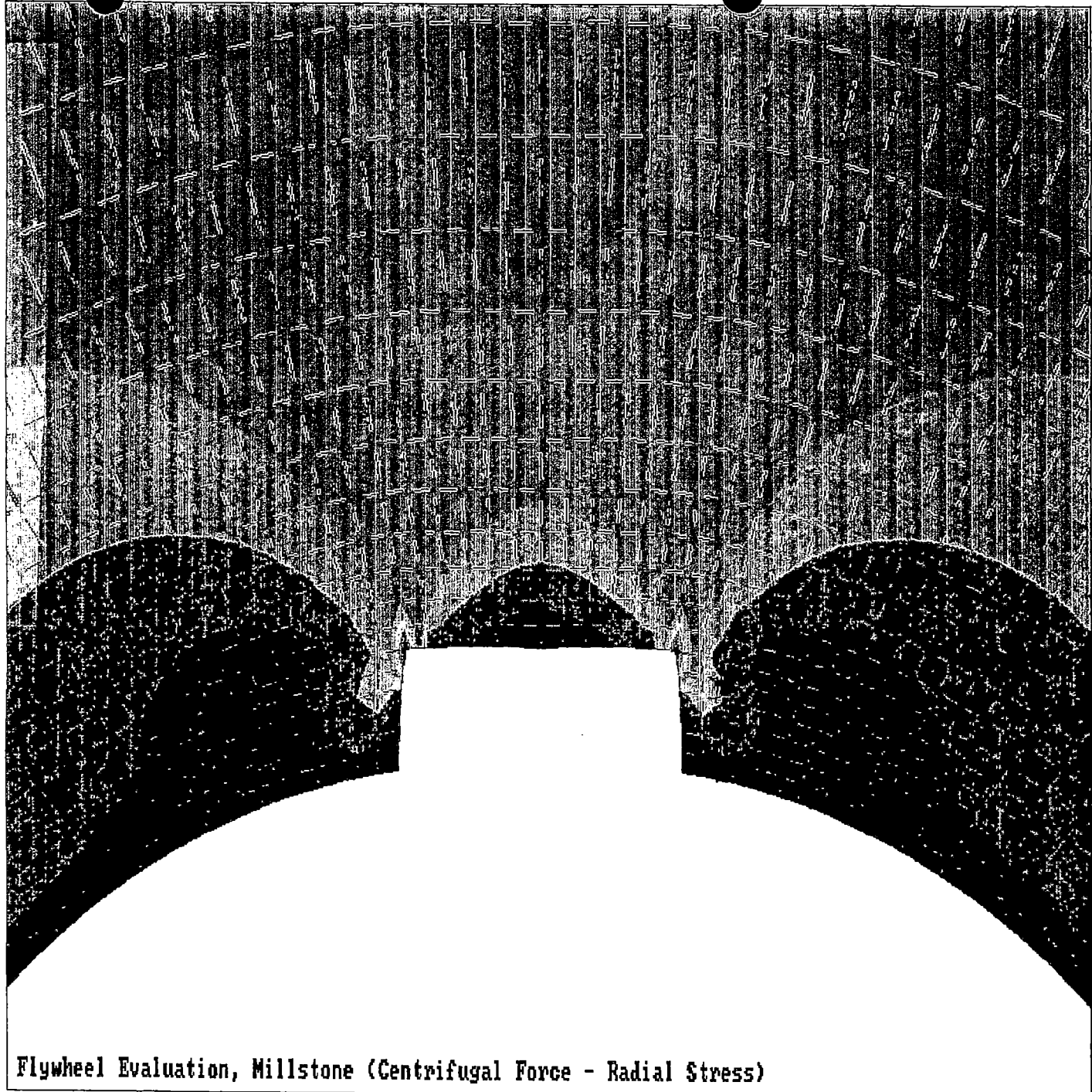
```
ANSYS-PC 4.4A1
OCT 25 1994
10:10:05
POST1 STRESS
STEP=1
ITER=1
SX    (AVG)
CSYS=1
DMX =0.00353
SMN =-521.061
SMNB=-5386
SMX =7105
SMXB=11964

ZV  =1
*DIST=5.343
*XF =0.068151
*YF =9.407
      -521.061
       326.309
       1174
       2021
       2868
       3716
       4563
       5411
       6258
       7105
```

Flywheel Evaluation, Millstone (Centrifugal Force - Radial Stress)

Figure 5-15. Details of Radial Stress Distribution in Keyway Region Due to Centrifugal Force (Millstone-2)

Figure 5-16. Overall Tangential Stress Distribution Due to Centrifugal Force (Palisades)

```
ANSYS-PC 4.4A1
OCT 25 1994
 8:56:30
POST1 STRESS
STEP=1
ITER=1
SY    (AVG)
CSYS=1
DMX =0.006364
SMN =-707.277
SMNB=-3492
SMX =15318
SMXB=19036

ZU  =1
*DIST=2.445
*XF  =0.011034
*YF  =16.127
     -707.277
      1073
      2854
      4634
      6415
      8196
      9976
      11757
      13537
      15318
```

Flywheel Evaluation, Palisades (Centrifugal Force - Tangential Stress)

Figure 5-17. Details of Tangential Stress Distribution in Keyway Region Due to Centrifugal Force (Palisades)

ANSYS-PC 4.4A1
OCT 25 1994
8:47:15
POST1 STRESS
STEP=1
ITER=1
SX   (AVG)
CSYS=1
DMX =0.006364
SMN =-645.235
SMNB=-4328
SMX =3551
SMXB=7019

ZV =1
DIST=39.6
   -645.235
   -178.946
   287.344
   753.633
   1220
   1686
   2153
   2619
   3085
   3551

Flywheel Evaluation, Palisades (Centrifugal Force - Radial Stress)

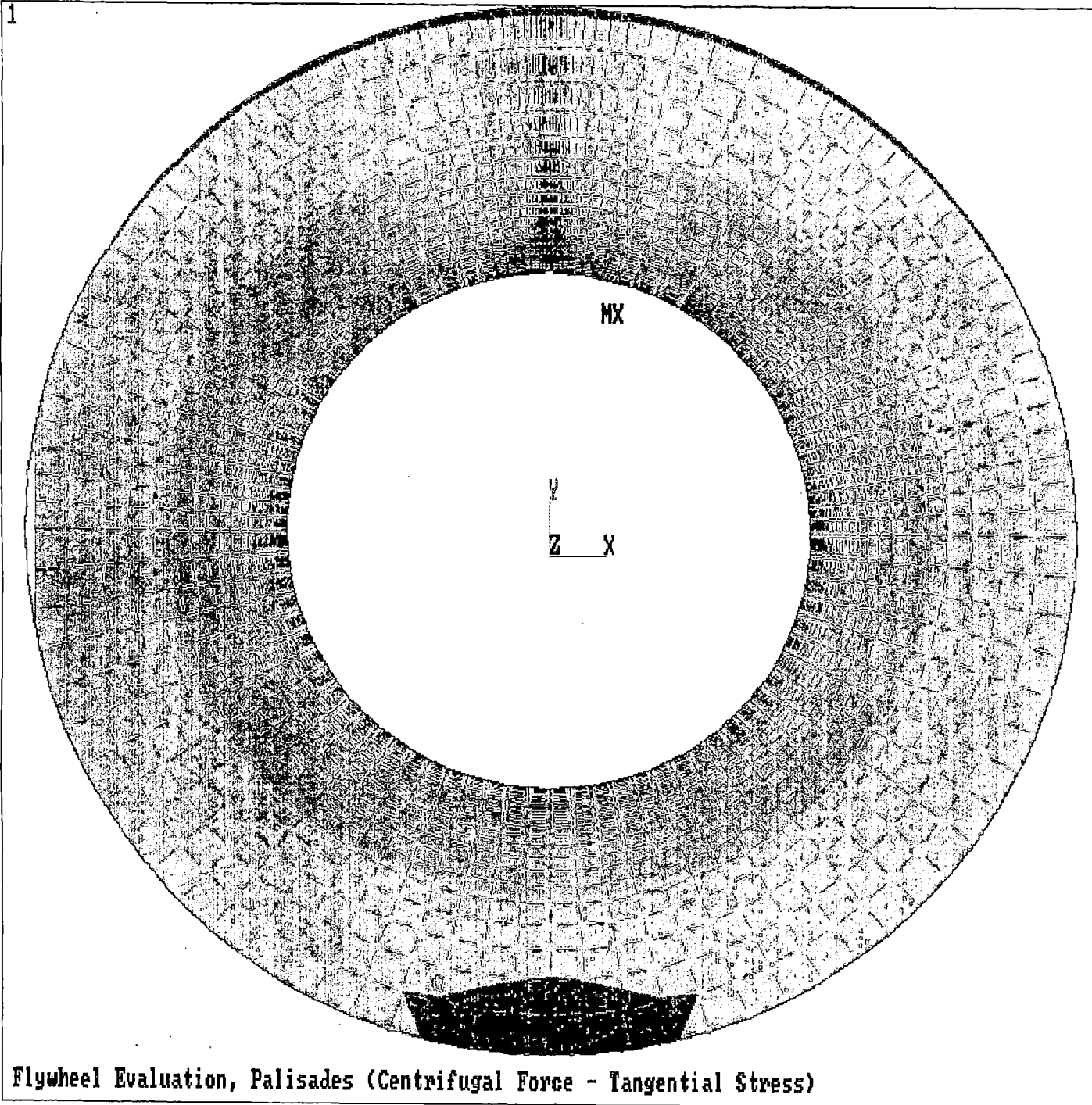Figure 5-18. Overall Radial Stress Distribution Due to Centrifugal Force (Palisades)

ANSYS-PC 4.4A1
OCT 25 1994
 9:04:41
POST1 STRESS
STEP=1
ITER=1
SX   (AVG)
CSYS=1
DMX =0.006364
SMN =-645.235
SMNB=-4328
SMX =3551
SMXB=7019

ZV =1
*DIST=4.604
*XF =-0.066263
*YF =17.843
-645.235
-178.946
287.344
753.633
1220
1686
2153
2619
3085
3551

MX

Flywheel Evaluation, Palisades (Centrifugal Force - Radial Stress)

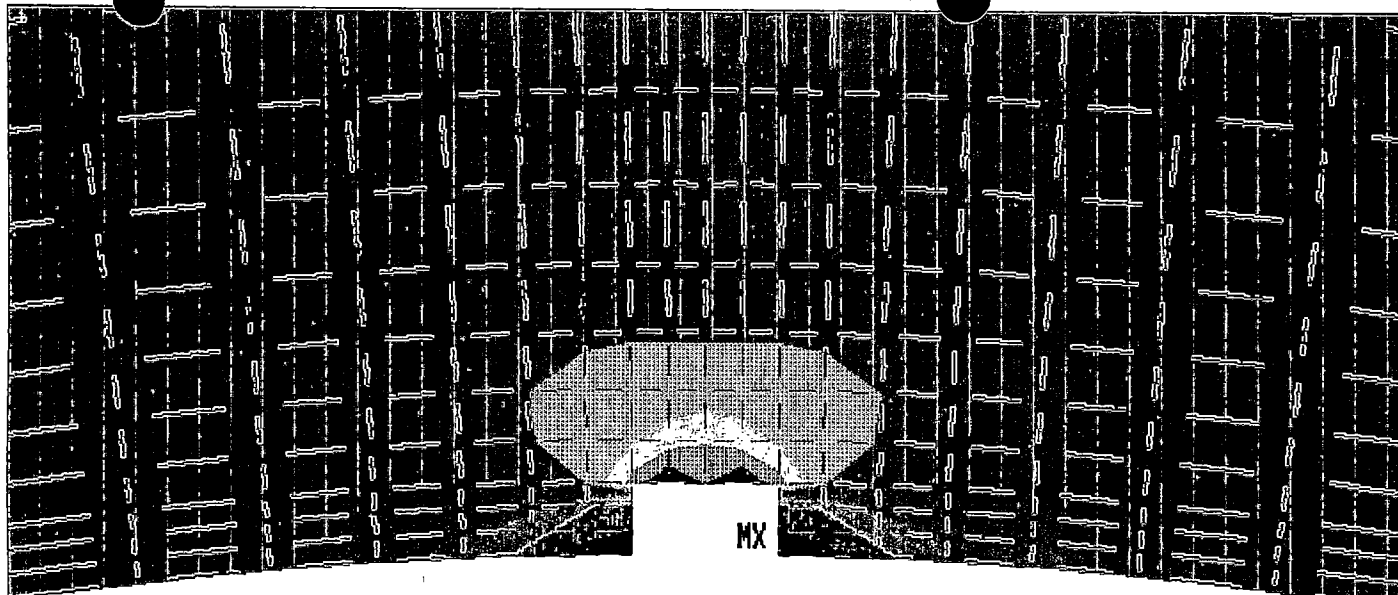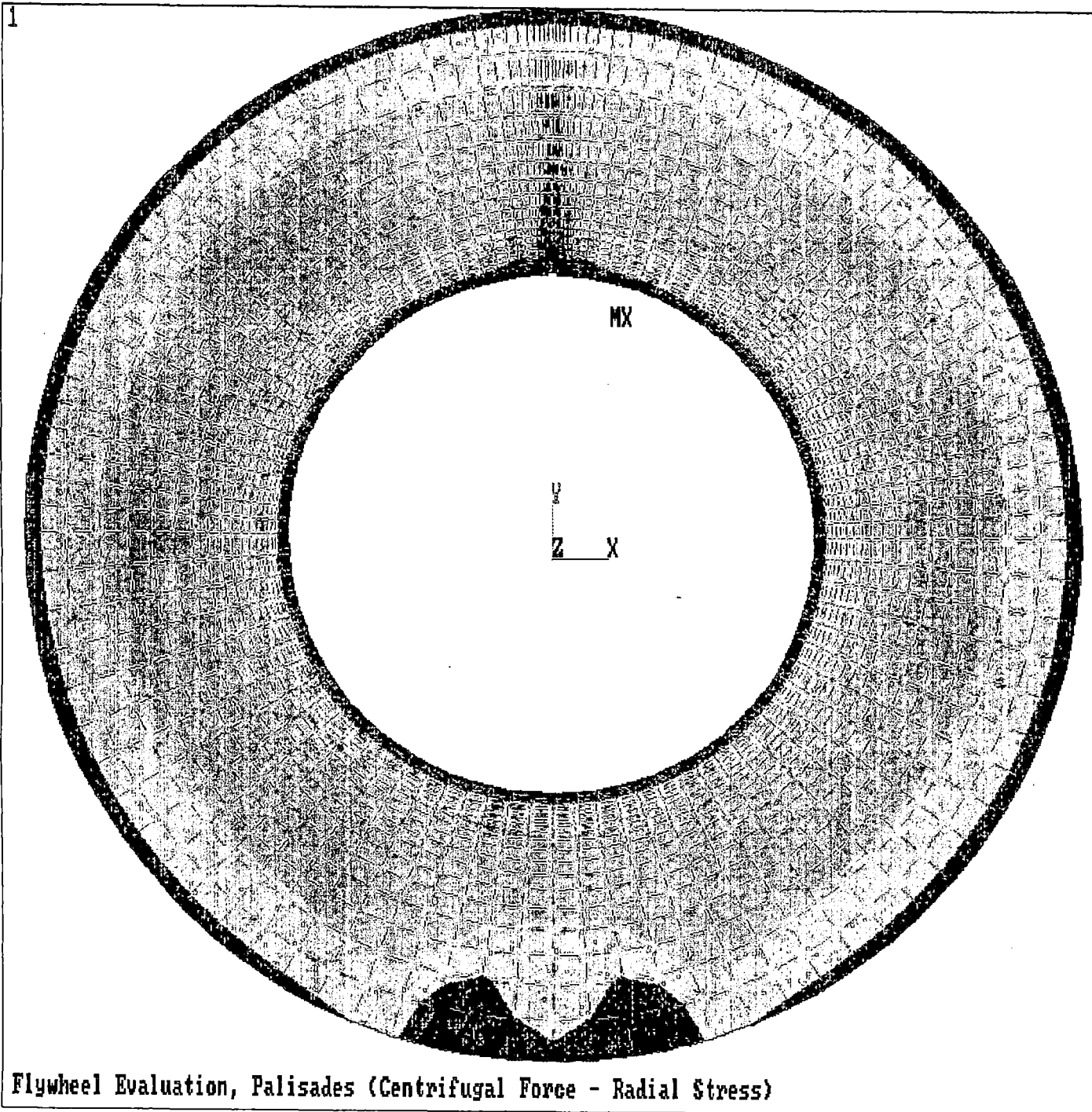Figure 5-19. Details of Radial Stress Distribution in Keyway Region Due to Centrifugal Force (Palisades)

```
ANSYS-PC 4.4A1
JAN 10 1995
10:40:59
POST1 STRESS
STEP=1
ITER=1
SY   (AVG)
CSYS=1
DMX =0.18204
SMN =-696.473
SMNB=-3886
SMX =15362
SMXB=20159

ZV  =1
DIST=39.6
      -696.473
      1088
      2872
      4656
      6441
      8225
      10009
      11794
      13578
      15362
```

CEOG Flywheel Evaluation, St. Lucie (Centrifugal Force)

Figure 5-20. Overall Tangential Stress Distribution Due to Centrifugal Force (St. Lucie)

```
ANSYS-PC 4.4A1
JAN 10 1995
10:52:31
POST1 STRESS
STEP=1
ITER=1
SY    (AVG)
CSYS=1
DMX =0.18204
SMN =-696.473
SMNB=-3886
SMX =15362
SMXB=20159

ZV  =1
*DIST=10.043
*XF  =0.017783
*YF  =13.665
     -696.473
      1088
      2872
      4656
      6441
      8225
      10009
      11794
      13578
      15362
```

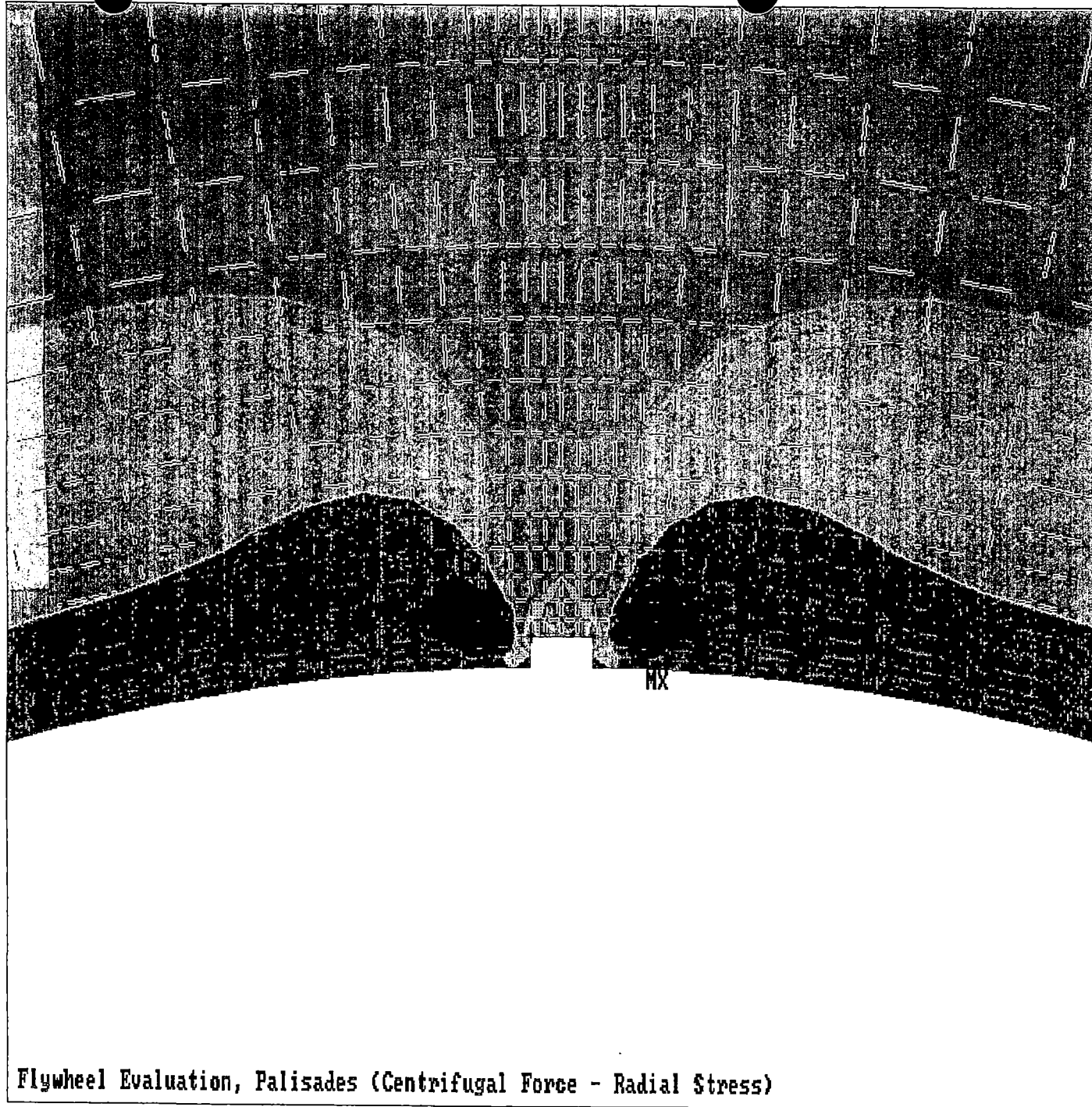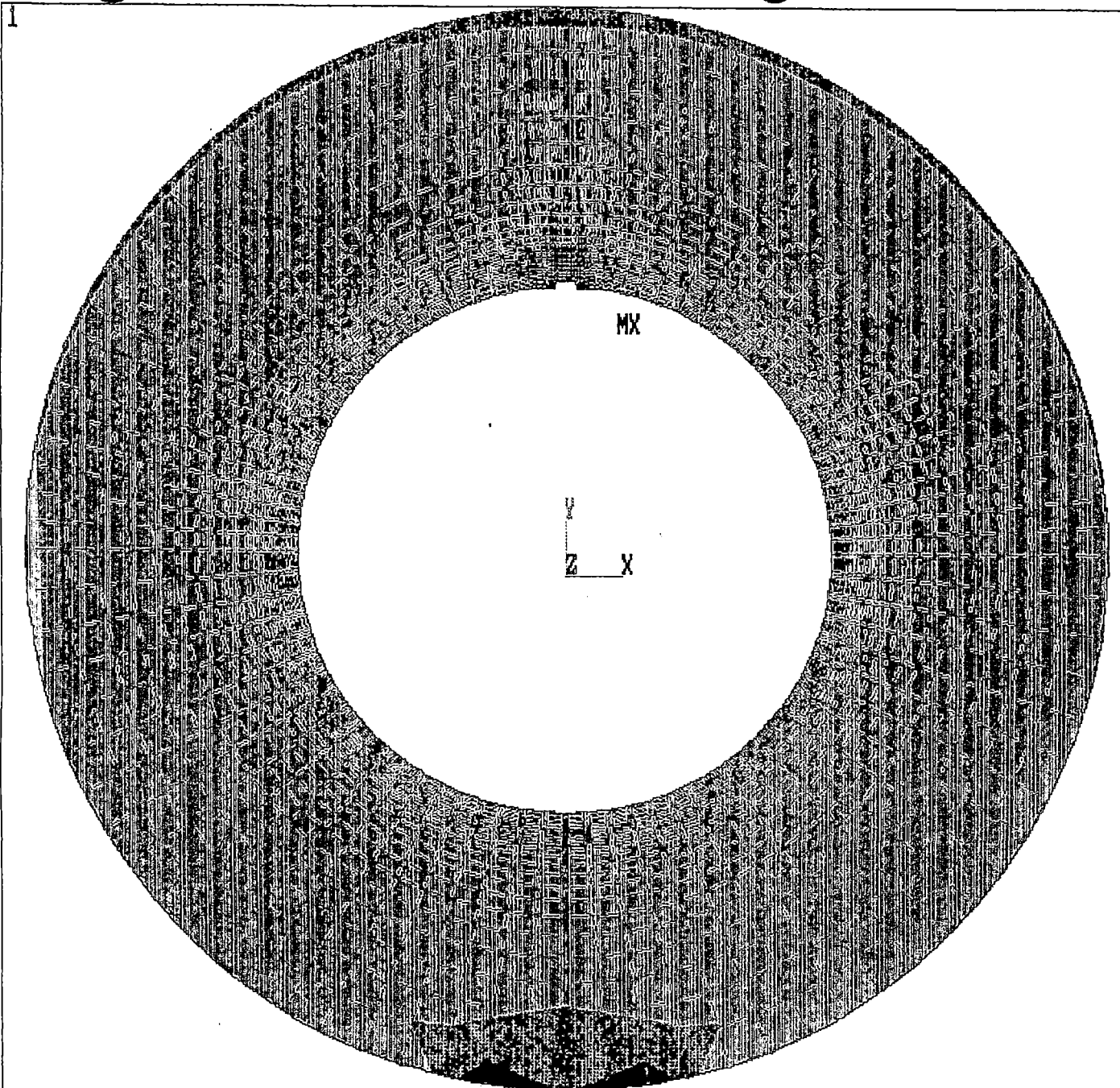CEOG Flywheel Evaluation, St. Lucie (Centrifugal Force)

Figure 5-21. Details of Tangential Stress Distribution in Keyway Region Due to Centrifugal Force (St. Lucie)

```
ANSYS-PC 4.4A1
JAN 10 1995
10:27:57
POST1 STRESS
STEP=1
ITER=1
SX   (AVG)
CSYS=1
DMX =0.18204
SMN =-680.318
SMNB=-5109
SMX =4395
SMXB=8627

ZV  =1
DIST=39.6
        -680.318
        -116.367
        447.584
        1012
        1575
        2139
        2703
        3267
        3831
        4395
```

CEOG Flywheel Evaluation, St. Lucie (Centrifugal Force)

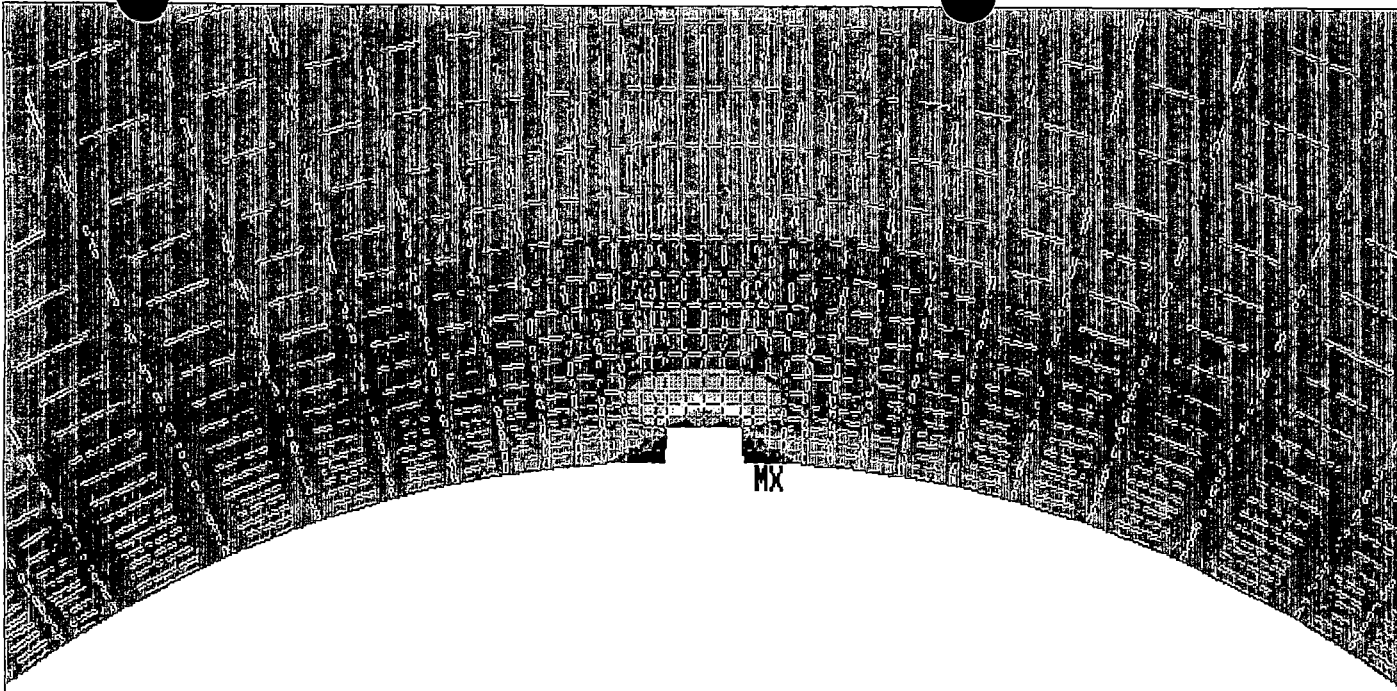Figure 5-22. Overall Radial Stress Distribution Due to Centrifugal Force (St. Lucie)

```
ANSYS-PC 4.4A1
JAN 10 1995
10:48:46
POST1 STRESS
STEP=1
ITER=1
SX    (AVG)
CSYS=1
DMX =0.18204
SMN =-680.318
SMNB=-5110
SMX =4395
SMXB=8655

ZV   =1
*DIST=10.043
*XF  =0.017783
*YF  =13.665
      -680.318
      -116.367
      447.584
      1012
      1575
      2139
      2703
      3267
      3831
      4395
```
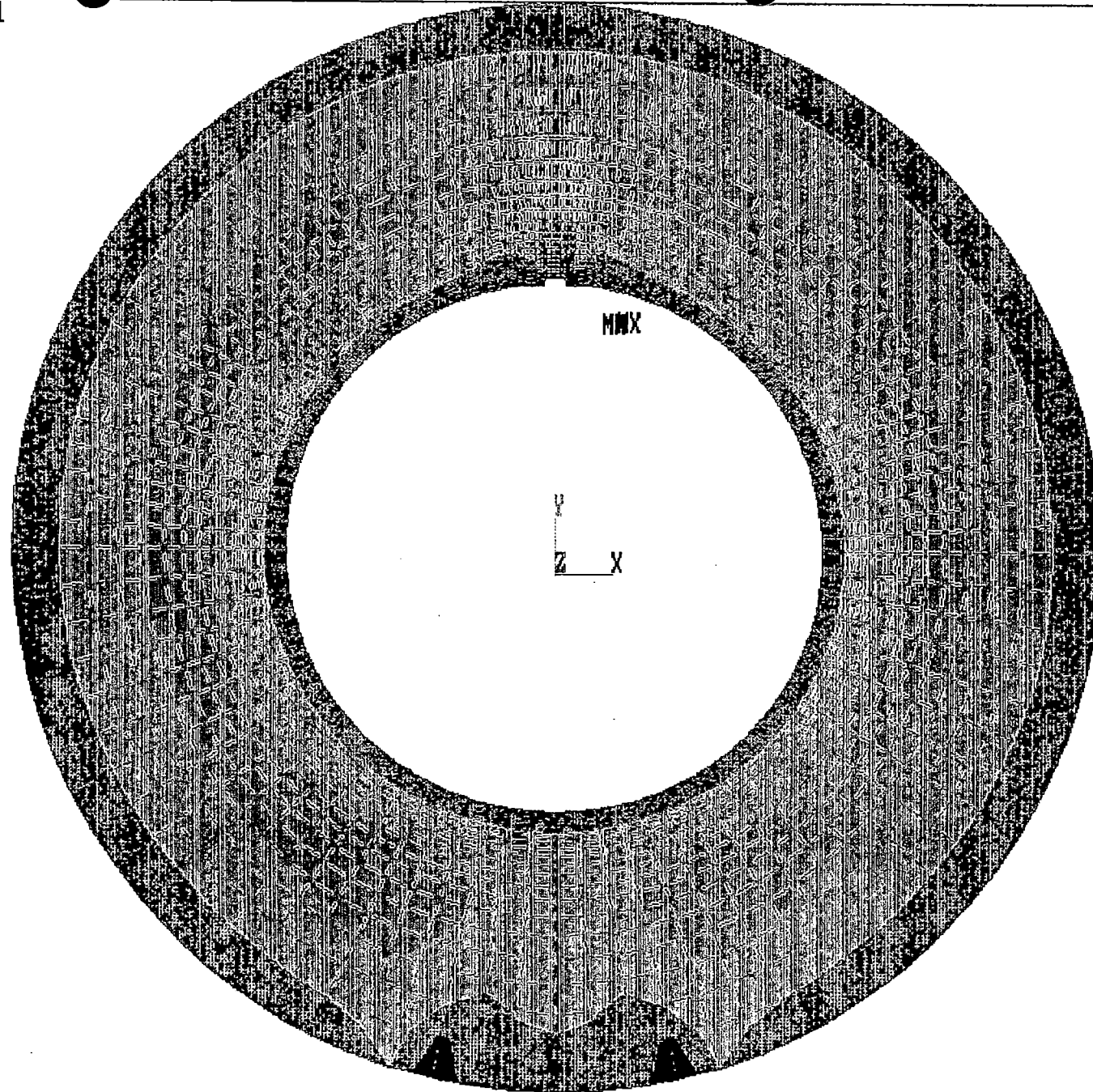
MN   MX

CEOG Flywheel Evaluation, St. Lucie (Centrifugal Force)

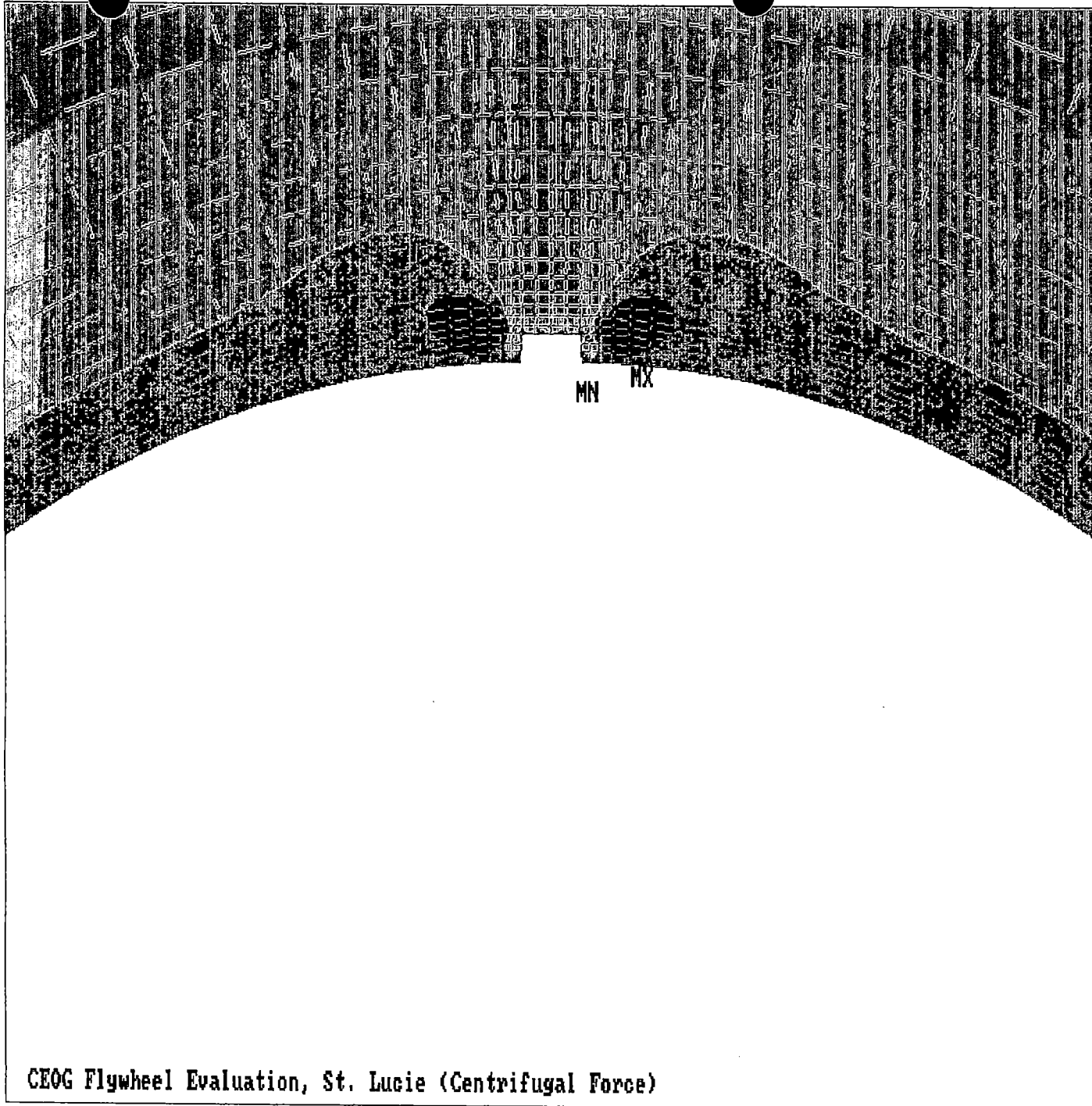Figure 5-23. Details of Radial Stress Distribution in Keyway Region Due to Centrifugal Force (St. Lucie)

Figure 5-24. Overall Tangential Stress Distribution Due to Centrifugal Force (Waterford-3)

```
ANSYS-PC 4.4A1
OCT 25 1994
 5:22:45
POST1 STRESS
STEP=1
ITER=1
SY    (AVG)
CSYS=1
DMX =0.00696
SMN =-784.598
SMNB=-2945
SMX =35256
SMXB=43791

ZV   =1
*DIST=4.378
*XF  =0.097076
*YF  =6.328
     -784.598
      3220
      7224
      11229
      15234
      19238
      23243
      27247
      31252
      35256
```

Flywheel Evaluation, Waterford (Centrifugal Force - Tangential Stress)

Figure 5-25. Details of Tangential Stress Distribution in Keyway Region Due to Centrifugal Force (Waterford-3)
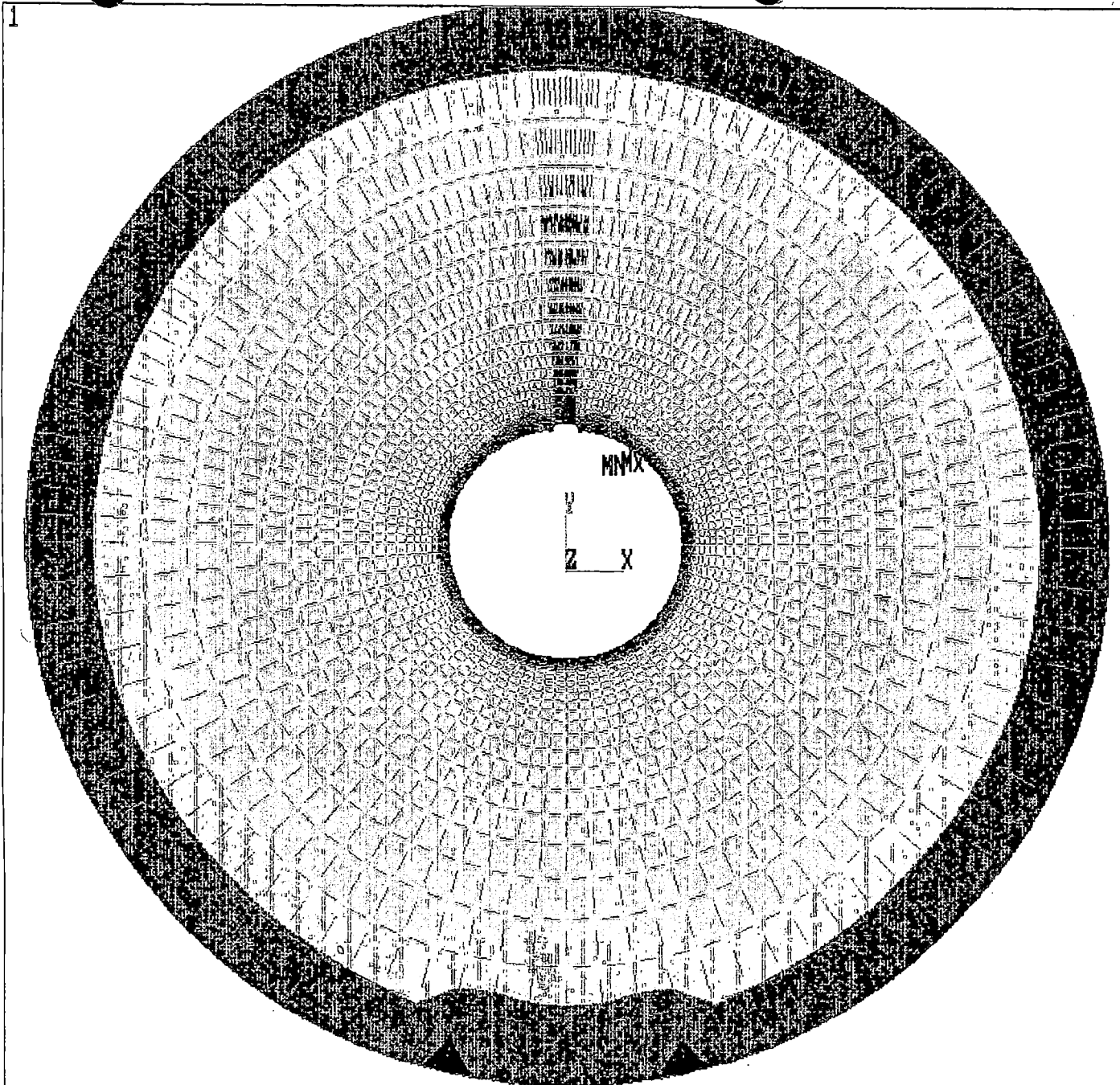
```
ANSYS-PC 4.4A1
OCT 25 1994
 5:10:37
POST1 STRESS
STEP=1
ITER=1
SX   (AVG)
CSYS=1
DMX =0.00696
SMN =-709.59
SMNB=-6255
SMX =10173
SMXB=18452

ZV  =1
DIST=42.9
        -709.59
        499.56
        1709
        2918
        4127
        5336
        6545
        7754
        8964
        10173
```

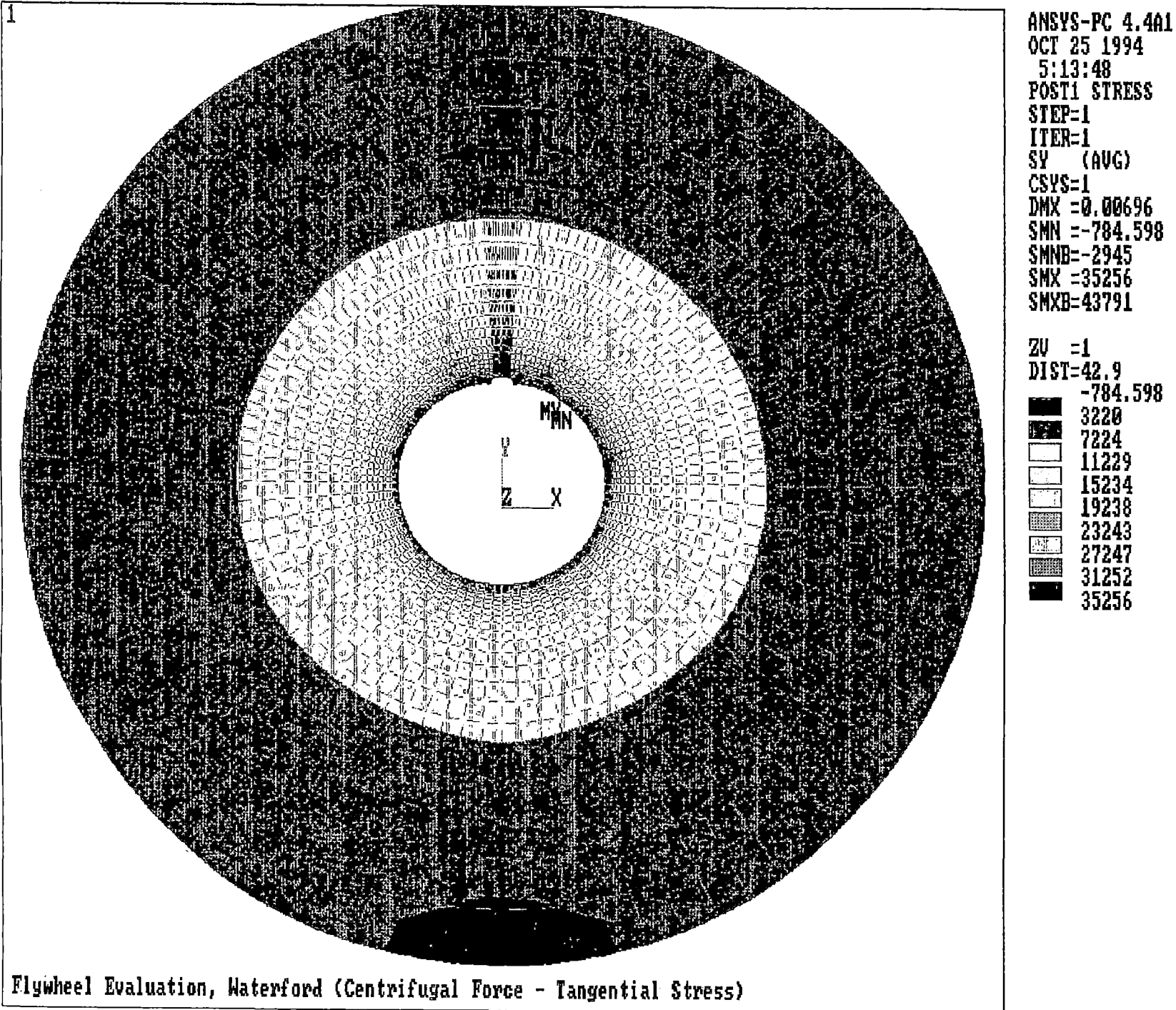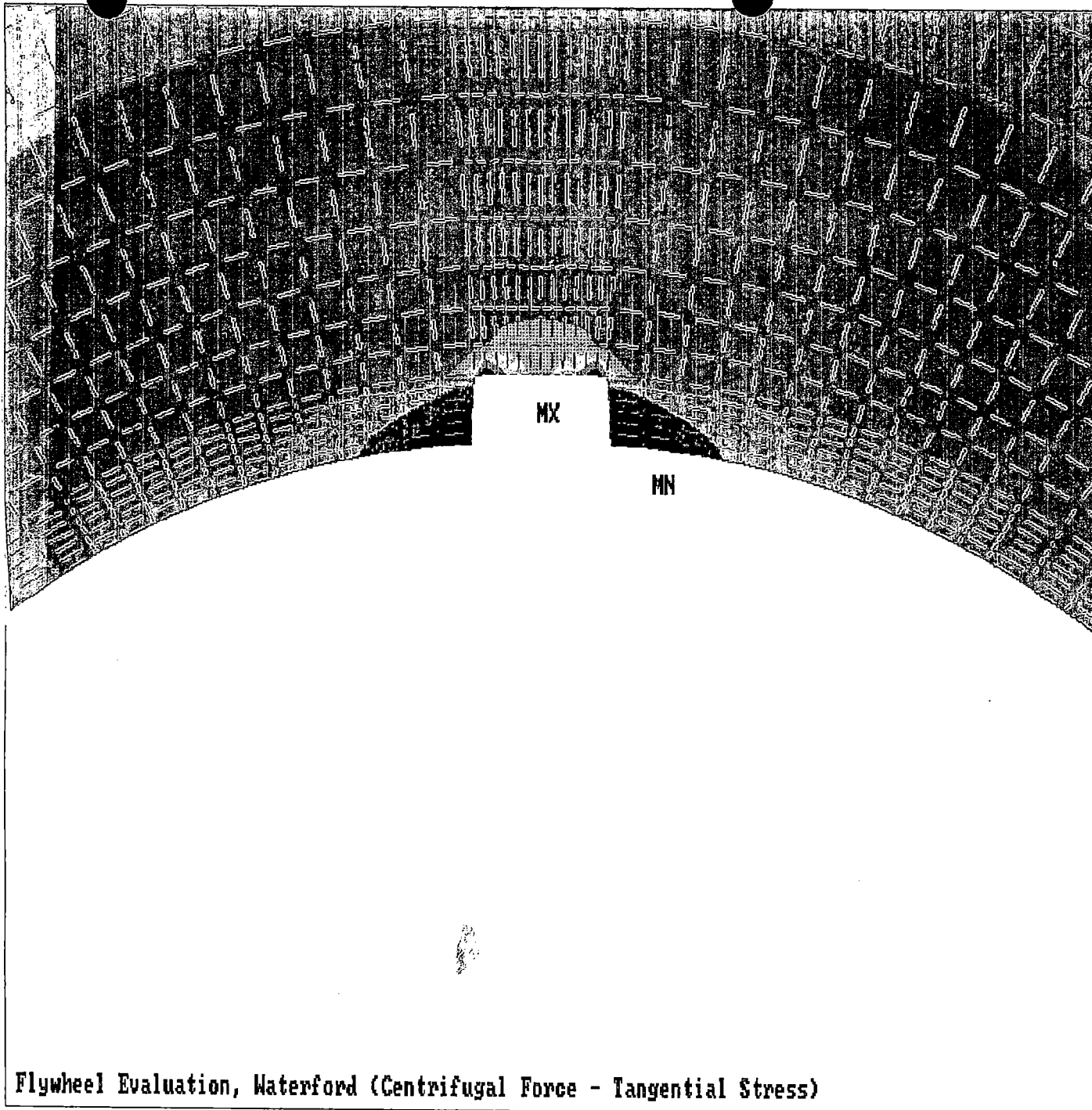Flywheel Evaluation, Waterford (Centrifugal Force - Radial Stress)

Figure 5-26. Overall Radial Stress Distribution Due to Centrifugal Force (Waterford-3)
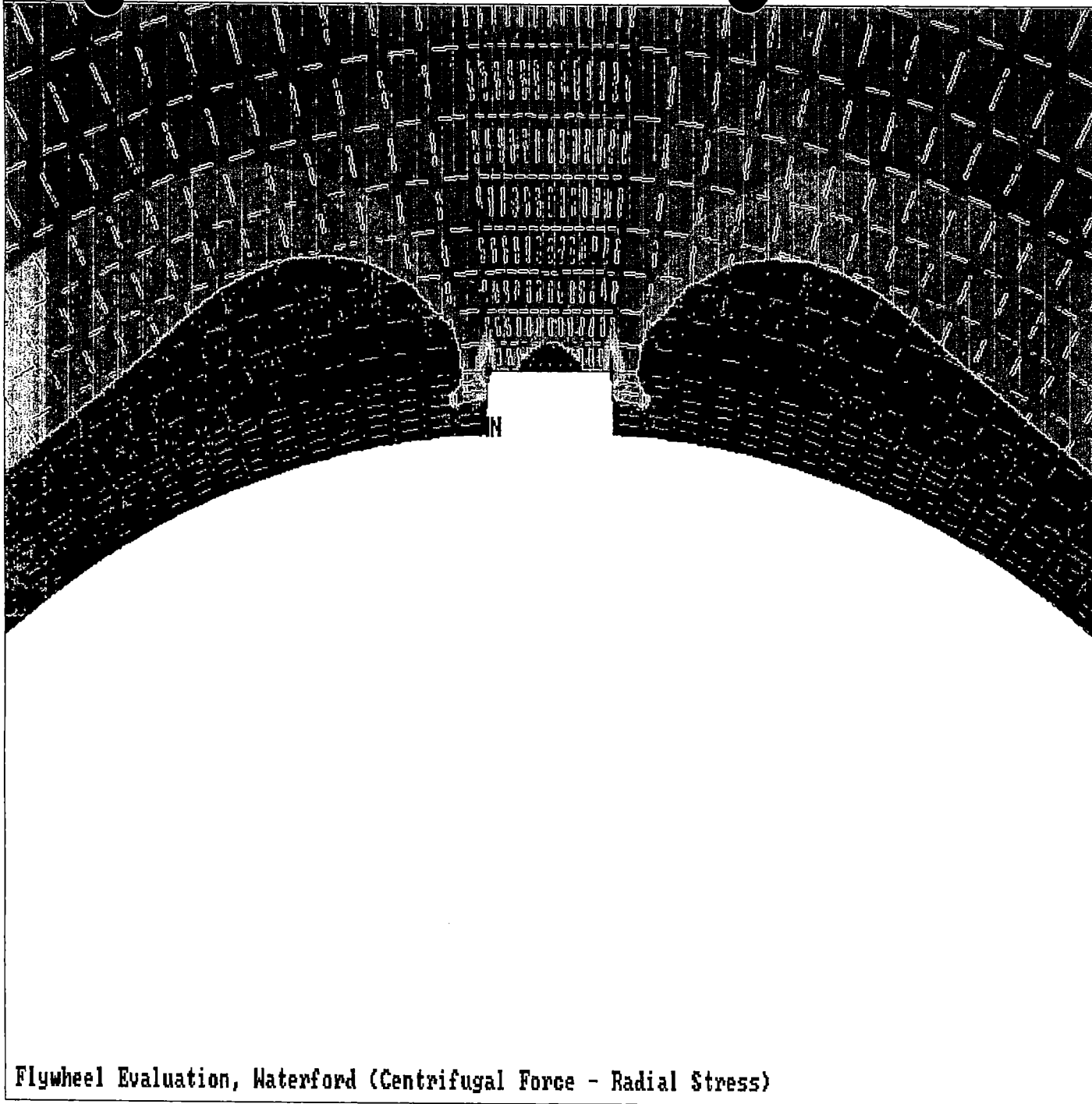
```
ANSYS-PC 4.4A1
OCT 25 1994
 5:29:36
POST1 STRESS
STEP=1
ITER=1
SX    (AVG)
CSYS=1
DMX =0.00696
SMN =-709.59
SMNB=-6255
SMX =10173
SMXB=18452

ZV   =1
*DIST=4.79
*XF  =0.011977
*YF  =6.233
       -709.59
       499.56
       1709
       2918
       4127
       5336
       6545
       7754
       8964
       10173
```

Flywheel Evaluation, Waterford (Centrifugal Force - Radial Stress)

Figure 5-27. Details of Radial Stress Distribution in Keyway Region Due to Centrifugal Force (Waterford-3)

Flywheel Dimensions:
Bore Diameter: 30.4"
Outer Diameter: 72"
Keyway Dimensions:
Length: .75"
Depth: .39"
Operating Speed: 1200 rpm

Radial (Remote) Tangential (Remote) Radial (Keyway) Tangential (Keyway)

Radial Distance
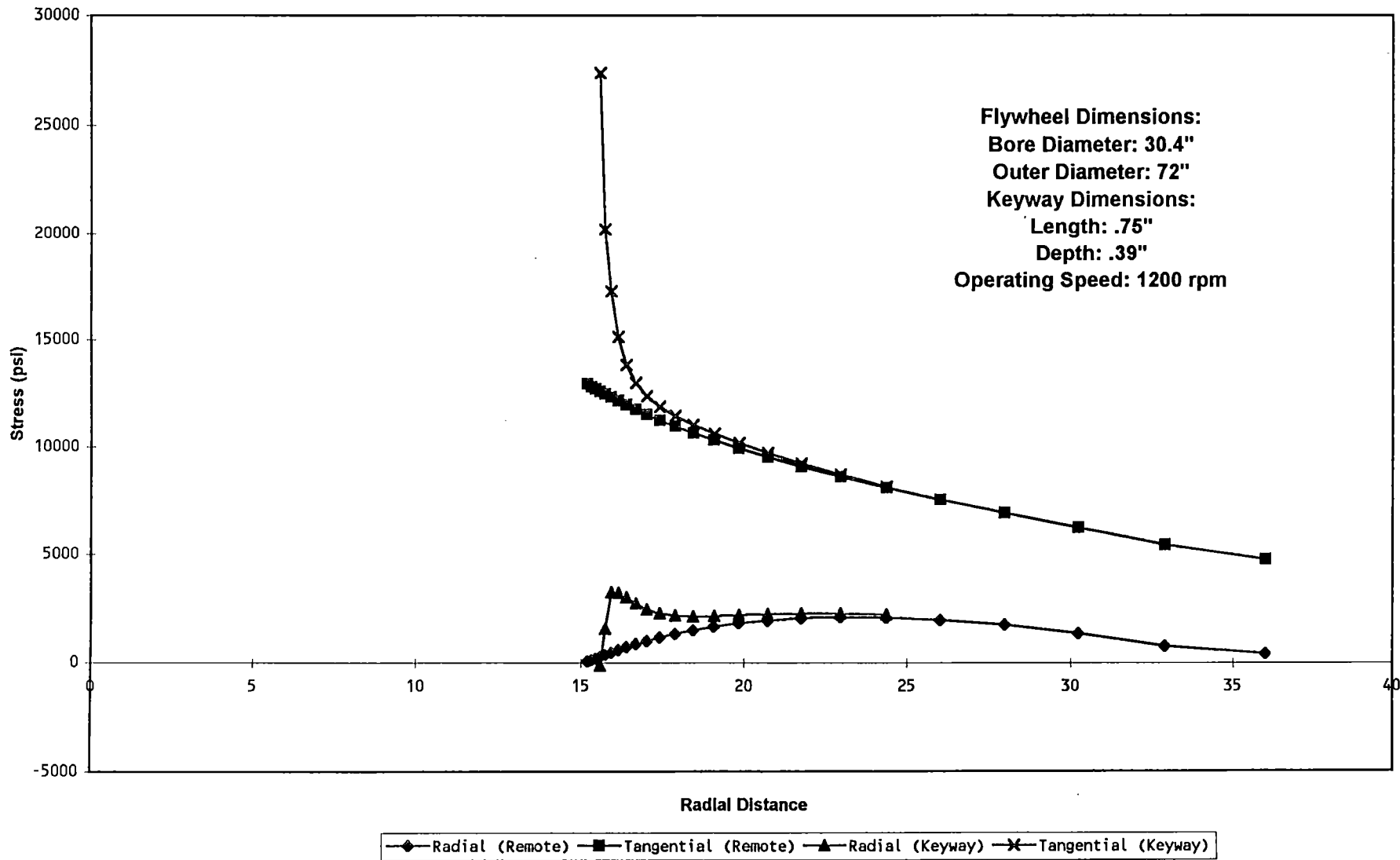
Figure 5-28. Tangential and Radial Stress Distribution from Bore to Outside Diameter (ANO-1)
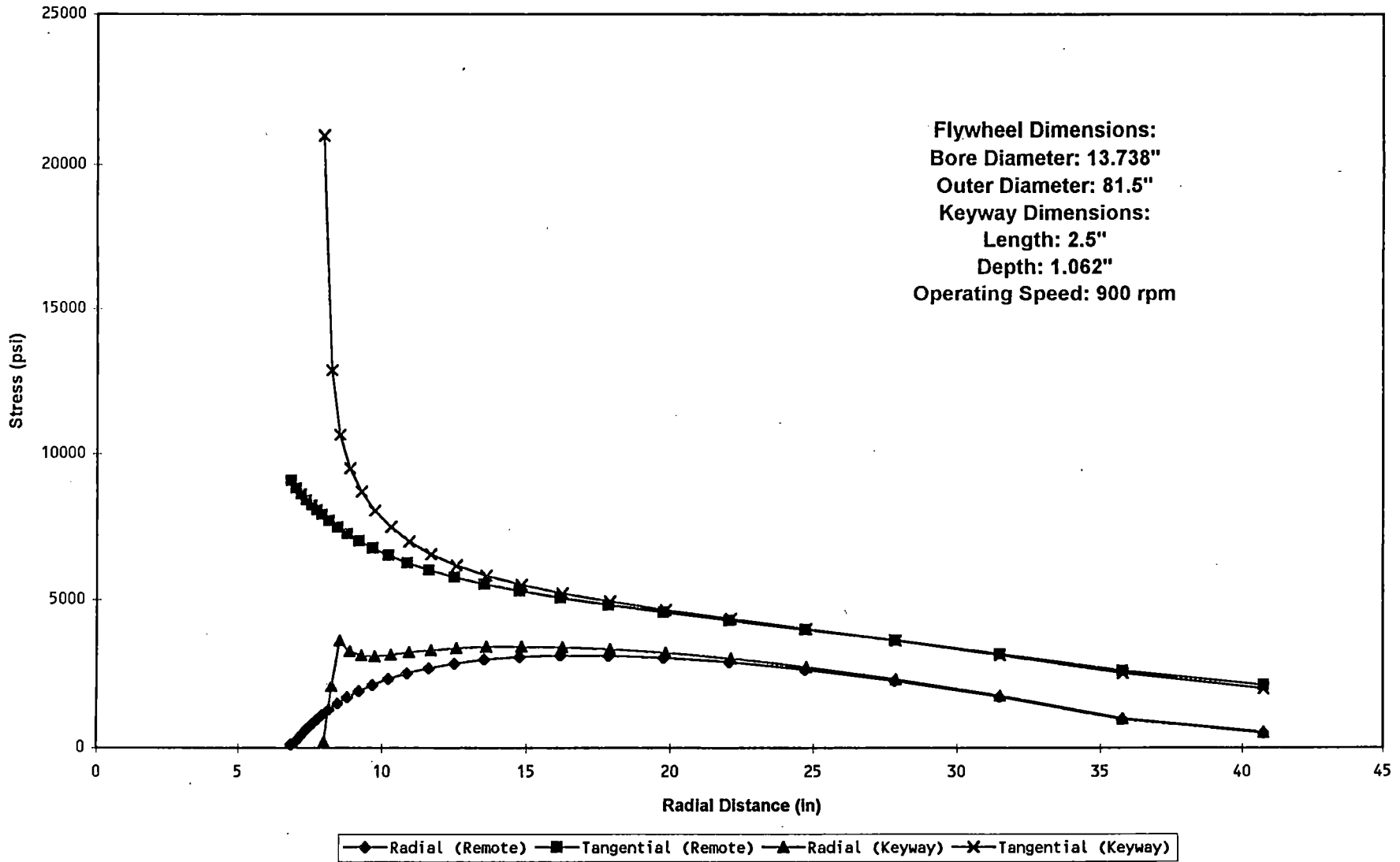
Figure 5-29. Tangential and Radial Stress Distribution from Bore to Outside Diameter (ANO-2)

Flywheel Dimensions:
Bore Diameter: 13.7415"
Outer Diameter: 75"
Keyway Dimensions:
Length: 2.5"
Depth: 1.062"
Operating Speed: 900 rpm

Stress (psi)

Radial Distance (In)

—◇—Radial (Remote) —■—Tangential (Remote) —△—Radial (Keyway) —✕—Tangential (Keyway)
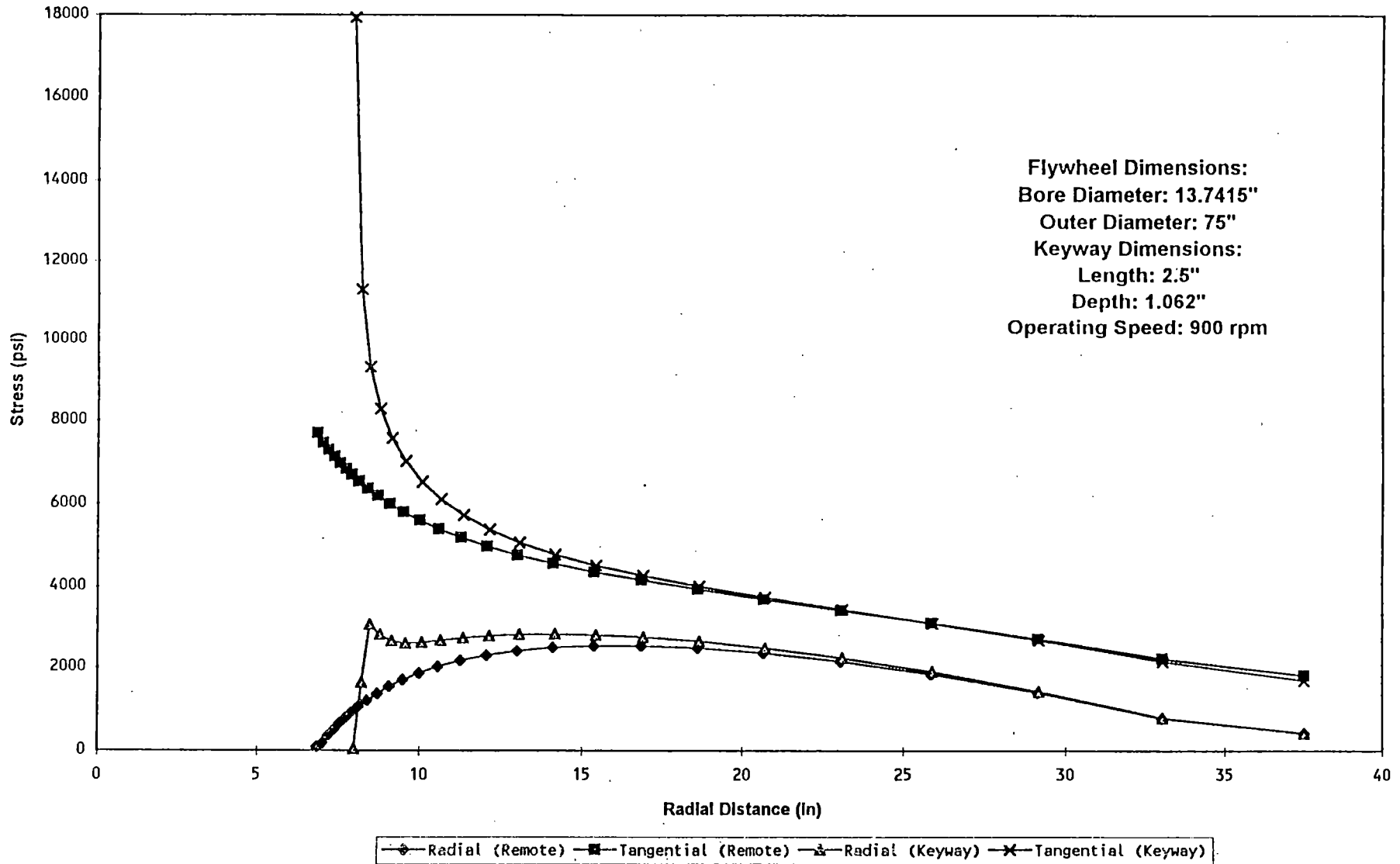
Figure 5-30. Tangential and Radial Stress Distribution from Bore to Outside Diameter (Millstone-2)

Flywheel Dimensions:
Bore Diameter: 32.9"
Outer Diameter: 72"
Keyway Dimensions:
Length: 0.5"
Depth: 0.25"
Operating Speed: 900 rpm

Legend: —◆— Radial (Remote)   —■— Tangential (Remote)   —▲— Radial (Keyway)   —✕— Tangential (Keyway)
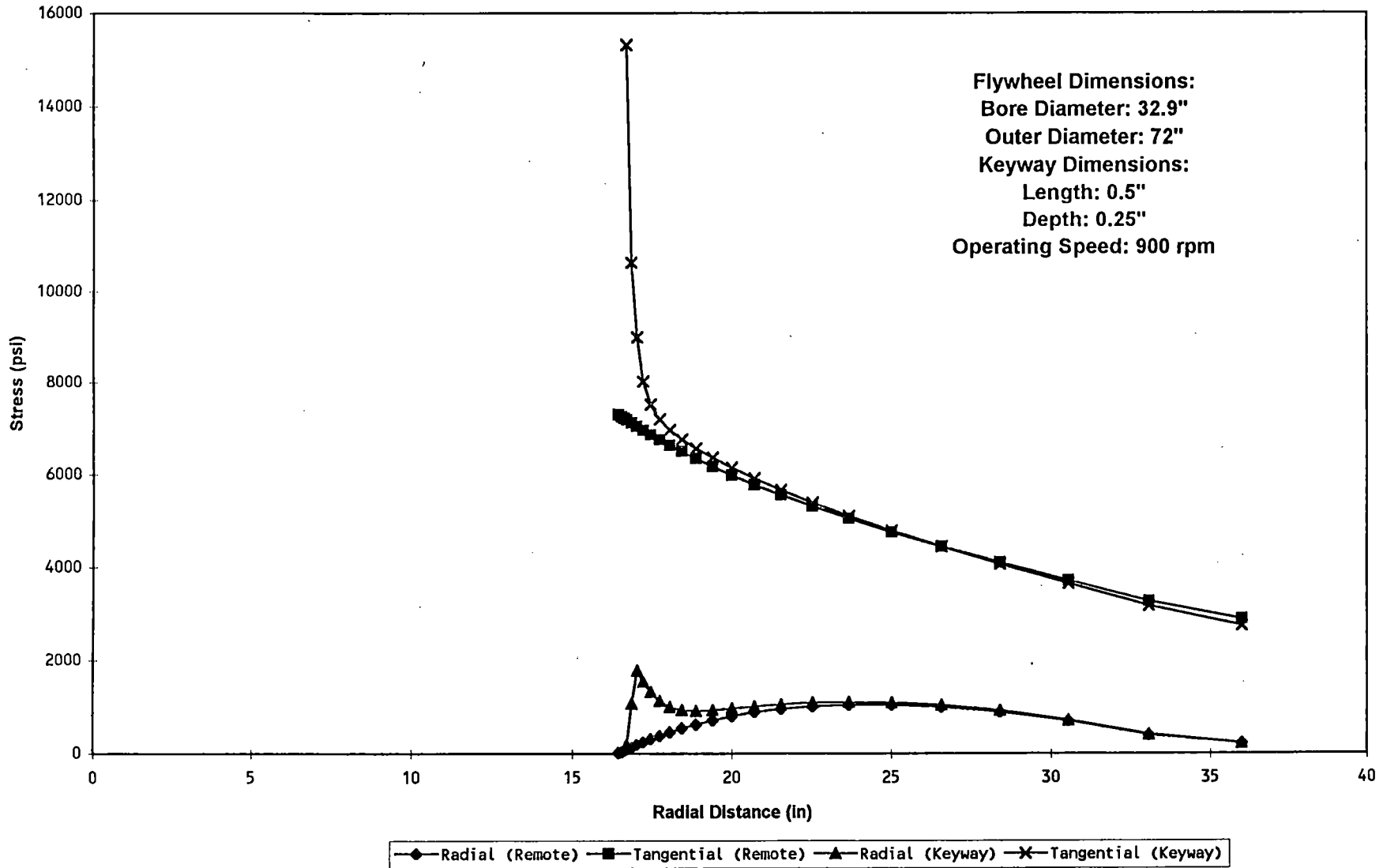
Figure 5-31. Tangential and Radial Stress Distribution from Bore to Outside Diameter (Palisades)

FIGURE 5

ST. LUCIE
CENTRIFUGAL STRESSES
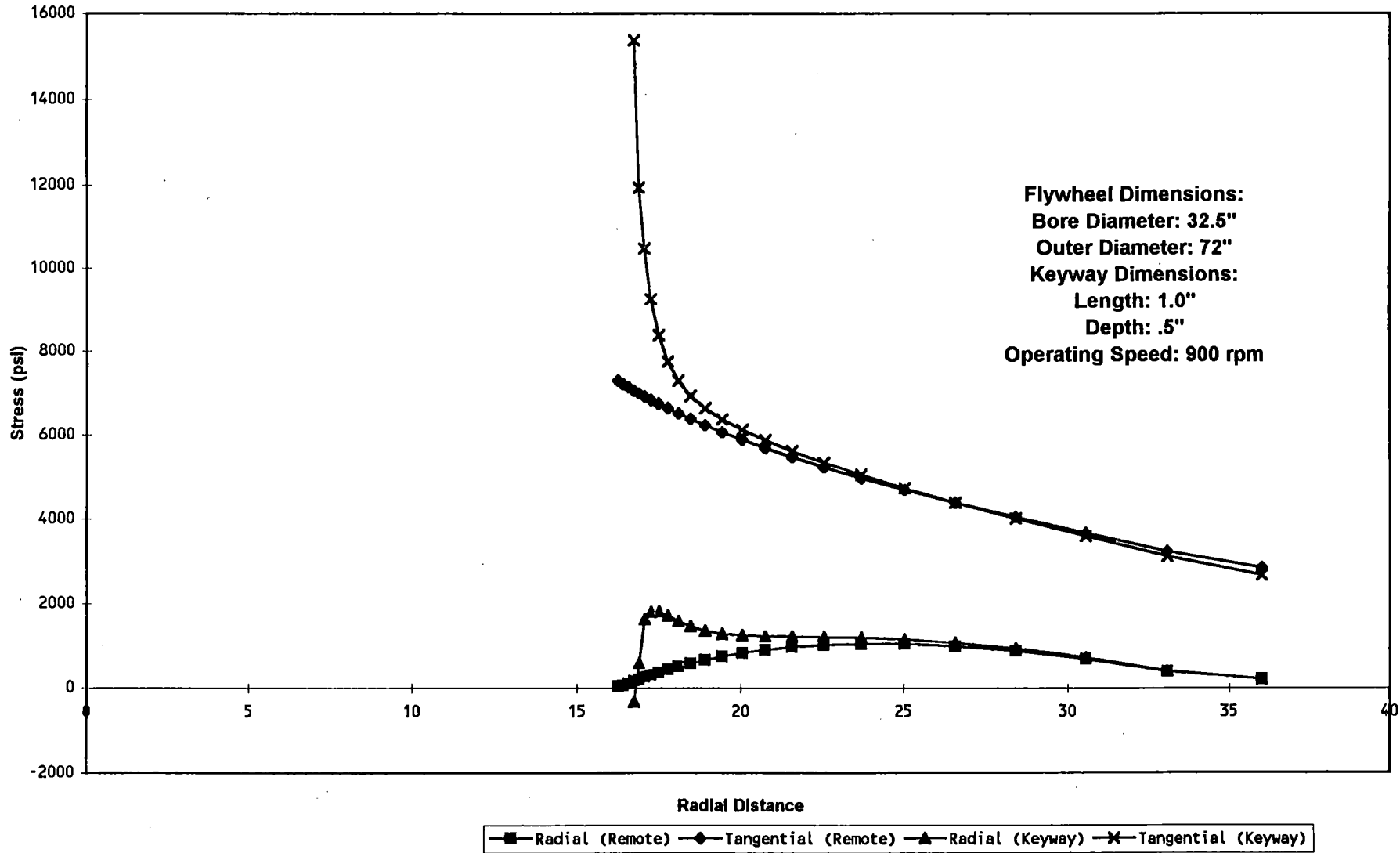
Figure 5-32. Tangential and Radial Stress Distribution from Bore to Outside Diameter (St. Lucie)

Flywheel Dimensions:
Bore Diameter = 13.75"
Outer Diameter = 78"
Keyway Dimensions:
Length = 1.0"
Depth 0.531"
Operating Speed : 1200 rpm

Stress (psi)

Radial Distance (In)

—◆— Radial (Remote) —■— Tangential (Remote) —▲— Radial (Keyway) —✕— Tangential (Keyway)
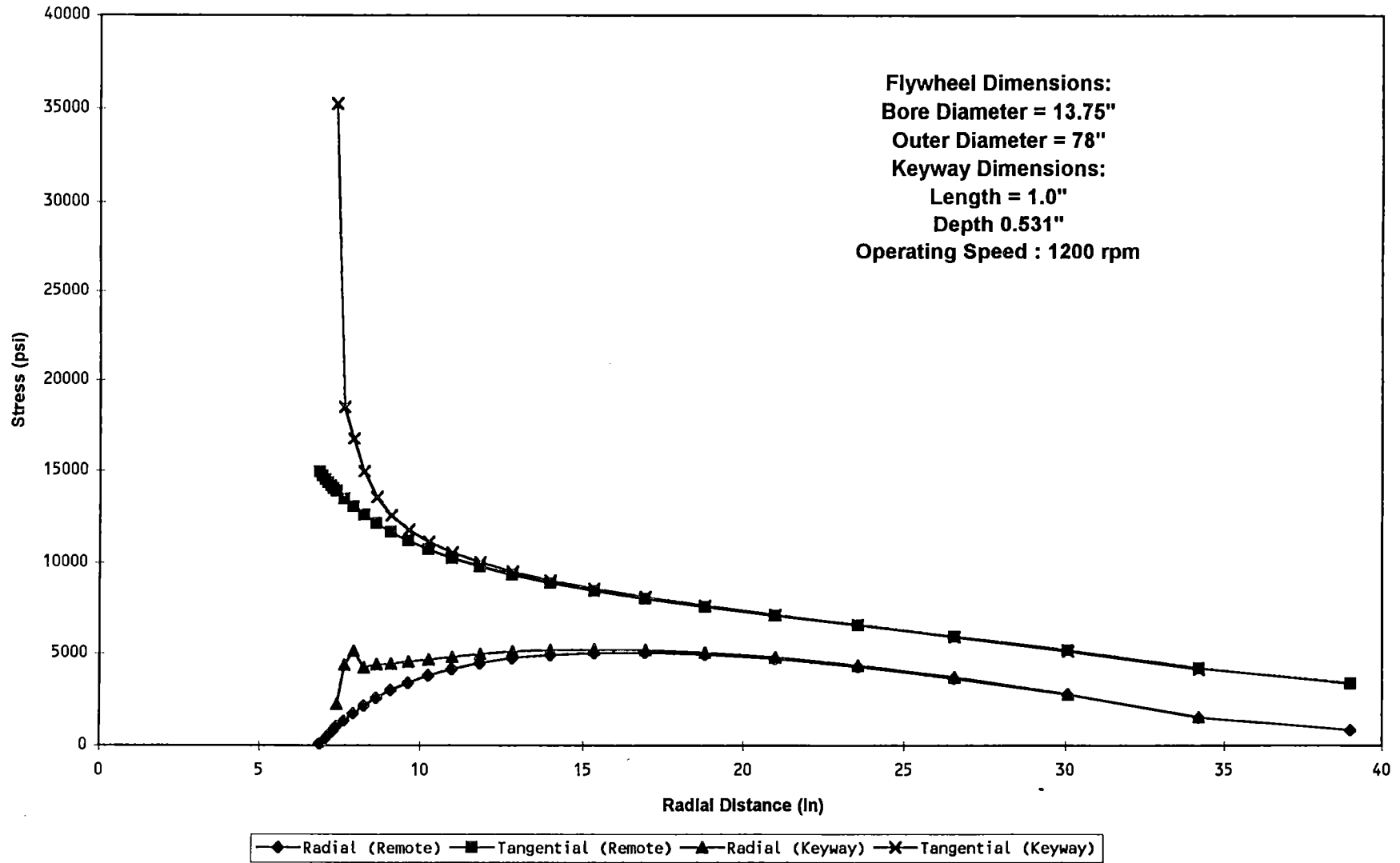
Figure 5-33. Tangential and Radial Stress Distribution from Bore to Outside Diameter (Waterford-3)
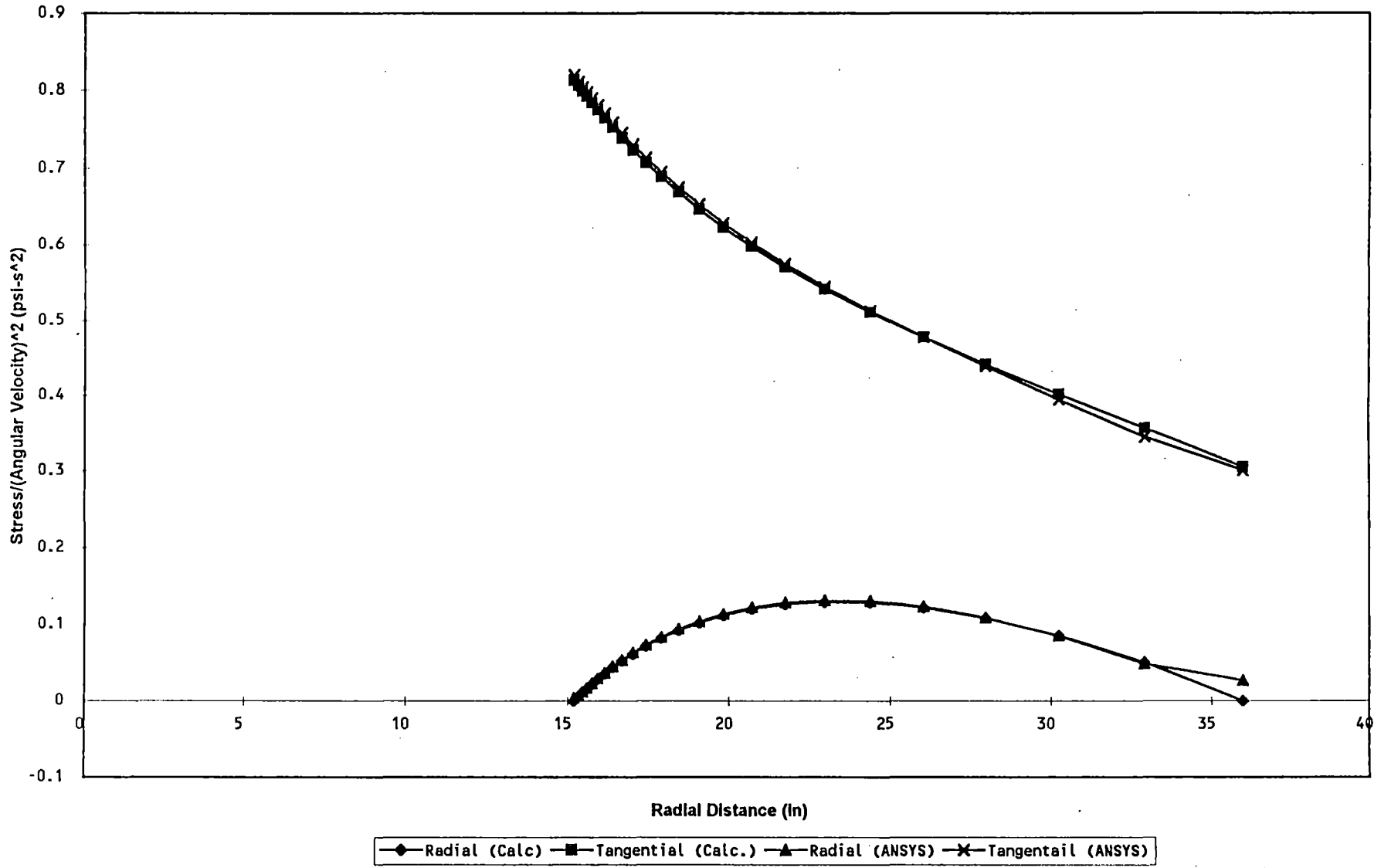
Figure 5-34. Comparison of Finite Element Results for Centrifugal Force With Theoretical Results (ANO-1)
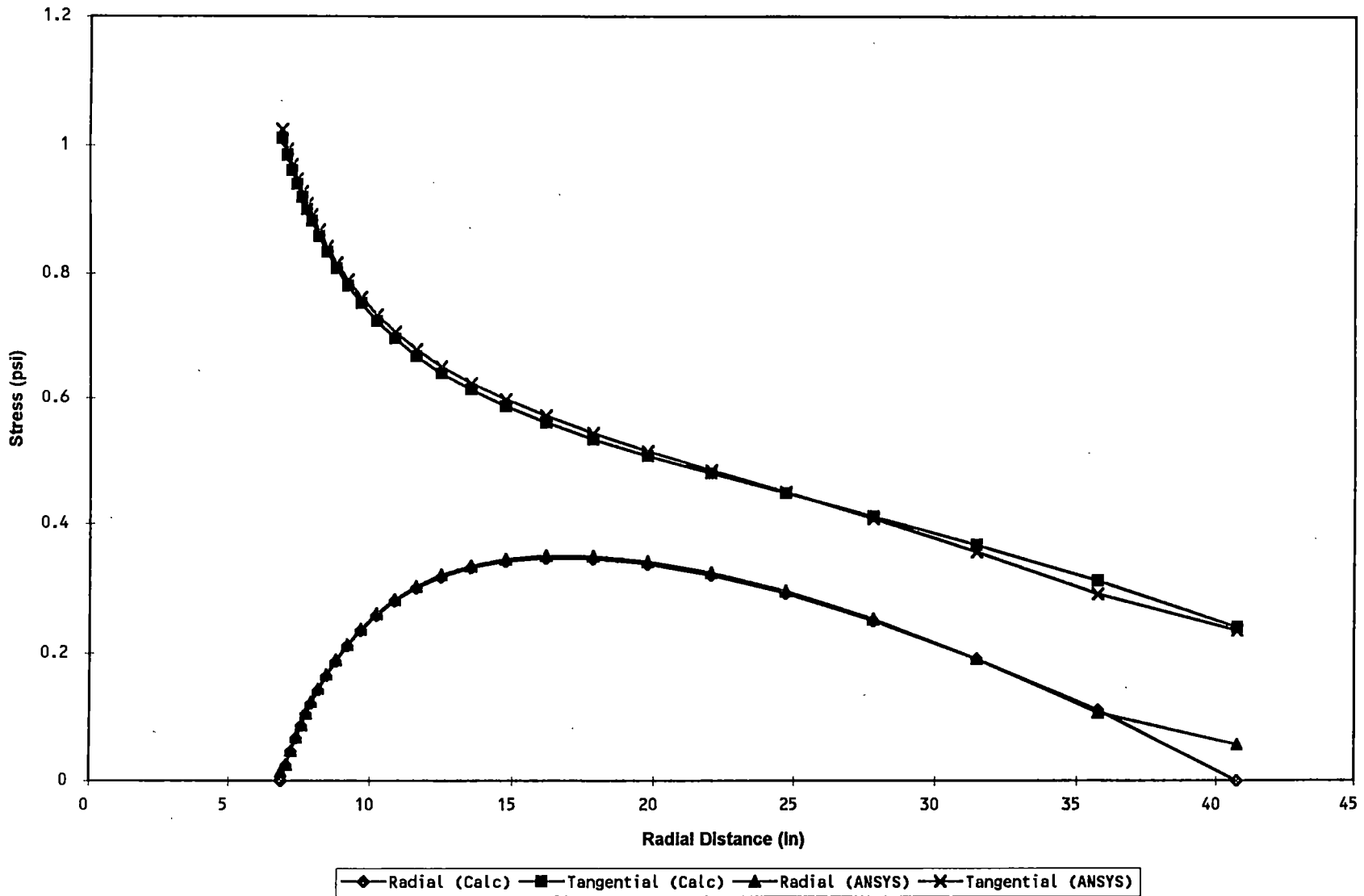
Figure 5-35. Comparison of Finite Element Results for Centrifugal Force With Theoretical Results (ANO-2)
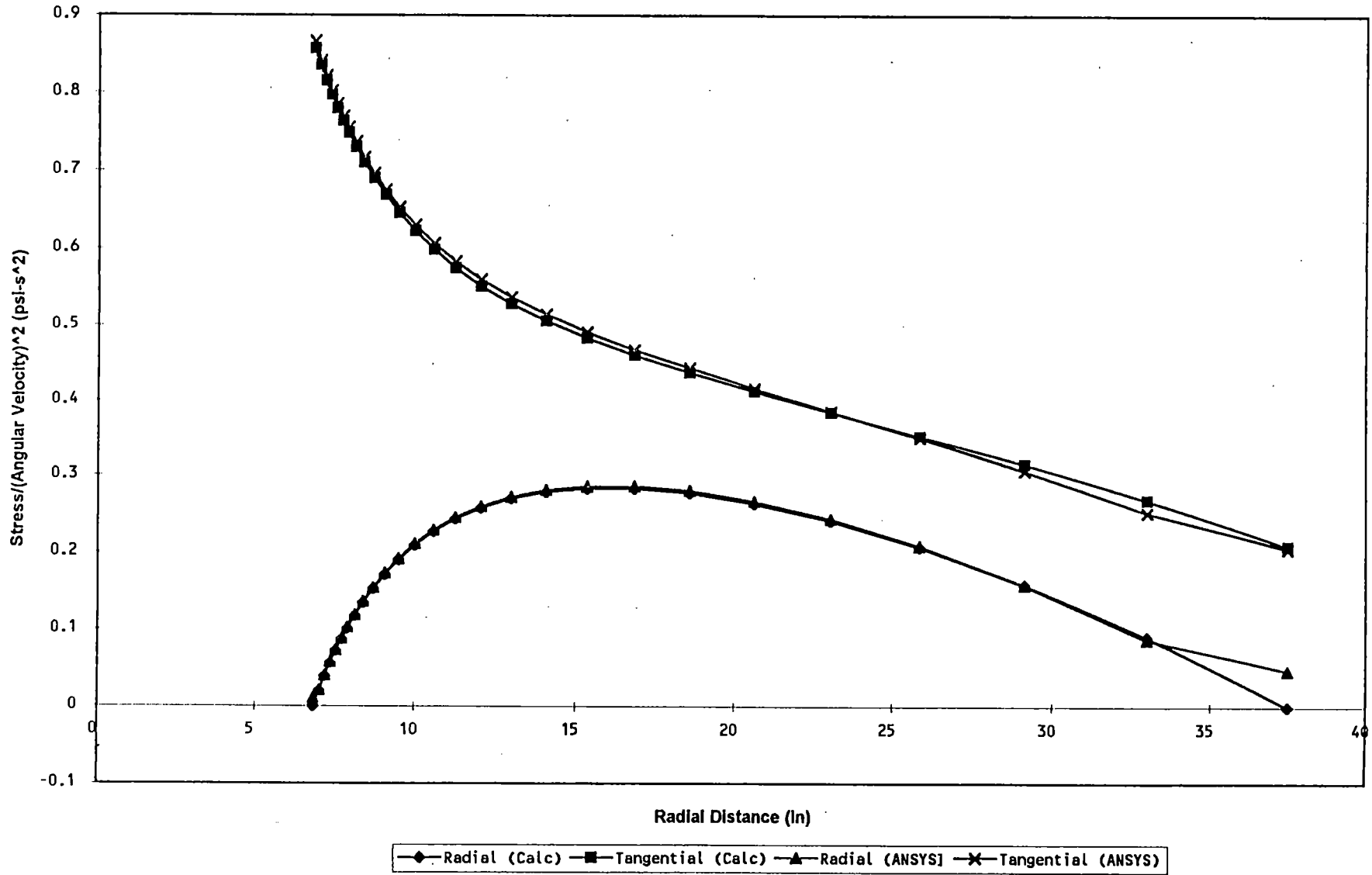
Figure 5-36. Comparison of Finite Element Results for Centrifugal Force With Theoretical Results (Millstone-2)
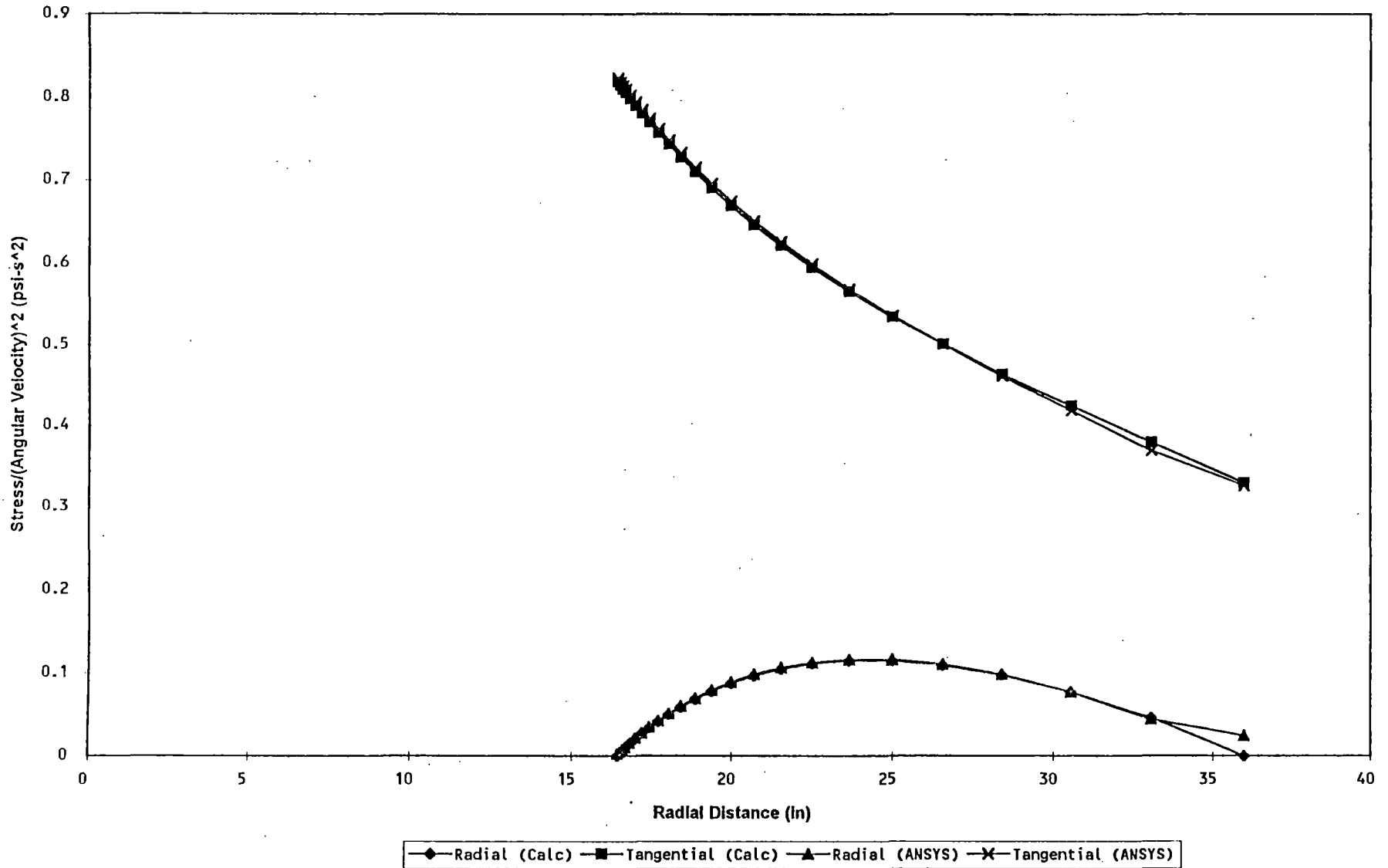
Figure 5-37. Comparison of Finite Element Results for Centrifugal Force With Theoretical Results (Palisades)

FIGURE 10

Structural Integrity Associates, Inc.

St. Lucie
Centrifugal Force
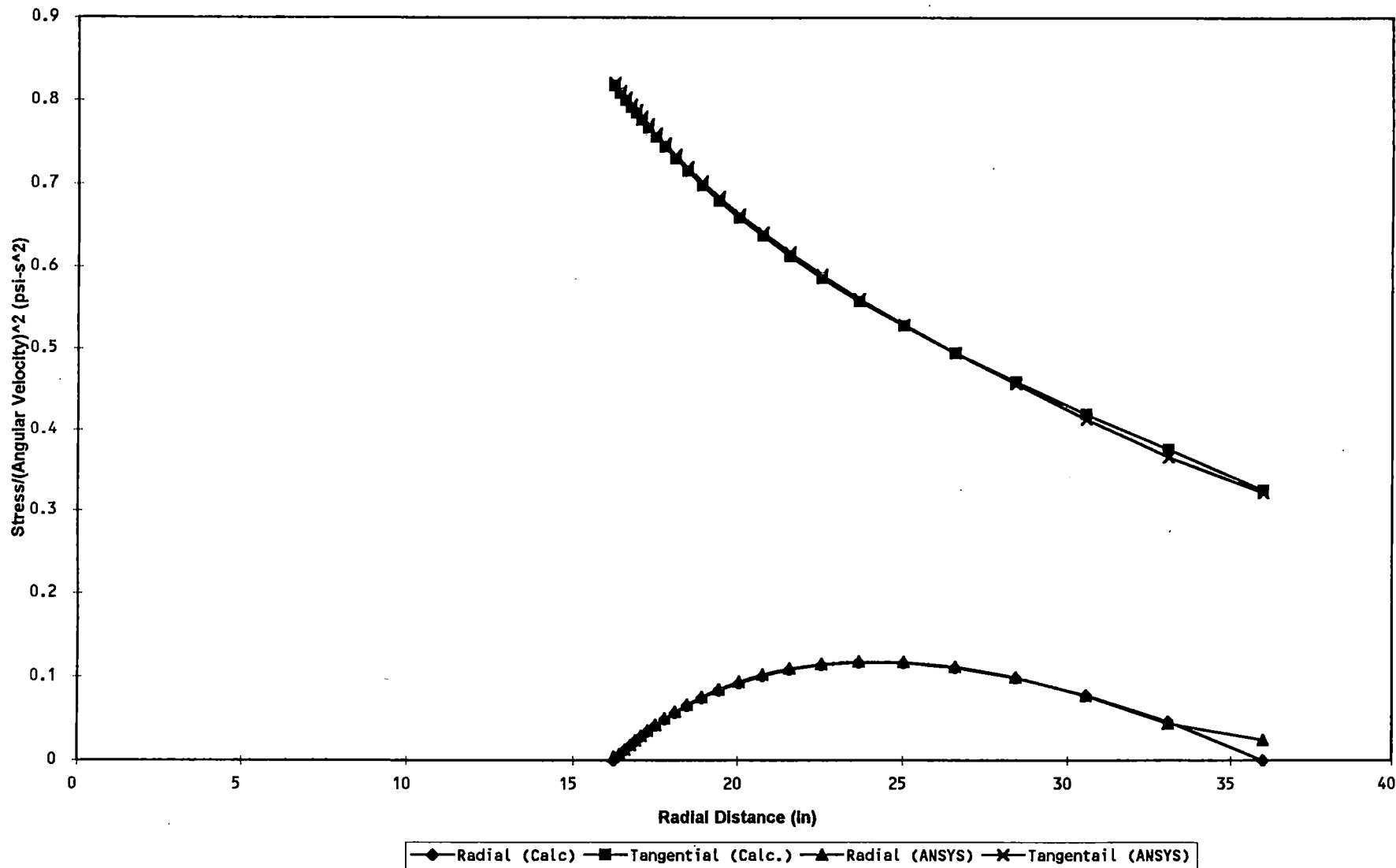
Figure 5-38. Comparison of Finite Element Results for Centrifugal Force With Theoretical Results (St. Lucie)
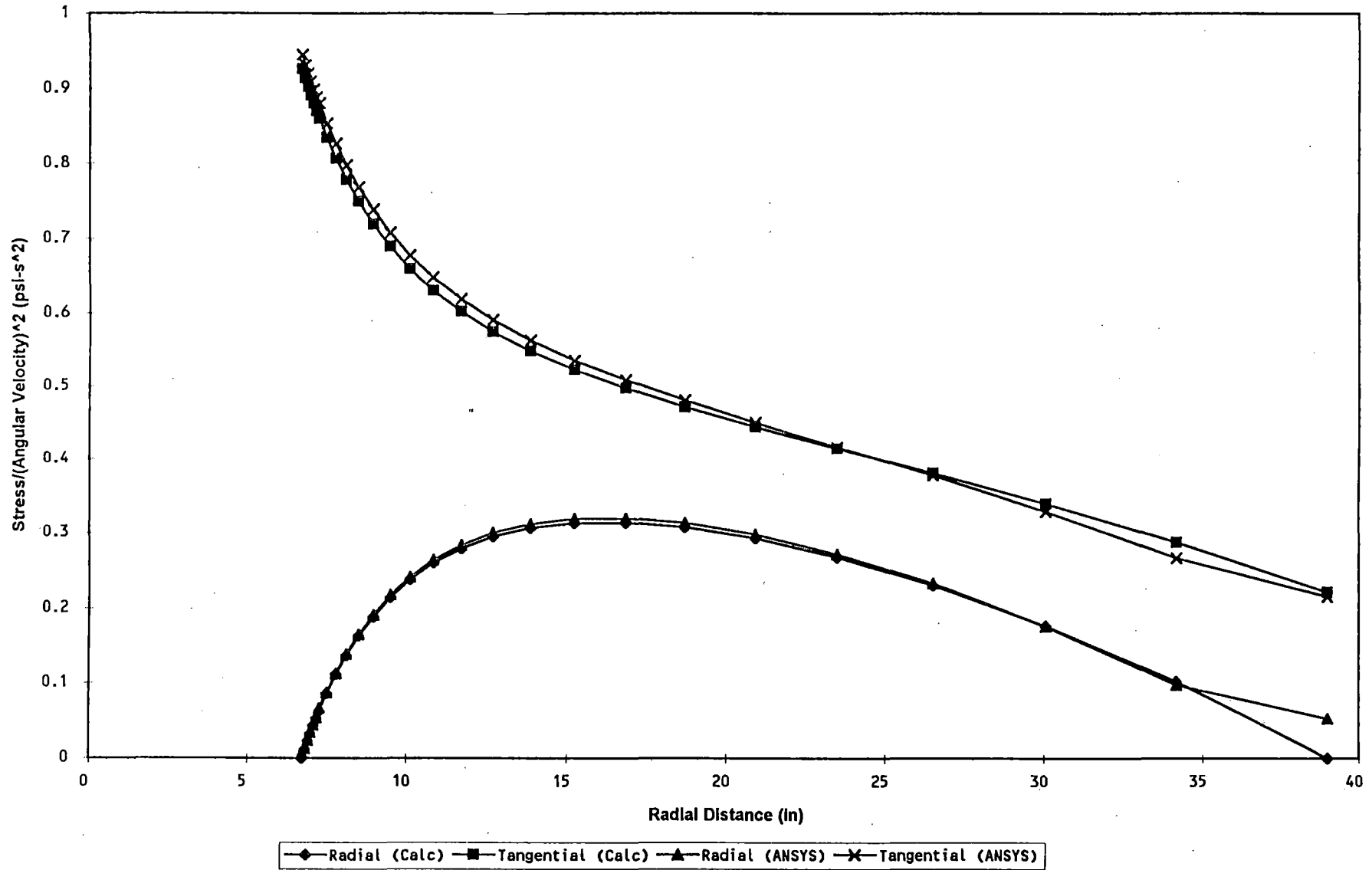
Figure 5-39. Comparison of Finite Element Results for Centrifugal Force With Theoretical Results (Waterford-3)

CEOG Flywheel Evaluation, ANO Unit 1 (Shrink Fit Force)
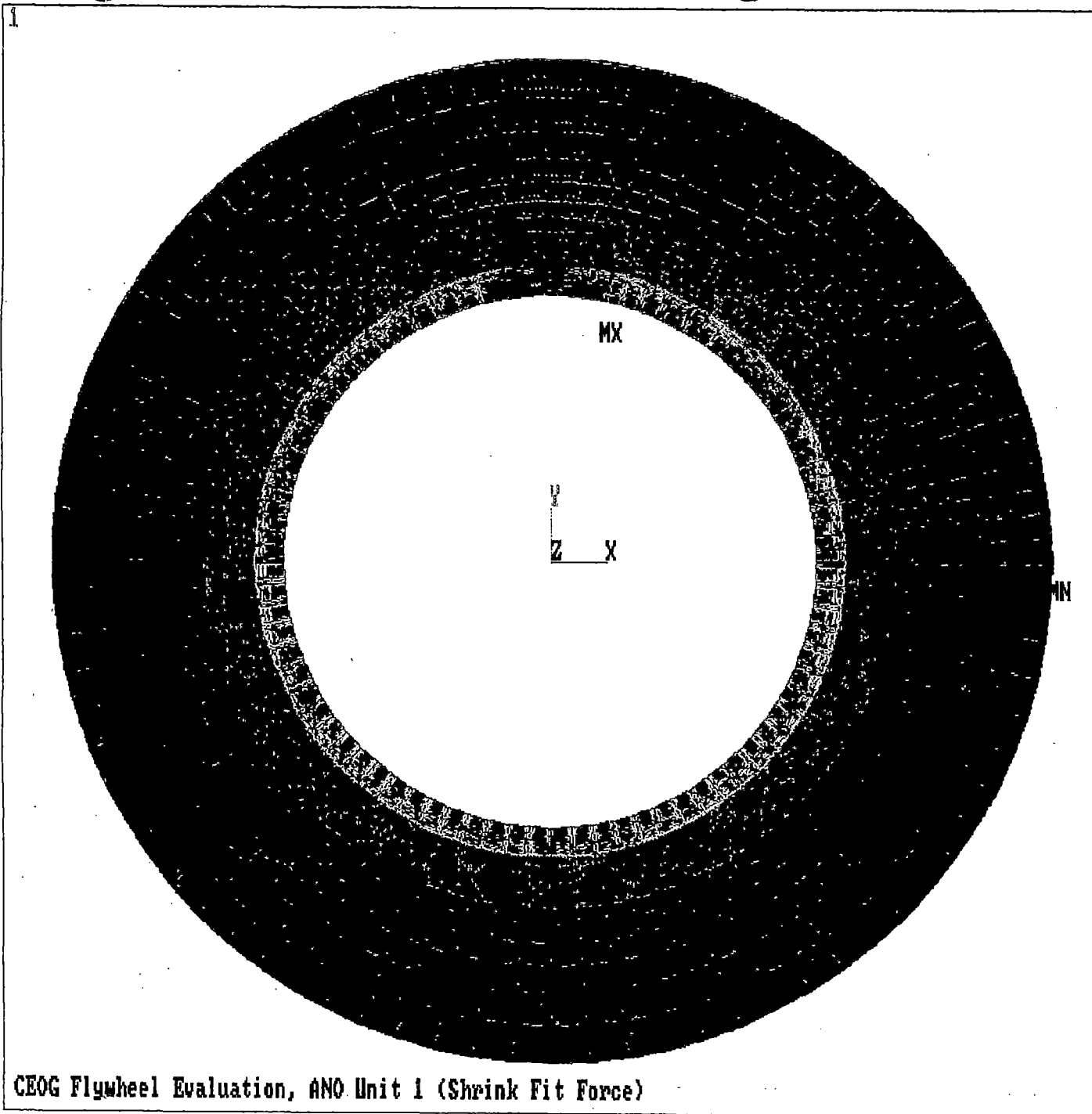
ANSYS-PC 4.4A1
AUG 23 1994
2:13:55
POST1 STRESS
STEP=1
ITER=1
SY   (AVG)
CSYS=1
DMX =0.001001
SMN =-499.622
SMNB=-1836
SMX =3781
SMXB=4349

ZV   =1
DIST=39.6
      -499.622
      -23.981
      451.659
      927.299
      1403
      1879
      2354
      2830
      3306
      3781

Figure 5-40. Overall Tangential Stress Distribution Due to Shrink-Fit Force (ANO-1)

```
ANSYS-PC 4.4A1
AUG 23 1994
  2:19:04
POST1 STRESS
STEP=1
ITER=1
SY    (AVG)
CSYS=1
DMX =0.001001
SMN =-499.622
SMNB=-1836
SMX =3781
SMXB=4349

ZV   =1
*DIST=9.055
*XF  =-0.147314
*YF  =11.914
       -499.622
       -23.981
       451.659
       927.299
       1403
       1879
       2354
       2830
       3306
       3781
```

MX

CEOG Flywheel Evaluation, ANO Unit 1 (Shrink Fit Force)

Figure 5-41. Details of Tangential Stress Distribution in Keyway Region Due to Shrink-Fit Force (ANO-1)

```
ANSYS-PC 4.4A1
AUG 23 1994
 2:12:17
POST1 STRESS
STEP=1
ITER=1
SX    (AVG)
CSYS=1
DMX =0.001001
SMN =-5882
SMNB=-7591
SMX =232.206
SMXB=1283

ZV  =1
DIST=39.6
        -5882
        -5202
        -4523
        -3844
        -3164
        -2485
        -1806
        -1126
        -447.099
        232.206
```

CEOG Flywheel Evaluation, ANO Unit 1 (Shrink Fit Force)

Figure 5-42. Overall Radial Stress Distribution Due to Shrink-Fit Force (ANO-1)

```
ANSYS-PC 4.4A1
AUG 23 1994
  2:17:28
POST1 STRESS
STEP=1
ITER=1
SX    (AVG)
CSYS=1
DMX =0.001001
SMN =-5882
SMNB=-7591
SMX =232.206
SMXB=1283

ZV  =1
*DIST=9.055
*XF  =-0.147314
*YF  =11.914
        -5882
        -5202
        -4523
        -3844
        -3164
        -2485
        -1806
        -1126
        -447.099
        232.206
```

CEOG Flywheel Evaluation, ANO Unit 1 (Shrink Fit Force)

Figure 5-43. Details of Radial Stress Distribution in Keyway Region Due to Shrink-Fit Force (ANO-1)
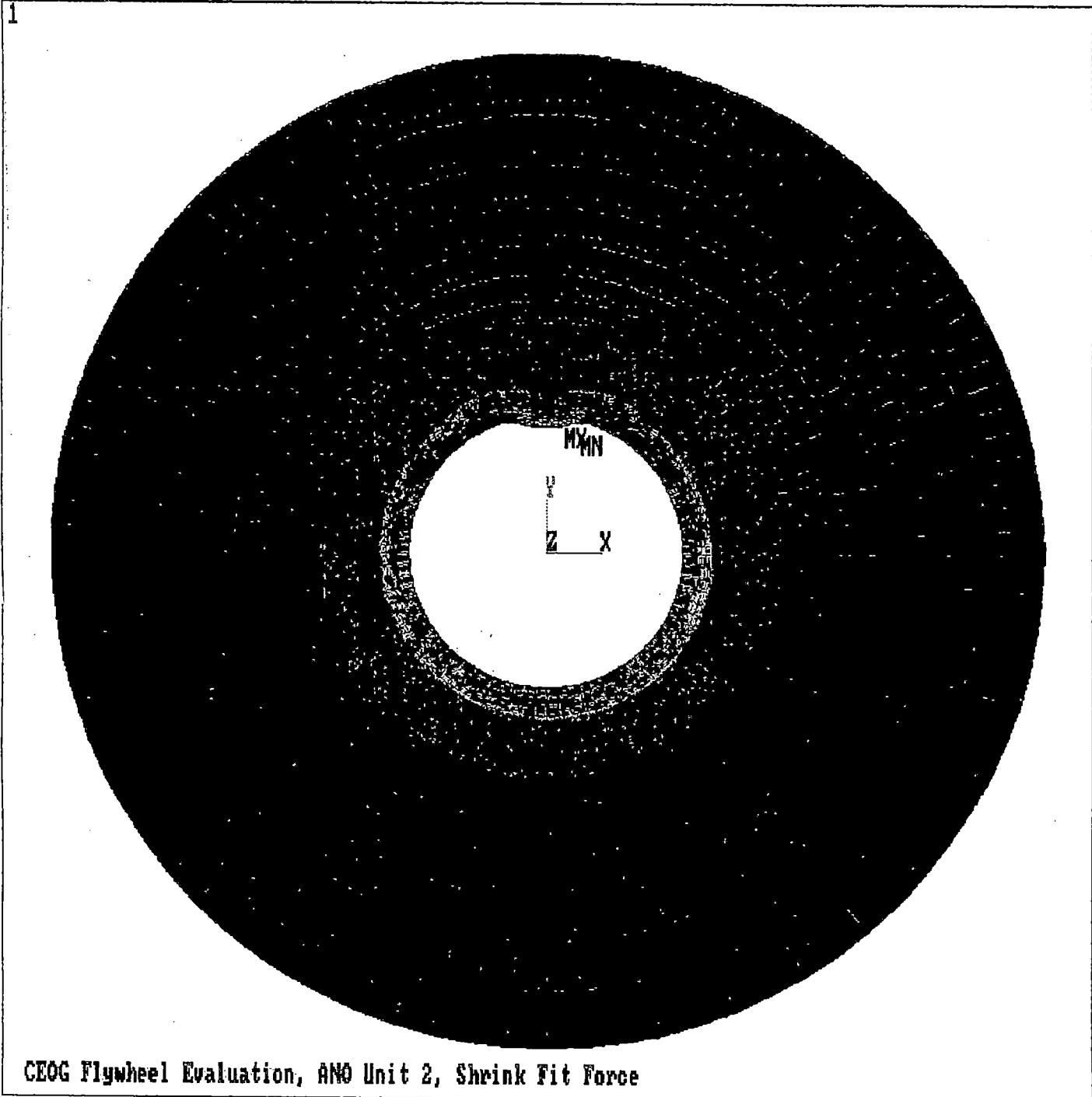
```
ANSYS-PC 4.4A1
AUG 23 1994
  3:52:11
POST1 STRESS
STEP=1
ITER=1
SY    (AVG)
CSYS=1
DMX =0.001033
SMN =-439.99
SMNB=-1694
SMX =6184
SMXB=7933

ZV   =1
DIST=44.825
     -439.99
      295.958
      1032
      1768
      2504
      3240
      3976
      4712
      5448
      6184
```

CEOG Flywheel Evaluation, ANO Unit 2, Shrink Fit Force

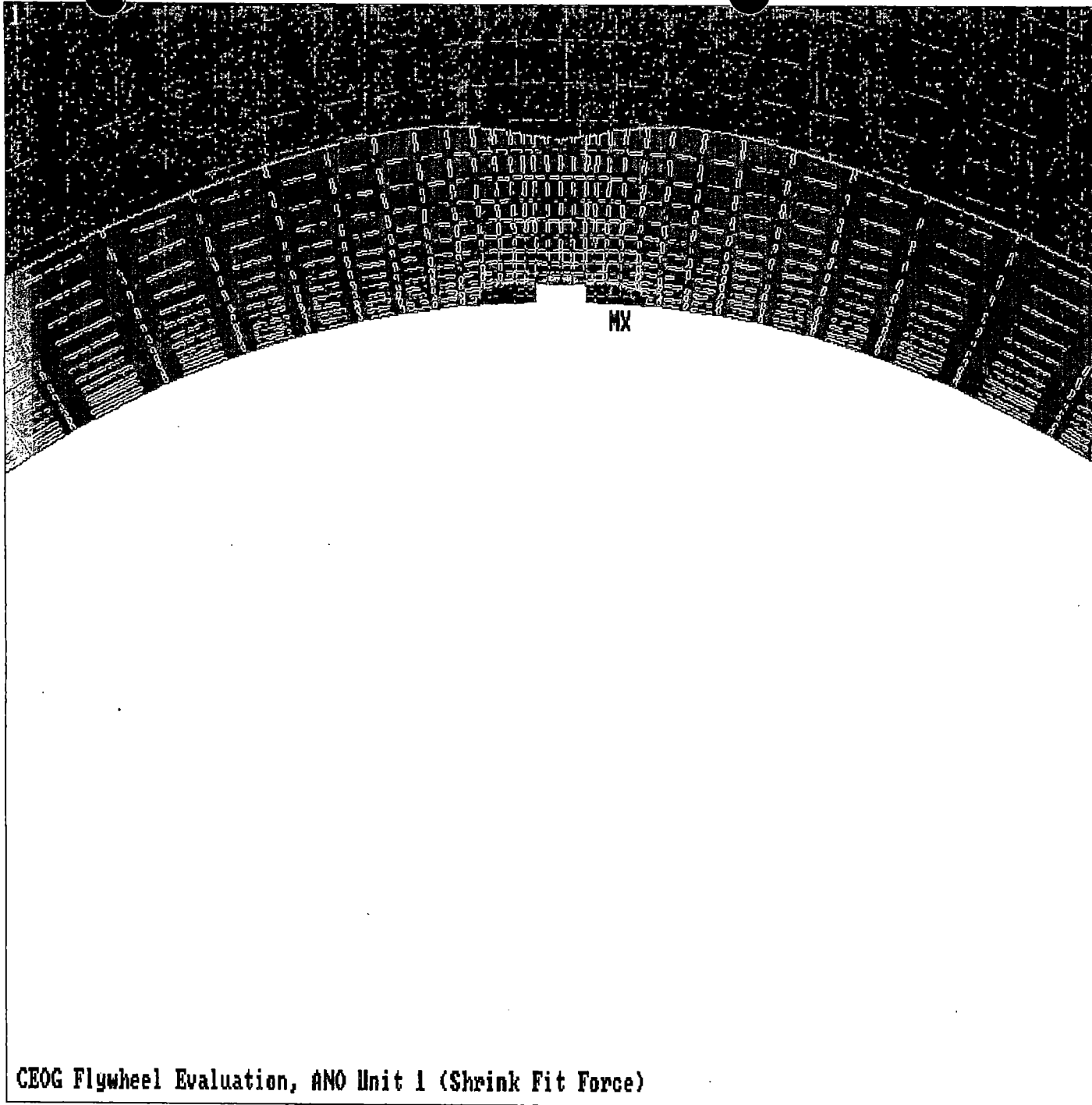Figure 5-44. Overall Tangential Stress Distribution Due to Shrink-Fit Force (ANO-2)
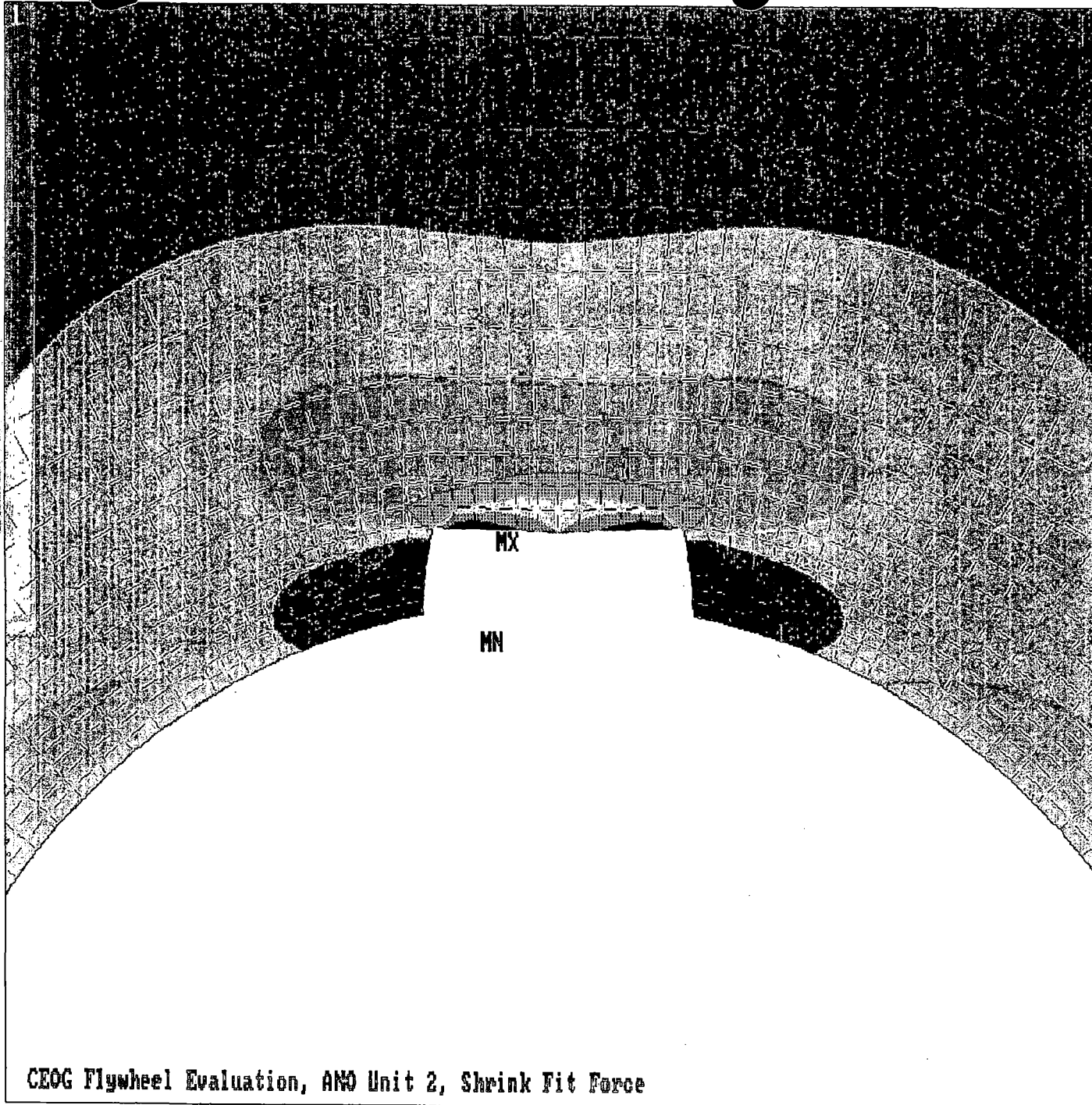
```
ANSYS-PC 4.4A1
AUG 23 1994
 4:00:13
POST1 STRESS
STEP=1
ITER=1
SY   (AVG)
CSYS=1
DMX =0.001033
SMN =-439.99
SMNB=-1694
SMX =6184
SMXB=7933

ZV  =1
*DIST=6.105
*XF =-0.075006
*YF =7.99
      -439.99
      295.958
      1032
      1768
      2504
      3240
      3976
      4712
      5448
      6184
```

MX

MN

CEOG Flywheel Evaluation, ANO Unit 2, Shrink Fit Force

Figure 5-45. Details of Tangential Stress Distribution in Keyway Region Due to Shrink-Fit Force (ANO-2)
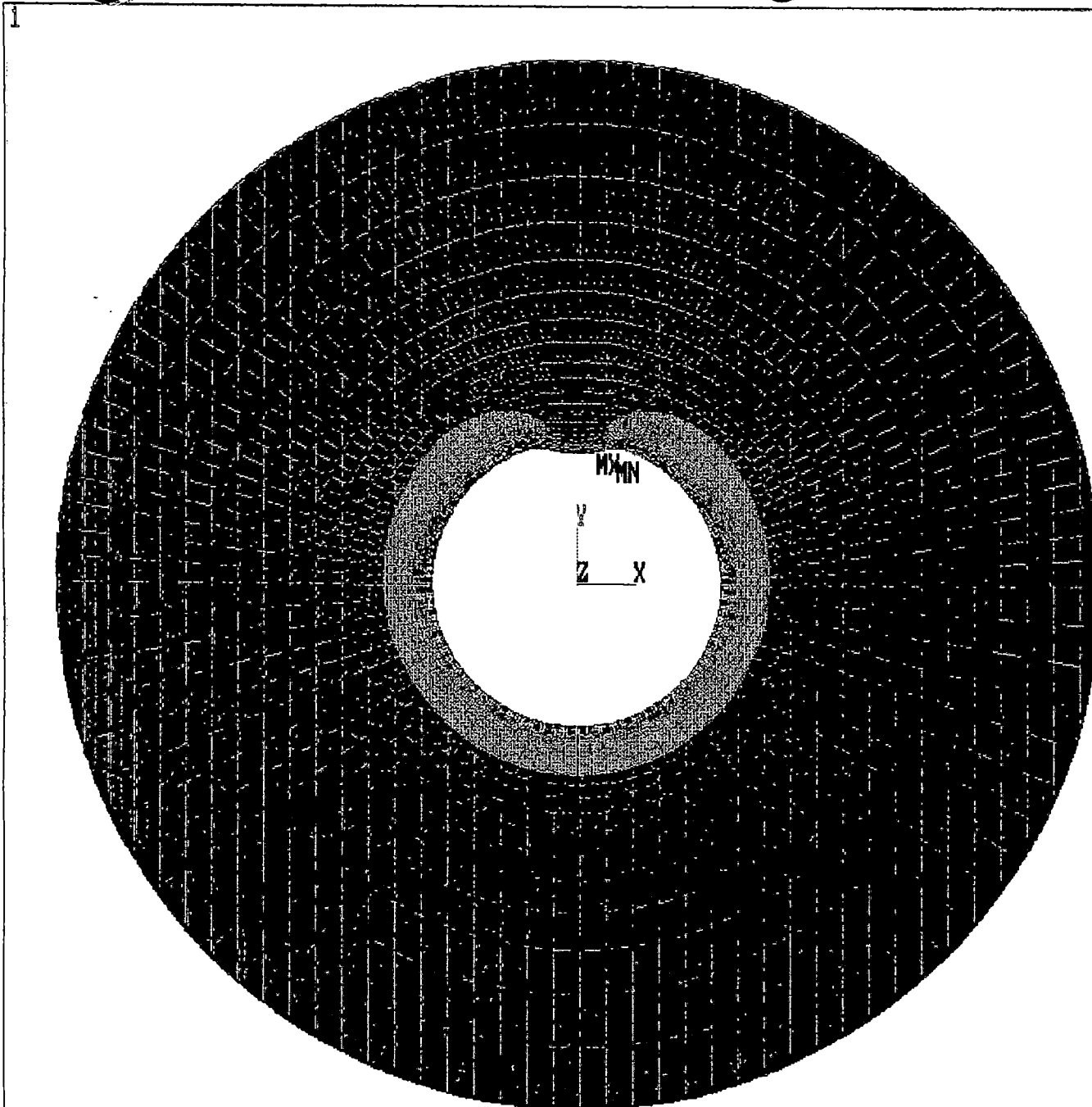
```
ANSYS-PC 4.4A1
AUG 23 1994
 3:50:31
POST1 STRESS
STEP=1
ITER=1
SX   (AVG)
CSYS=1
DMX =0.001033
SMN =-12173
SMNB=-13516
SMX =172.898
SMXB=1922

ZV  =1
DIST=44.825
        -12173
        -10801
        -9429
        -8057
        -6686
        -5314
        -3942
        -2571
        -1199
        172.898
```

CEOG Flywheel Evaluation, ANO Unit 2, Shrink Fit Force

Figure 5-46. Overall Radial Stress Distribution Due to Shrink-Fit Force (ANO-2)

ANSYS-PC 4.4A1
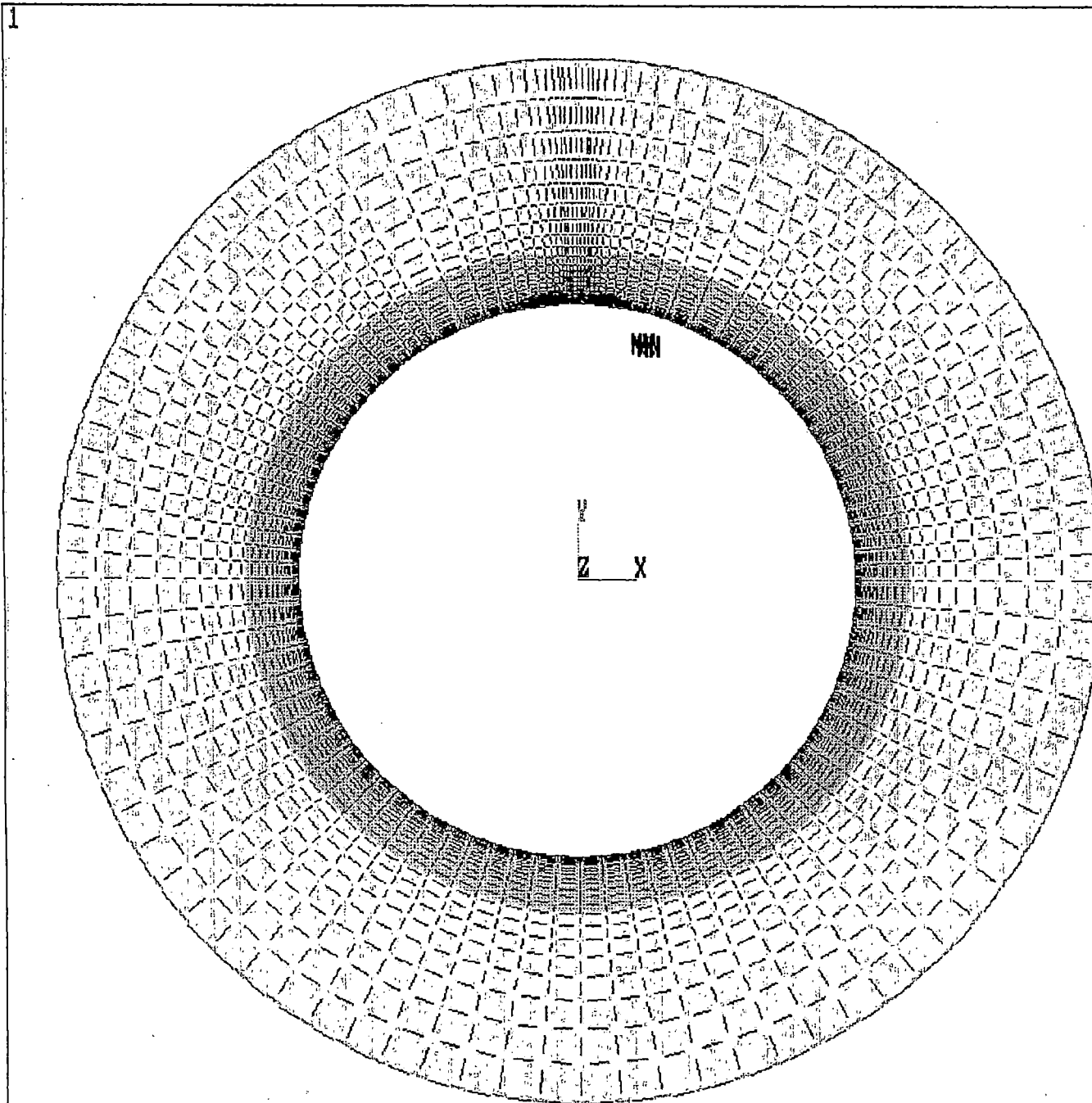AUG 23 1994
3:58:34
POST1 STRESS
STEP=1
ITER=1
SX   (AVG)
CSYS=1
DMX =0.001033
SMN =-12173
SMNB=-13516
SMX =172.898
SMXB=1922

ZV =1
*DIST=6.105
*XF =-0.075006
*YF =7.99
    -12173
    -10801
    -9429
    -8057
    -6686
    -5314
    -3942
    -2571
    -1199
    172.898

MX

MN

CEOG Flywheel Evaluation, ANO Unit 2, Shrink Fit Force

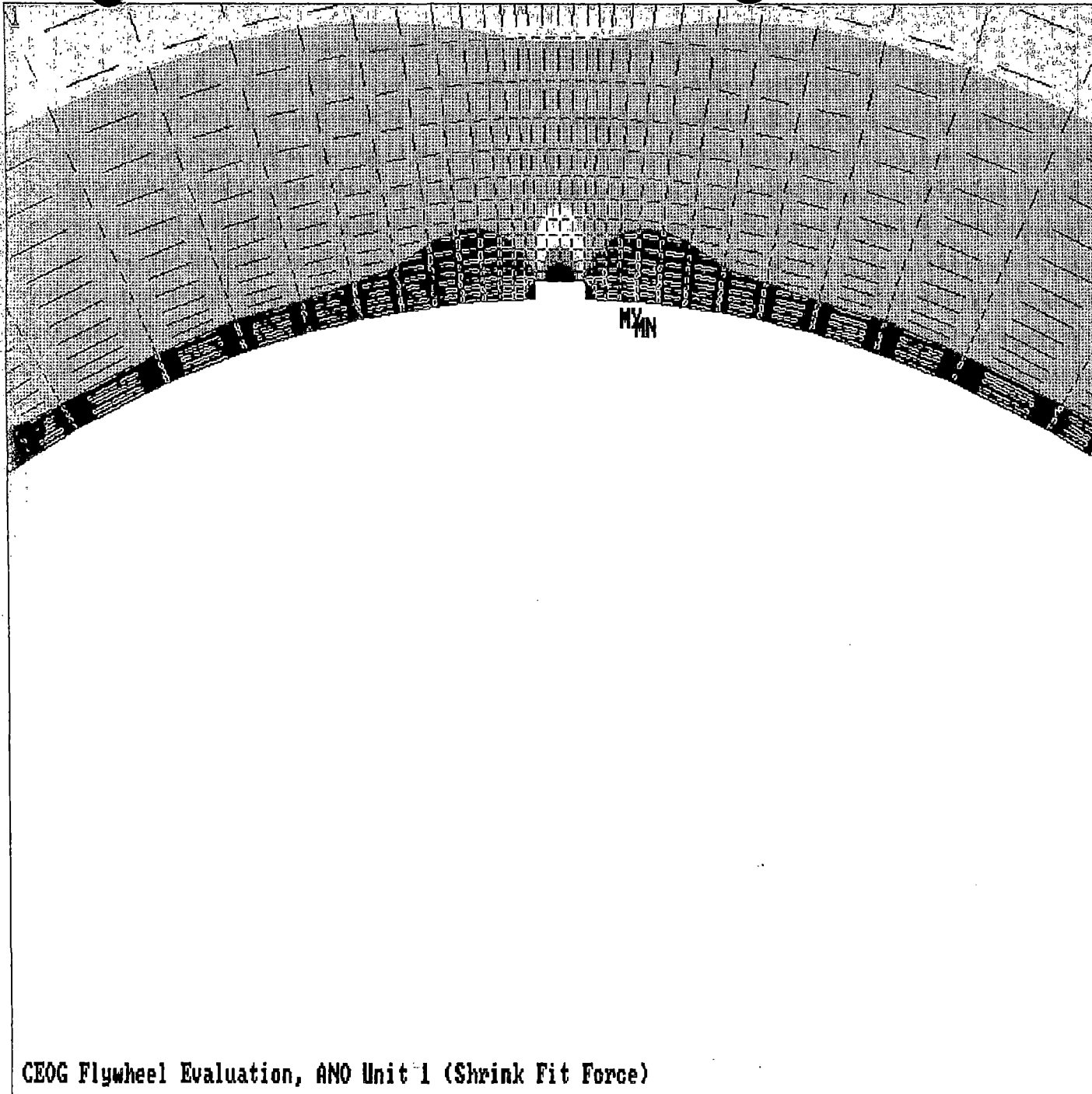Figure 5-47. Details of Radial Stress Distribution in Keyway Region Due to Shrink-Fit Force (ANO-2)

```
ANSYS-PC 4.4A1
AUG 23 1994
  5:53:36
POST1 STRESS
STEP=1
ITER=1
SY   (AVG)
CSYS=1
DMX =0.001033
SMN =-451.372
SMNB=-1728
SMX =6254
SMXB=8072

ZV  =1
DIST=41.25
     -451.372
     293.712
     1039
     1784
     2529
     3274
     4019
     4764
     5509
     6254
```

CEOG Flywheel Evaluation, Millstone, (Shrink Fit Force)

Figure 5-48.   Overall Tangential Stress Distribution Due to Shrink-Fit Force (Millstone-2)

ANSYS-PC 4.4A1
AUG 23 1994
5:59:26
POST1 STRESS
STEP=1
ITER=1
SY   (AVG)
CSYS=1
DMX =0.001033
SMN =-451.372
SMNB=-1728
SMX =6254
SMXB=8072

ZV   =1
*DIST=6.166
*XF =0.342495
*YF =8.174
          -451.372
          293.712
          1039
          1784
          2529
          3274
          4019
          4764
          5509
          6254

CEOG Flywheel Evaluation, Millstone, (Shrink Fit Force)

Figure 5-49. Details of Tangential Stress Distribution in Keyway Region Due to Shrink-Fit Force (Millstone-2)
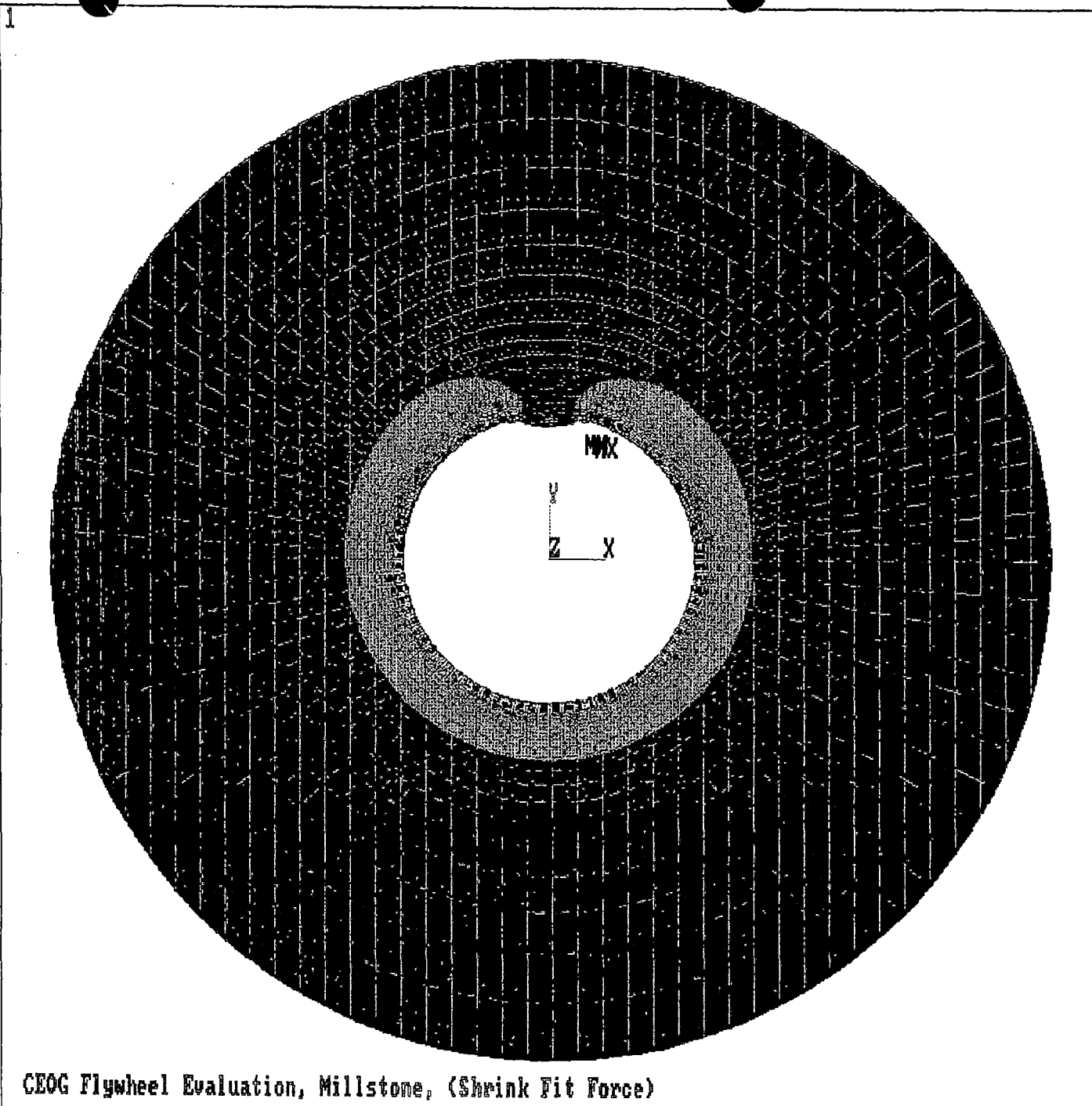
```
ANSYS-PC 4.4A1
AUG 23 1994
 5:47:26
POST1 STRESS
STEP=1
ITER=1
SX   (AVG)
CSYS=1
DMX =0.001033
SMN =-12421
SMNB=-13791
SMX =213.45
SMXB=2031

ZU  =1
DIST=41.25
      -12421
      -11017
      -9614
      -8210
      -6806
      -5402
      -3998
      -2594
      -1190
      213.45
```

CEOG Flywheel Evaluation, Millstone, (Shrink Fit Force)

Figure 5-50. Overall Radial Stress Distribution Due to Shrink-Fit Force (Millstone-2)

Figure 5-51. Details of Radial Stress Distribution in Keyway Region Due to Shrink-Fit Force (Millstone-2)
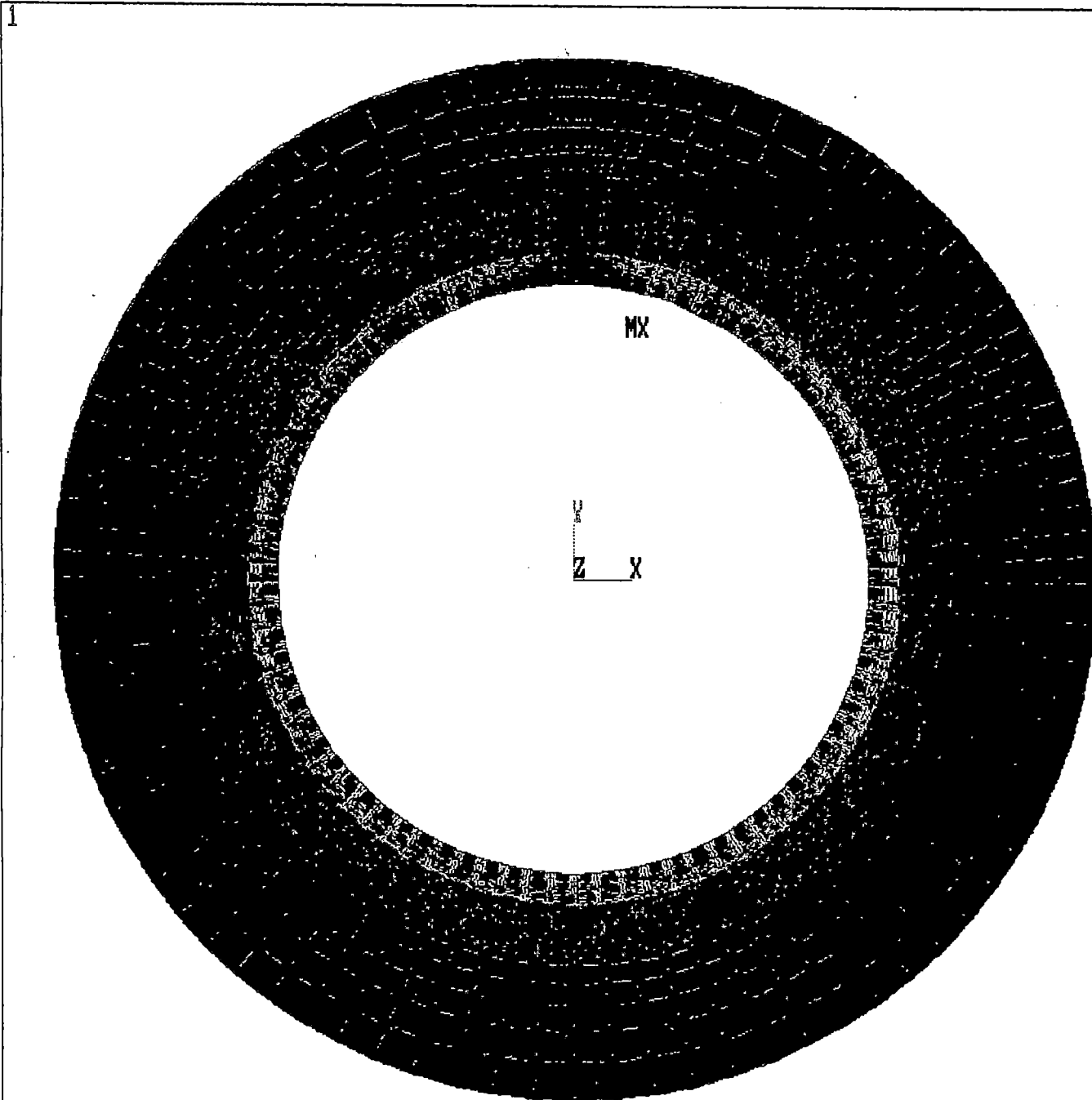
```
ANSYS-PC 4.4A1
AUG 23 1994
 6:16:34
POST1 STRESS
STEP=1
ITER=1
SY   (AVG)
CSYS=1
DMX =0.001
SMN =-571.937
SMNB=-1568
SMX =3505
SMXB=4206

ZV  =1
DIST=39.6
     -571.937
     -118.995
     333.947
     786.889
     1240
     1693
     2146
     2599
     3052
     3505
```

MX

Z   X

CEOG Flywheel Evaluation, Palisades, (Shrink Fit Force)

Figure 5-52. Overall Tangential Stress Distribution Due to Shrink-Fit Force (Palisades)

```
ANSYS-PC 4.4A1
AUG 23 1994
 6:21:44
POST1 STRESS
STEP=1
ITER=1
SY    (AVG)
CSYS=1
DMX =0.001
SMN =-571.937
SMNB=-1568
SMX =3505
SMXB=4206

ZV   =1
*DIST=3.703
*XF  =0.0572
*YF  =14.846
     -571.937
     -118.995
      333.947
      786.889
      1240
      1693
      2146
      2599
      3052
      3505
```

CEOG Flywheel Evaluation, Palisades, (Shrink Fit Force)

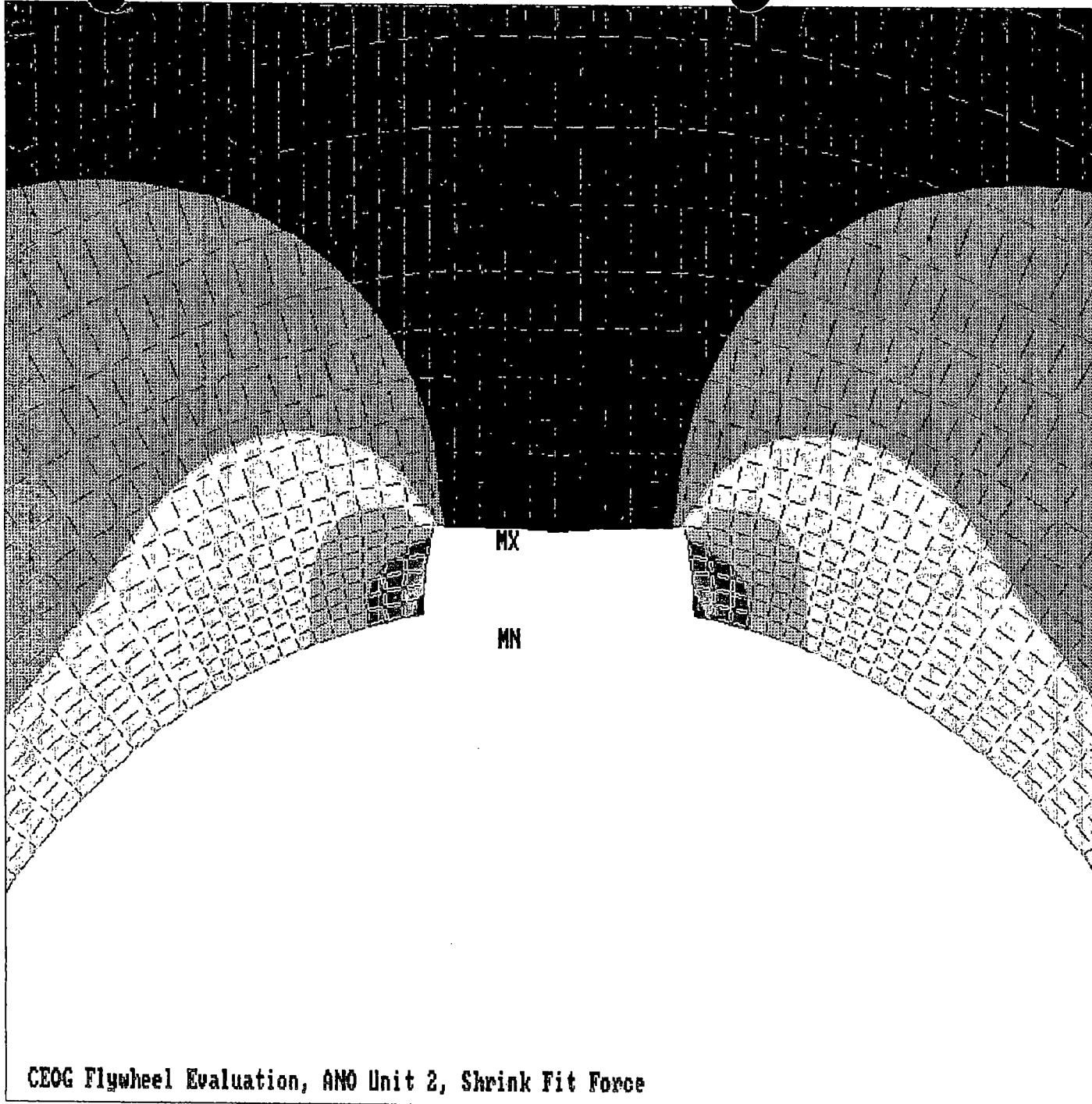Figure 5-53. Details of Tangential Stress Distribution in Keyway Region Due to Shrink-Fit Force (Palisades)

ANSYS-PC 4.4A1
AUG 23 1994
6:14:56
POST1 STRESS
STEP=1
ITER=1
SX   (AVG)
CSYS=1
DMX =0.001
SMN =-5870
SMNB=-7368
SMX =72.403
SMXB=1056

ZV =1
DIST=39.6
-5870
-5209
-4549
-3889
-3229
-2568
-1908
-1248
-587.815
72.403

MIN

CEOG Flywheel Evaluation, Palisades, (Shrink Fit Force)

Figure 5-54. Overall Radial Stress Distribution Due to Shrink-Fit Force (Palisades)

```
ANSYS-PC 4.4A1
AUG 23 1994
  6:19:51
POST1 STRESS
STEP=1
ITER=1
SX   (AVG)
CSYS=1
DMX =0.001
SMN =-5870
SMNB=-7368
SMX =72.403
SMXB=1056

ZV  =1
*DIST=3.703
*XF =0.0572
*YF =14.846
    -5870
    -5209
    -4549
    -3889
    -3229
    -2568
    -1908
    -1248
    -587.815
    72.403
```

CEOG Flywheel Evaluation, Palisades, (Shrink Fit Force)

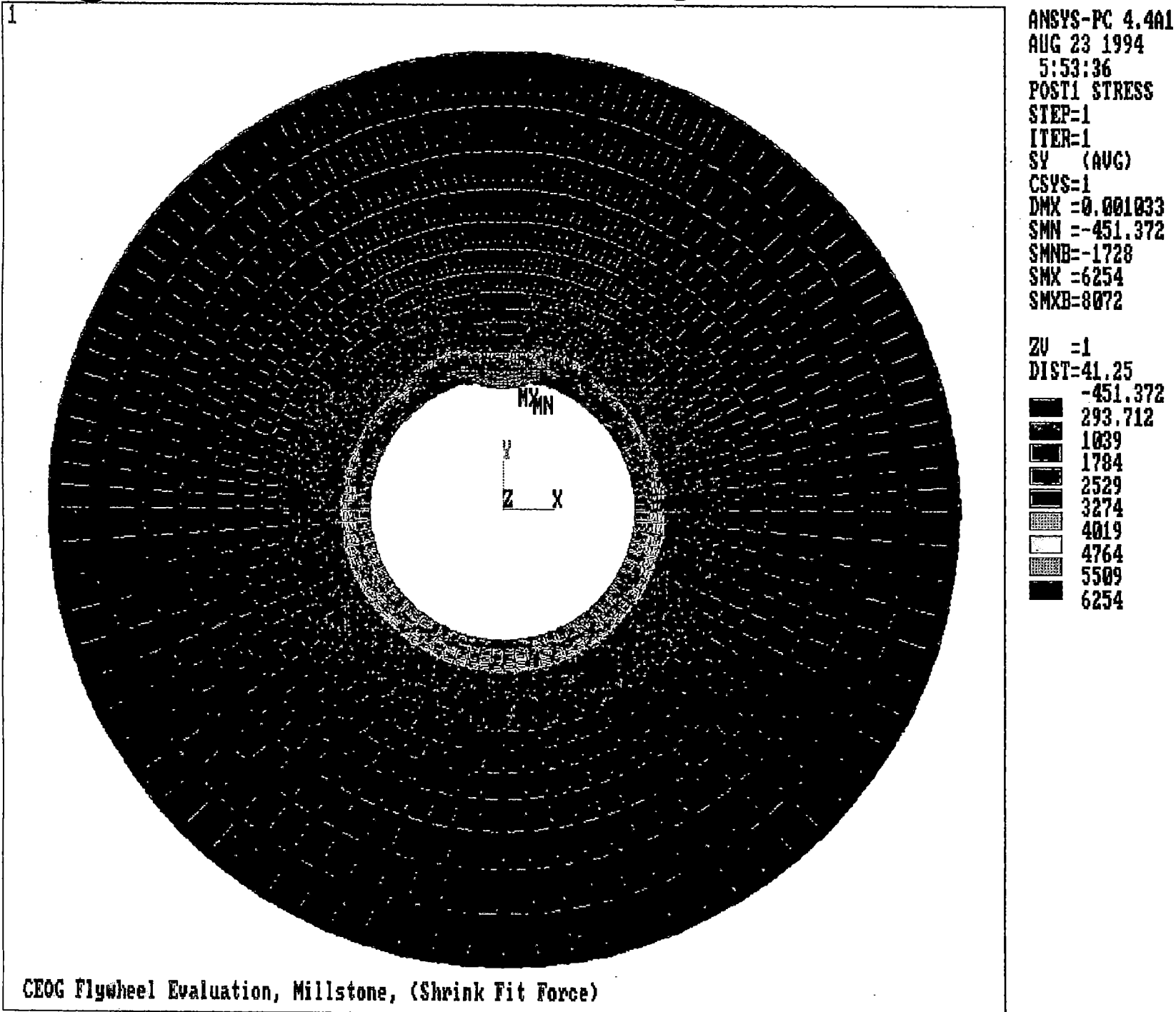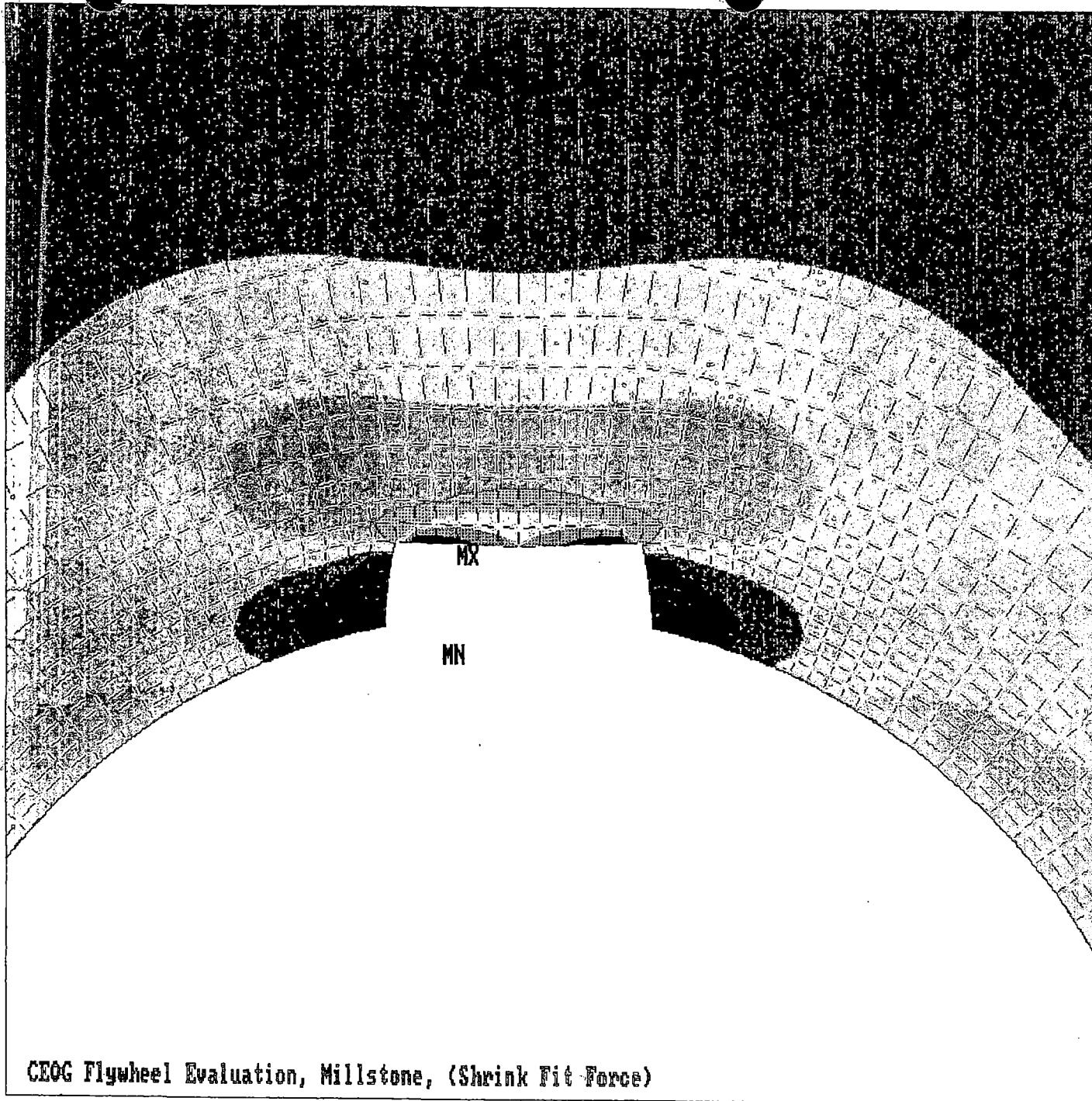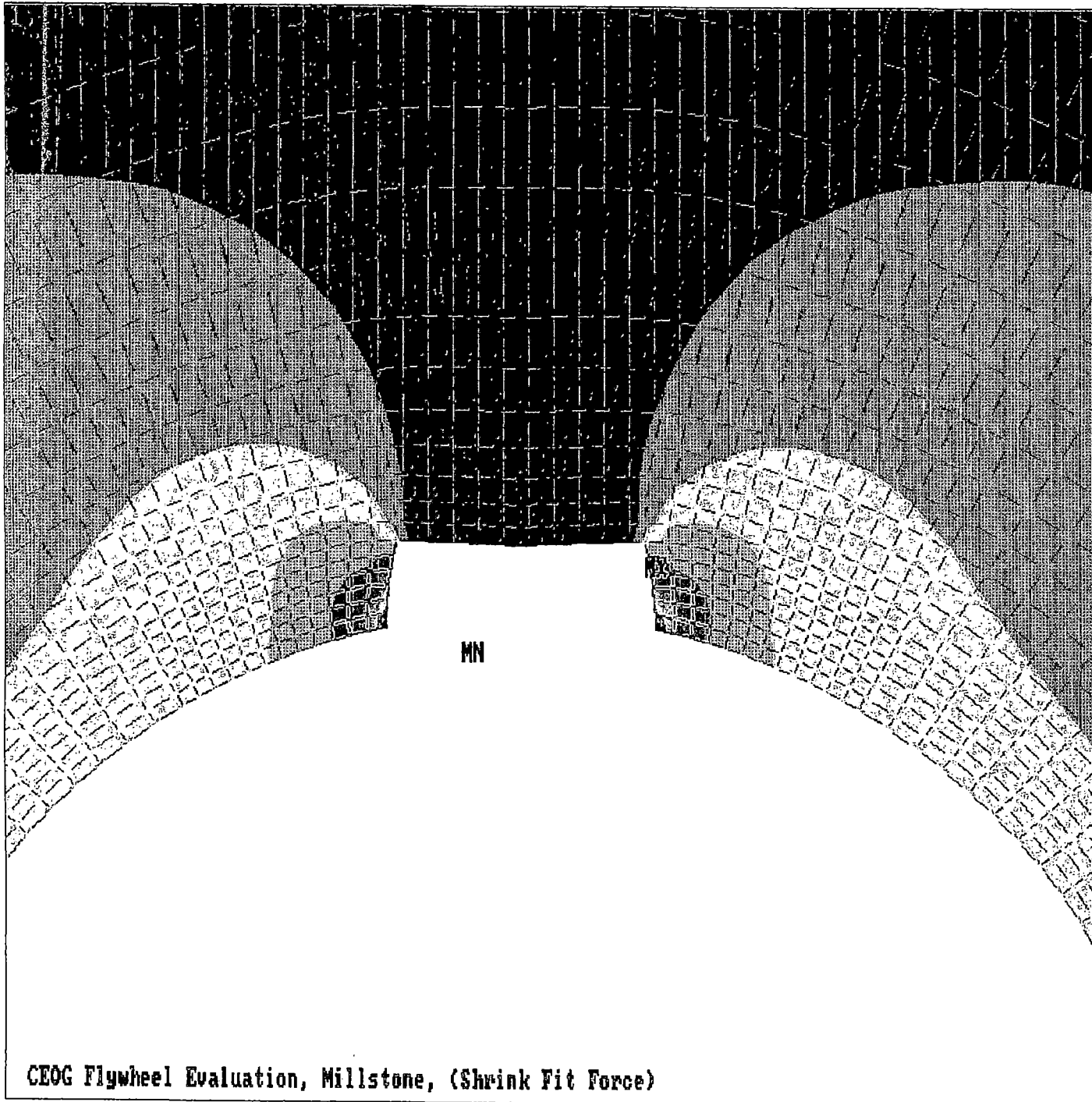Figure 5-55. Details of Radial Stress Distribution in Keyway Region Due to Shrink-Fit Force (Palisades)

ANSYS-PC 4.4A1
JAN 10 1995
16:01:35
POST1 STRESS
STEP=1
ITER=1
SY   (AVG)
CSYS=1
DMX =0.001001
SMN =-561.45
SMNB=-2025
SMX =3651
SMXB=4298

ZV =1
DIST=39.6
         -561.45
         -93.378
         374.695
         842.767
         1311
         1779
         2247
         2715
         3183
         3651

MX

Y
Z   X

CEOG Flywheel Evaluation, St. Lucie (Shrink Fit Force)

Figure 5-56. Overall Tangential Stress Distribution Due to Shrink-Fit Force (St. Lucie)

```
ANSYS-PC 4.4A1
JAN 10 1995
16:09:46
POST1 STRESS
STEP=1
ITER=1
SY    (AVG)
CSYS=1
DMX =0.001001
SMN =-561.45
SMNB=-2025
SMX =3651
SMXB=4298

ZV  =1
*DIST=3.814
*XF =0.065425
*YF =18.632
        -561.45
        -93.378
        374.695
        842.767
        1311
        1779
        2247
        2715
        3183
        3651
```

CEOG Flywheel Evaluation, St. Lucie (Shrink Fit Force)

Figure 5-57. Details of Tangential Stress Distribution in Keyway Region Due to Shrink-Fit Force (St. Lucie)
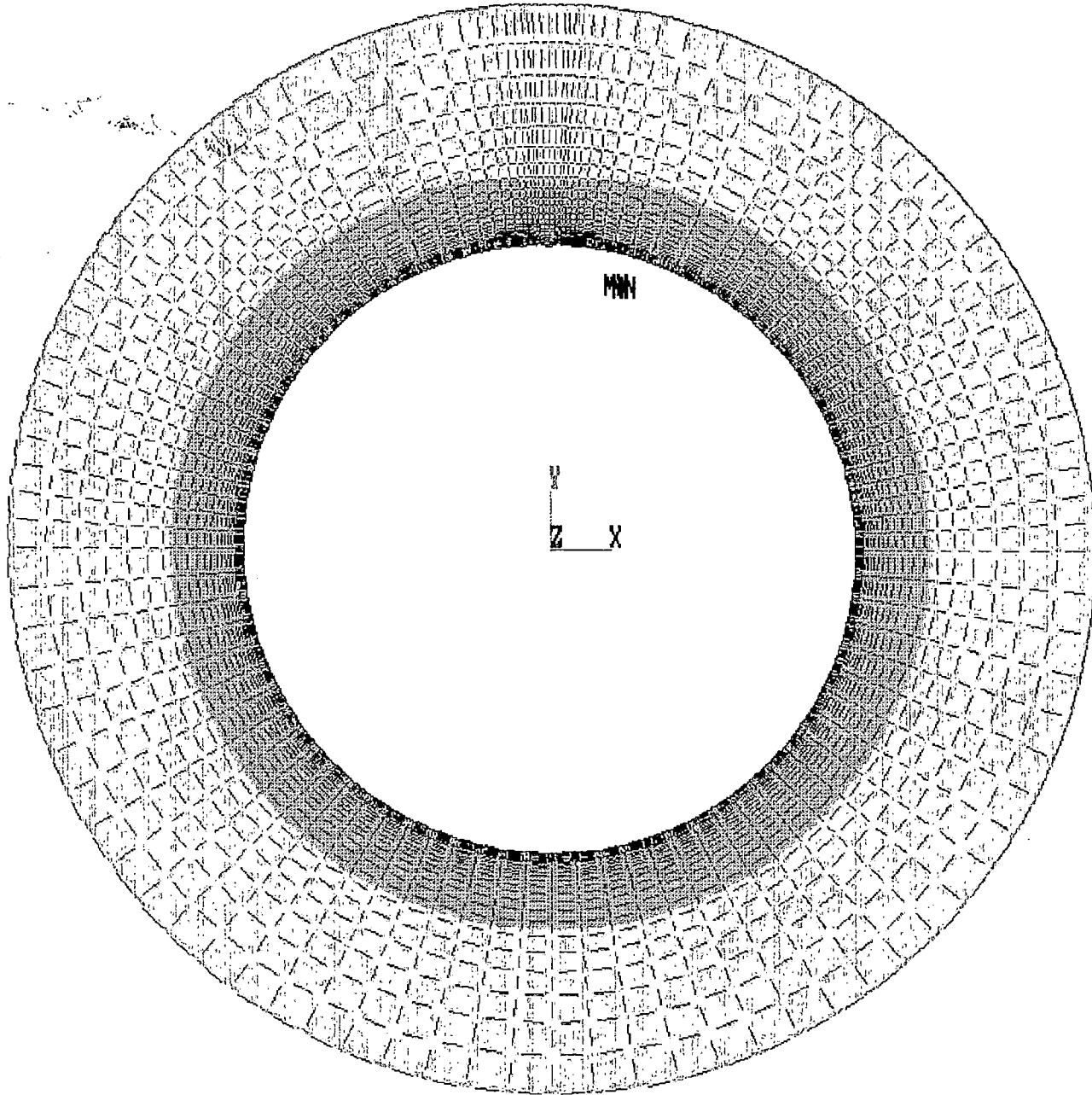
```
1                                                    ANSYS-PC 4.4A1
                                                     JAN 10 1995
                                                     15:58:26
                                                     POST1 STRESS
                                                     STEP=1
                                                     ITER=1
                                                     SX   (AVG)
                                                     CSYS=1
                                                     DMX =0.001001
                                                     SMN =-6097
                                                     SMNB=-7986
                                                     SMX =358.555
                                                     SMXB=1519

                                                     ZV  =1
                                                     DIST=39.6
                                                         -6097
                                                         -5380
                                                         -4662
                                                         -3945
                                                         -3228
                                                         -2511
                                                         -1793
                                                         -1076
                                                         -358.737
                                                         358.555

CE0G Flywheel Evaluation, St. Lucie (Shrink Fit Force)
```
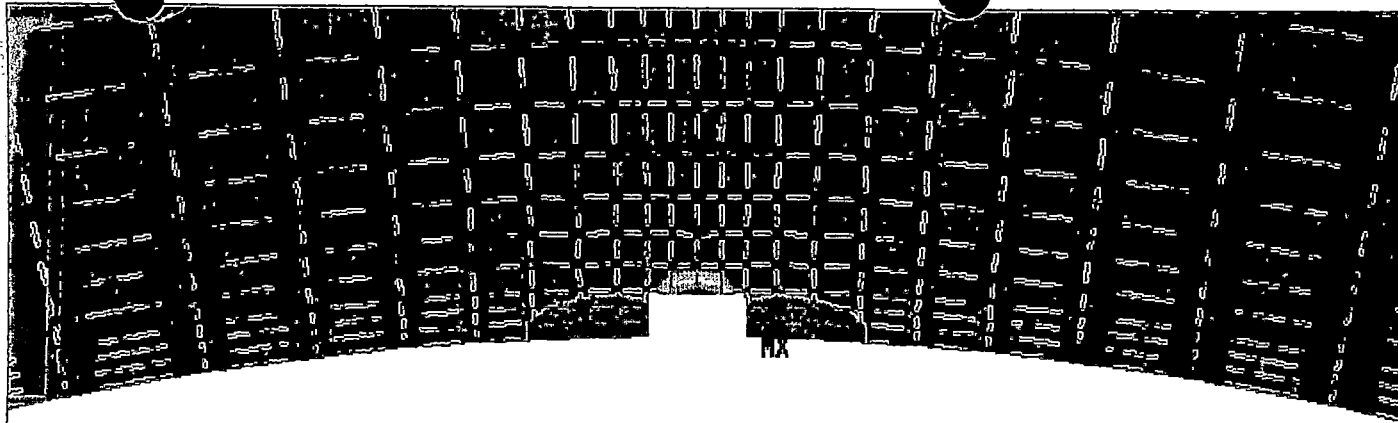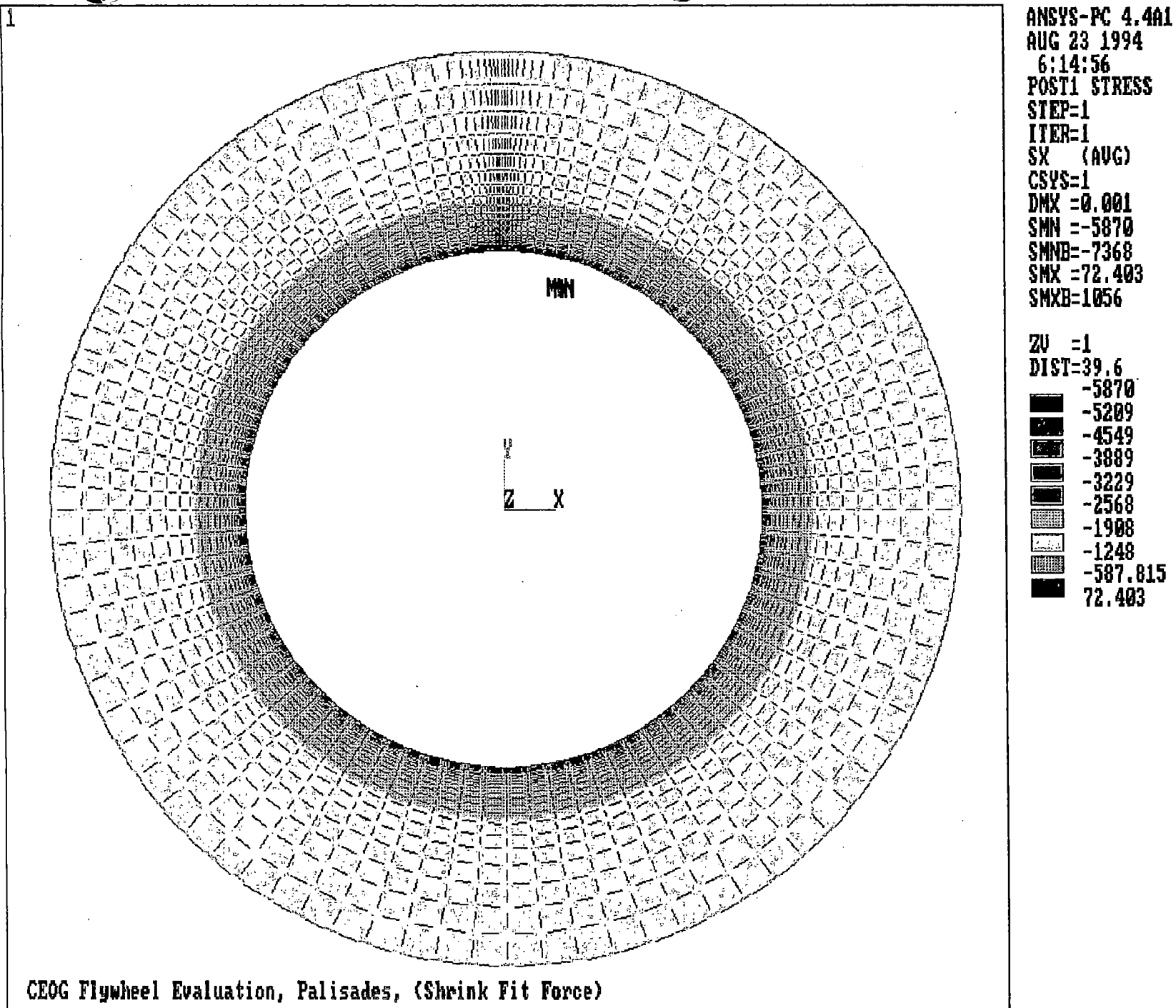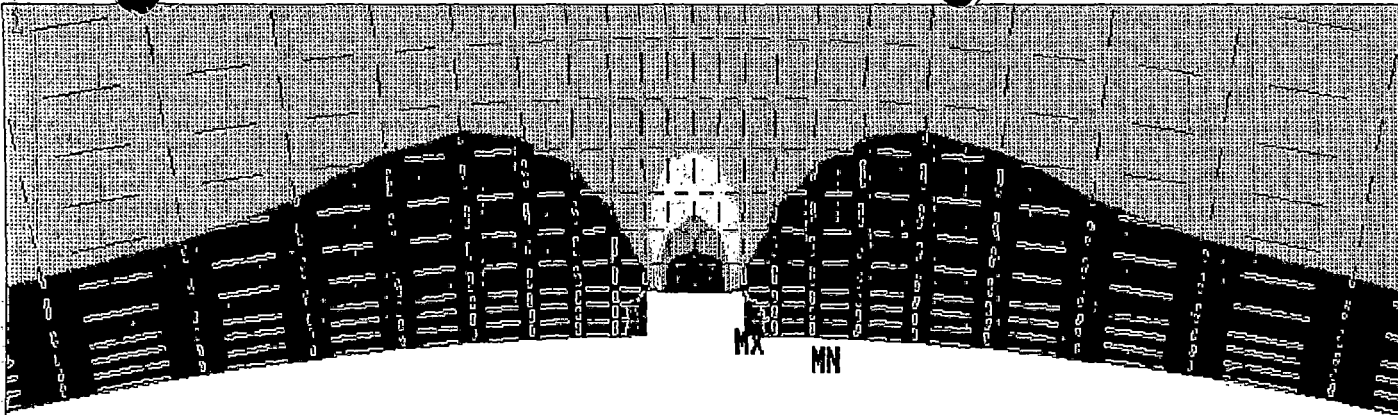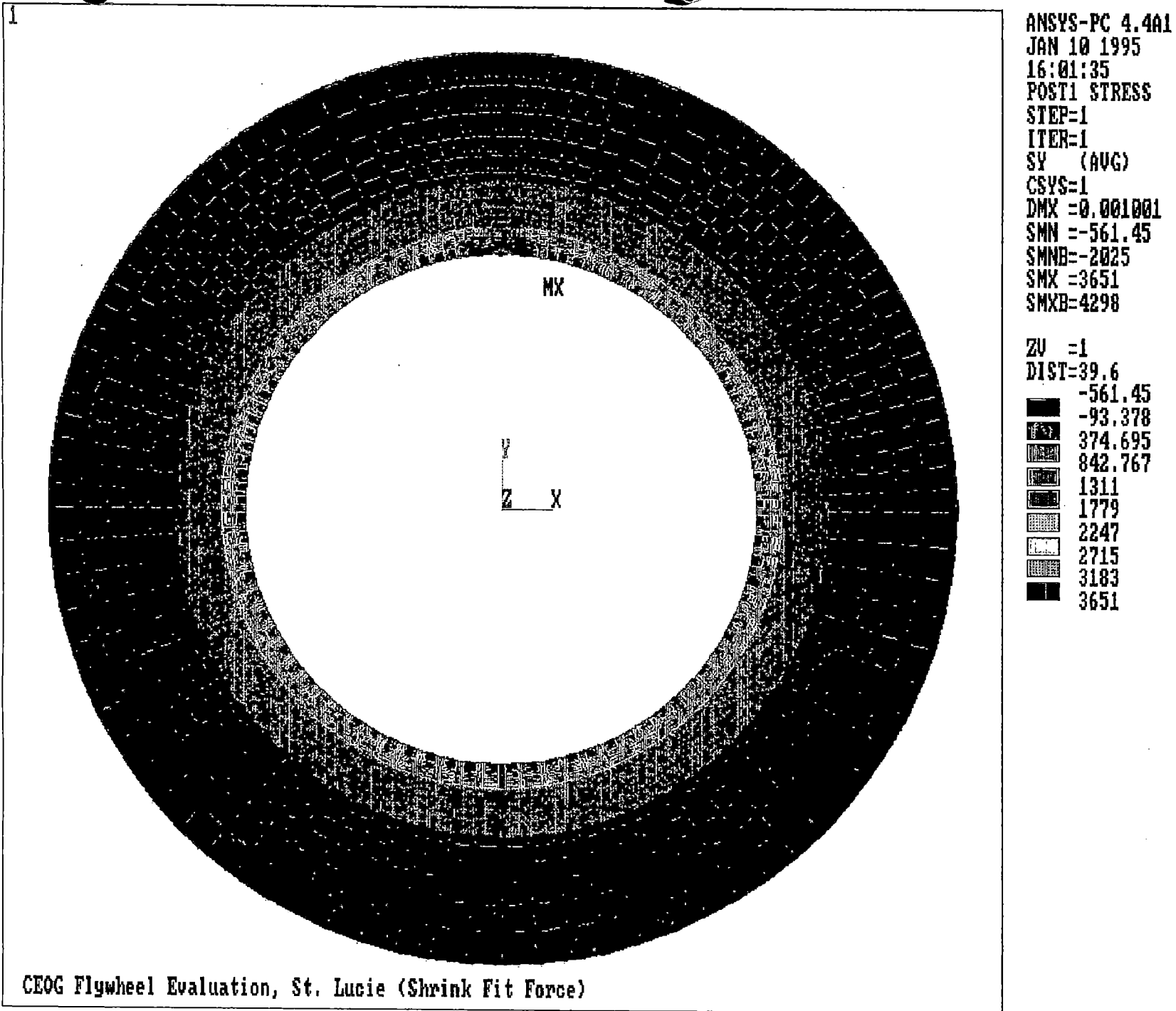
Figure 5-58. Overall Radial Stress Distribution Due to Shrink-Fit Force (St. Lucie)

ANSYS-PC 4.4A1
JAN 10 1995
16:06:14
POST1 STRESS
STEP=1
ITER=1
SX   (AVG)
CSYS=1
DMX =0.001001
SMN =-6097
SMNB=-7986
SMX =358.555
SMXB=1519

ZV =1
*DIST=3.814
*XF =0.065425
*YF =18.632
     -6097
     -5380
     -4662
     -3945
     -3228
     -2511
     -1793
     -1076
     -358.737
     358.555

CEOG Flywheel Evaluation, St. Lucie (Shrink Fit Force)

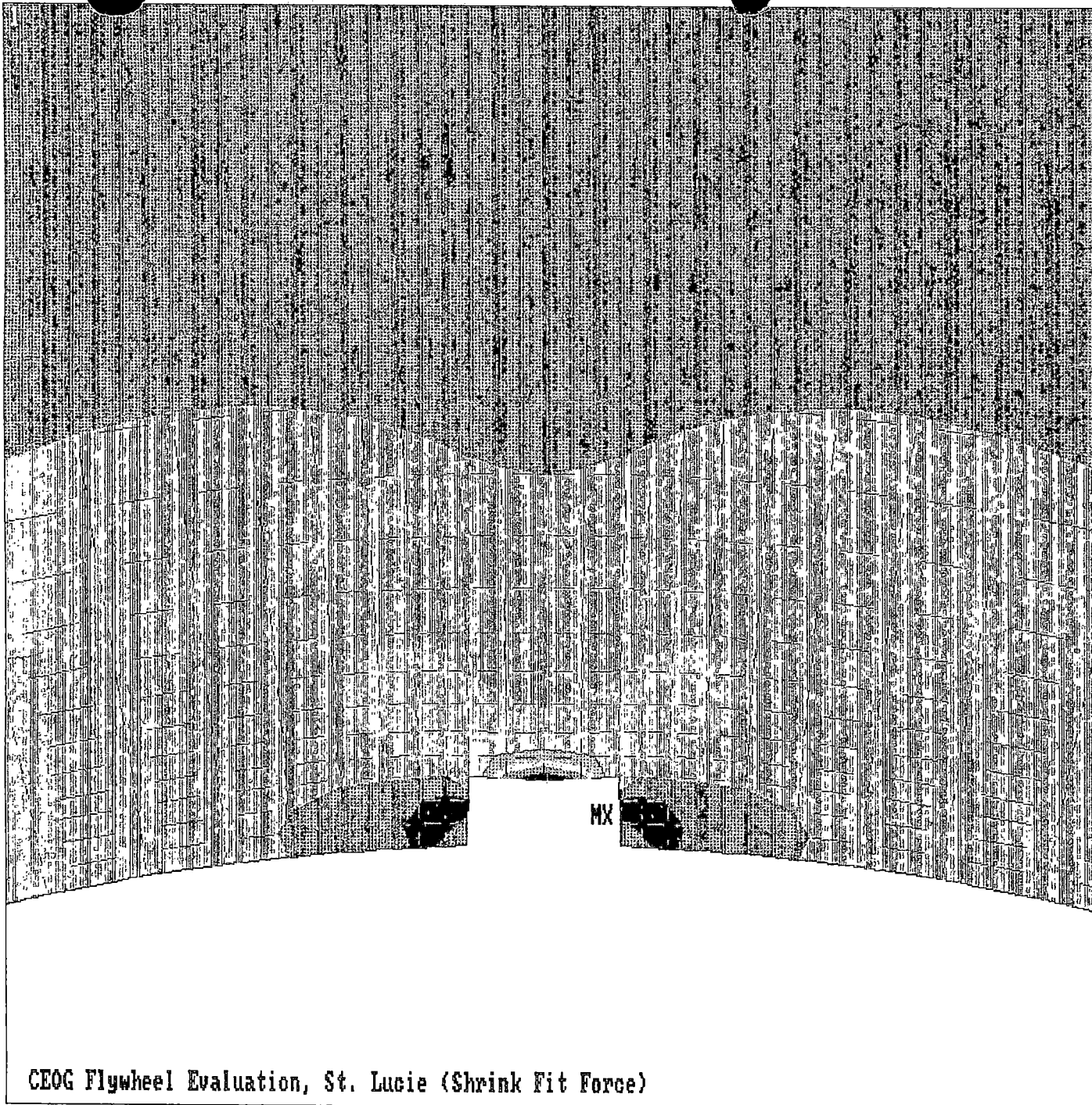Figure 5-59. Details of Radial Stress Distribution in Keyway Region Due to Shrink-Fit Force (St. Lucie)

```
ANSYS-PC 4.4A1
AUG 22 1994
 2:51:15
POST1 STRESS
STEP=1
ITER=1
SY   (AVG)
CSYS=1
DMX =0.001007
SMN =-170.567
SMNB=-1098
SMX =7444
SMXB=8830

ZV  =1
DIST=42.9
     -170.567
     675.45
     1521
     2367
     3214
     4060
     4906
     5752
     6598
     7444
```

CEOG Flywheel Evaluation, Waterford, Shrink Fit Force

Figure 5-60. Overall Tangential Stress Distribution Due to Shrink-Fit Force (Waterford-3)

Figure 5-61. Details of Tangential Stress Distribution in Keyway Region Due to Shrink-Fit Force (Waterford-3)

```
1                                                    ANSYS-PC 4.4A1
                                                     NOV  1 1994
                                                     22:11:57
                                                     POST1 STRESS
                                                     STEP=1
                                                     ITER=1
                                                     SX   (AVG)
                                                     CSYS=1
                                                     DMX =0.001007
                                                     SMN =-10050
                                                     SMNB=-10351
                                                     SMX =11.985
                                                     SMXB=1430

                                                     ZV  =1
                                                     DIST=42.9
                                                          -10050
                                                          -8932
                                                          -7814
                                                          -6696
                                                          -5578
                                                          -4460
                                                          -3342
                                                          -2224
                                                          -1106
                                                          11.985

CEOG Flywheel Evaluation, Waterford, Shrink Fit Force
```
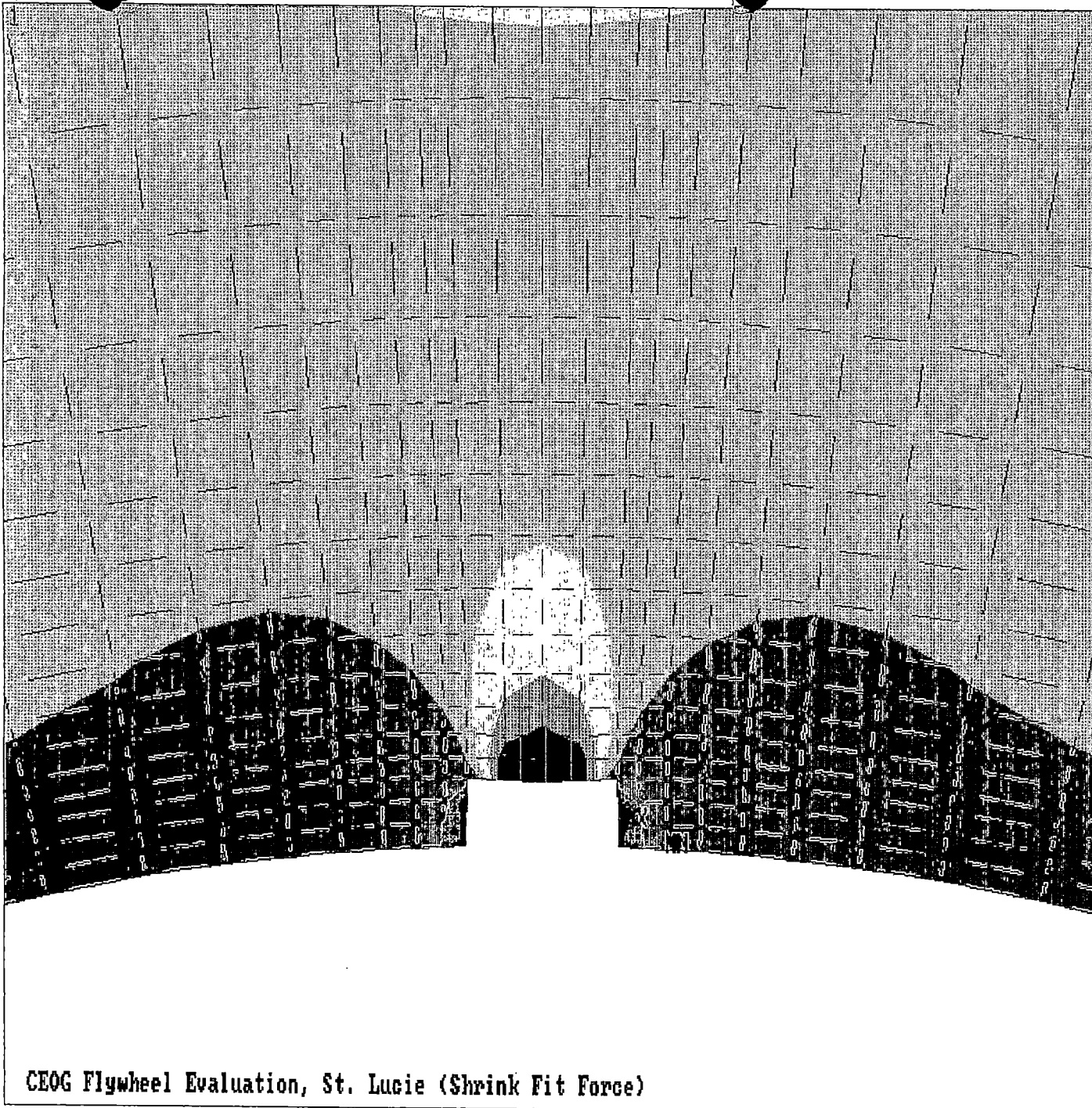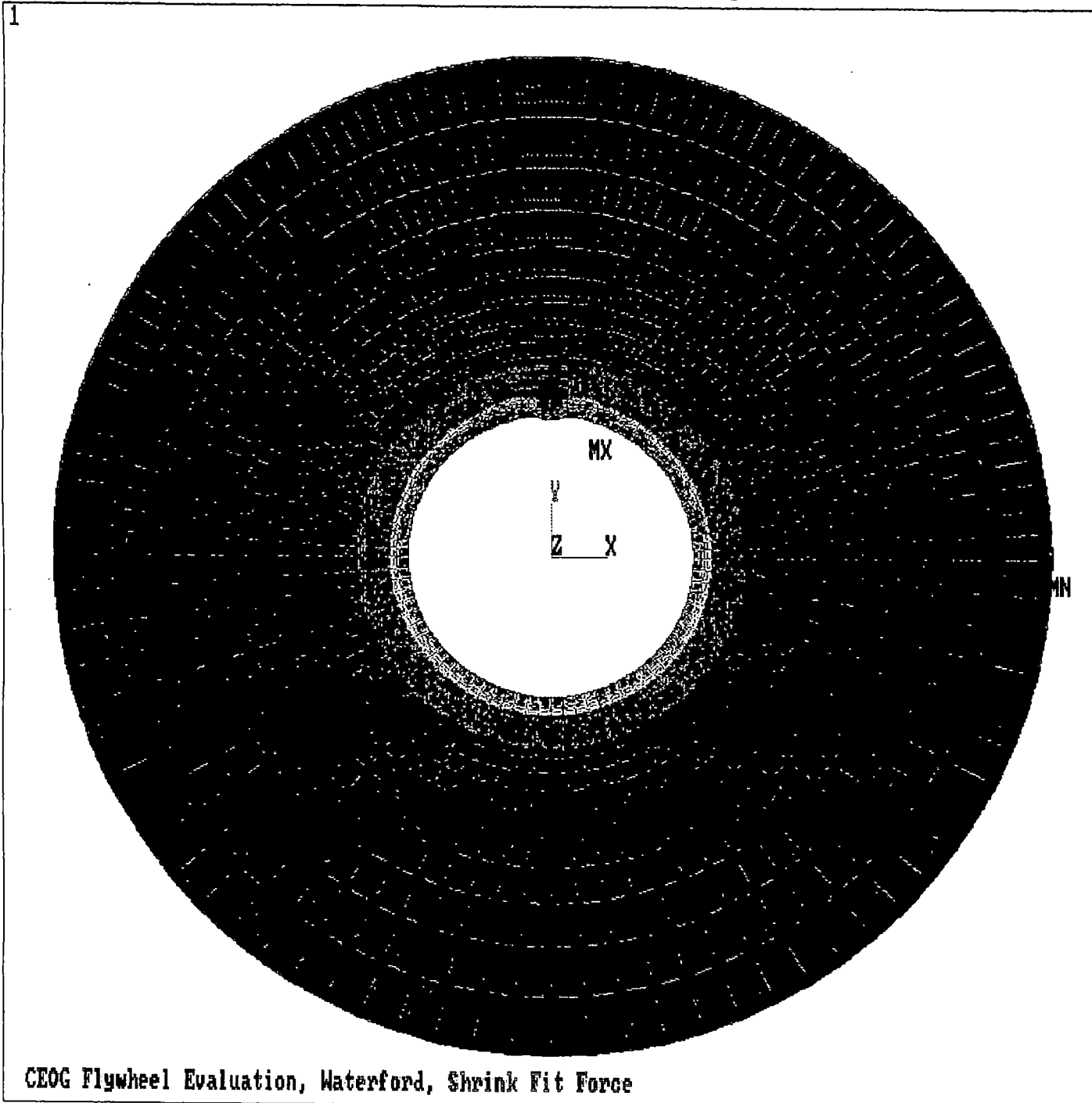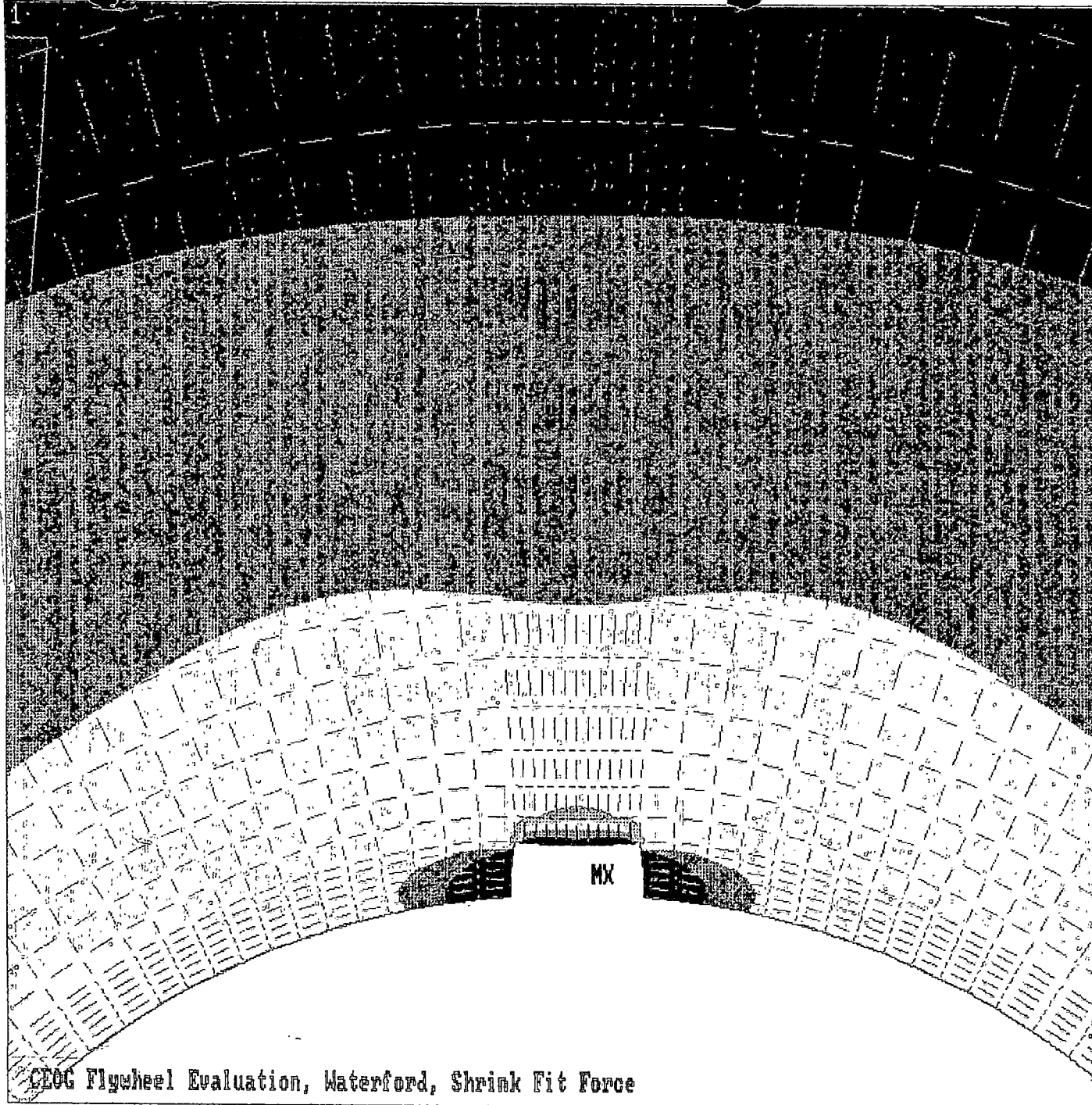
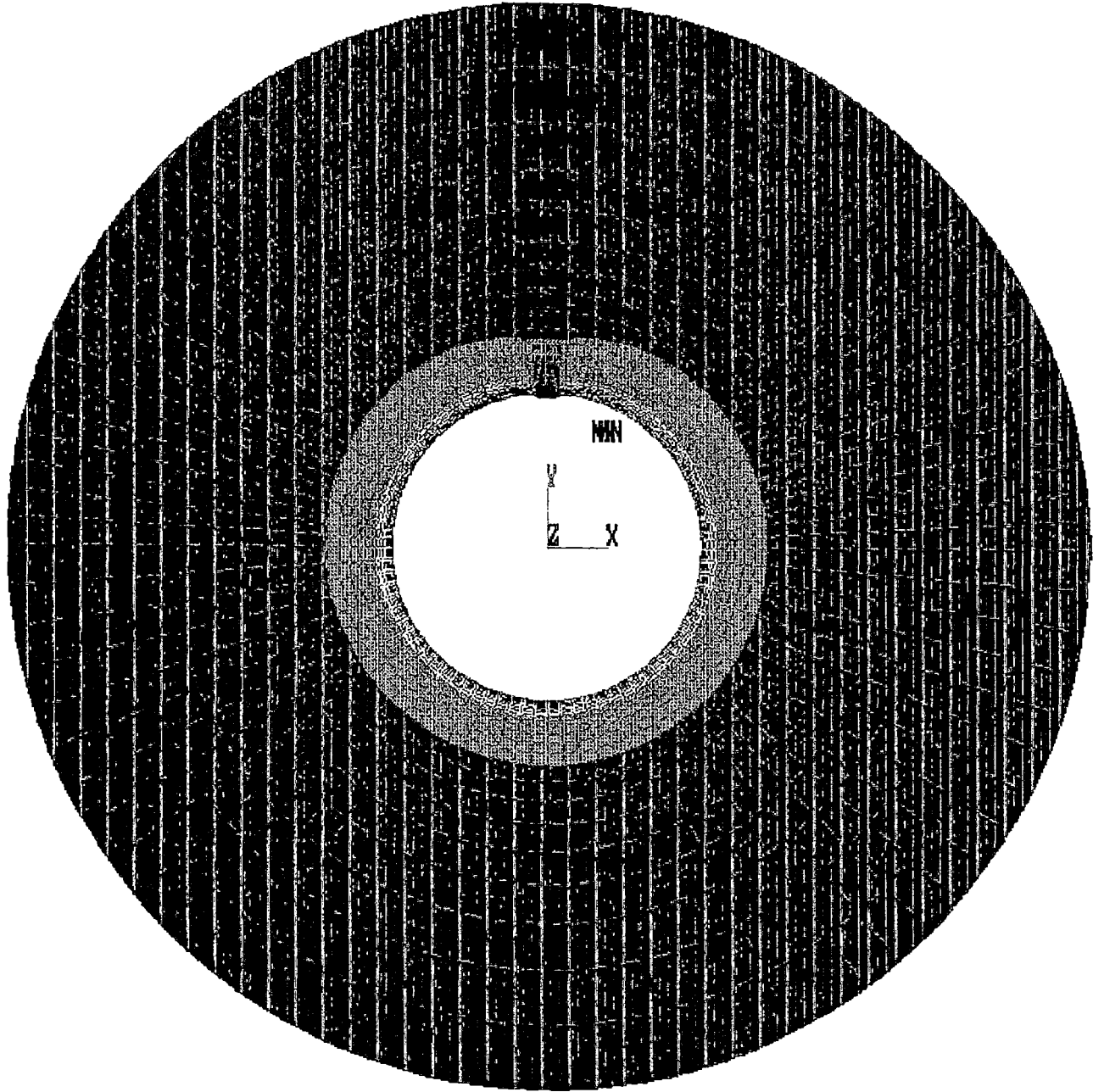Figure 5-62. Overall Radial Stress Distribution Due to Shrink-Fit Force (Waterford-3)

ANSYS-PC 4.4A1
AUG 22 1994
2:55:53
POST1 STRESS
STEP=1
ITER=1
SX   (AVG)
CSYS=1
DMX =0.001007
SMN =-10050
SMNB=-10351
SMX =11.985
SMXB=1430

ZV =1
*DIST=4.854
*XF =-0.214447
*YF =10.354
       -10050
       -8932
       -7814
       -6696
       -5578
       -4460
       -3342
       -2224
       -1106
       11.985

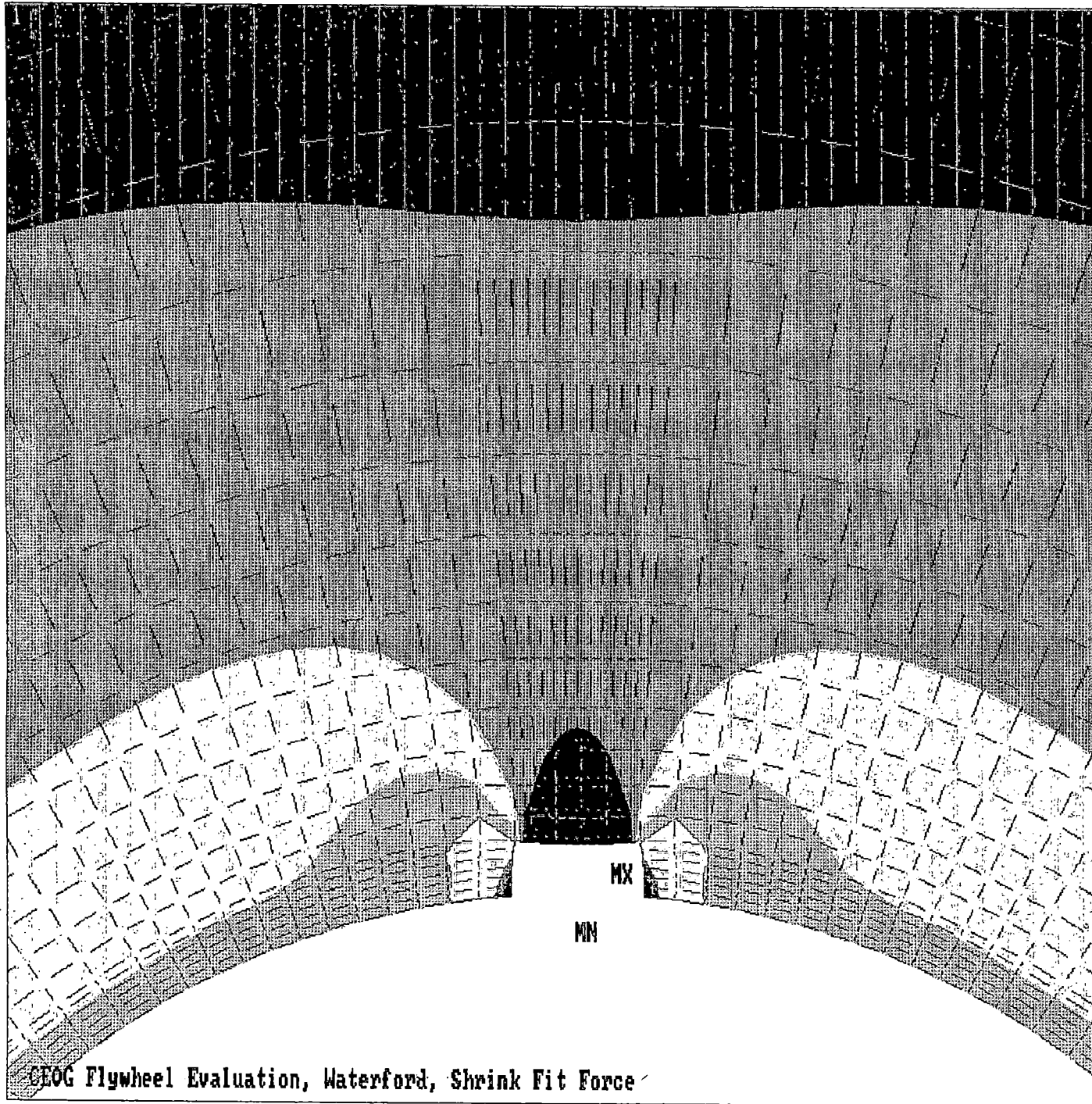CEOG Flywheel Evaluation, Waterford, Shrink Fit Force

Figure 5-63. Details of Radial Stress Distribution in Keyway Region Due to Shrink-Fit Force (Waterford-3)

6.0 FRACTURE MECHANICS EVALUATION

All of the flywheels considered in this evaluation are ferritic steels fabricated either from low alloy pressure vessel steel or carbon steel plate material. For the ferritic steels, the traditional concept used for fracture mechanics analyses in the ASME Code is linear elastic fracture mechanics (LEFM) in which the toughness of the material is assumed to be in the lower-shelf region and hence, the failure mode is brittle fracture.

Even though it can be argued that the flywheels under consideration may be in the transition to the upper-shelf region which will justify the use of elastic-plastic fracture mechanics (EPFM) analyses, LEFM principles are conservatively used in this section to determine allowable flaw sizes and crack growth for the various flywheels. These will then be used to establish safe operating periods which will serve as the basis for establishing alternate inspection intervals for the flywheels.

6.1 Fracture Mechanics Models and Stress Intensity Factor Determination

6.1.1 Centrifugal Stresses

If local discontinuities such as the keyway and the bolt holes are neglected, the stress intensity factor (K_I) for a radial crack emanating from the bore of the flywheel can be calculated using the model of Williams and Isherwood [14], which assumes the flywheel to be a rotating disc. In this model, the expression for K_I is given by

$$K_I = \rho \omega^2 b^{5/2} \phi \left[\frac{\pi(\frac{c}{b} - \frac{a}{b})}{(1-v^2)} \right]^{1/2} \tag{6-1}$$

Structural Integrity Associates, Inc.

where:

$$\phi = \left(\frac{3+v}{32}\right)\left[3\left\{\left[1+\frac{a^2}{b^2}\right]+3\left(\frac{a}{b}\right)\left(\frac{b}{c}\right)+\left[1+\frac{a}{b}+\frac{a^2}{b^2}\right]\frac{\left(1-\frac{a}{b}\right)}{\left(1-\frac{c}{b}\right)}\right\}\right]-\left(\frac{1+3v}{32}\right)$$

$$\left[\frac{\left(\frac{c}{b}\right)^3-\left(\frac{a}{b}\right)^3}{\left(\frac{c}{b}-\frac{a}{b}\right)}+\frac{1}{3}\frac{\left(1-\frac{a}{b}\right)^3}{\left(1-\frac{c}{b}\right)}\right]$$

(6-2)

where:

a = bore radius (in.)

b = outer radius (in.)

c = crack depth measured from the center of flywheel (in.)

ρ = mass density (lb/in^3)

ω = rotational speed (rad/s)

v = Poisson's ratio

As explained in Reference 12, this model can be used for a crack emanating from a keyway except that in this case, the keyway depth is included as part of the total crack depth. It is also explained in Reference 12 that the above equations give an erroneous value of stress intensity for zero crack depth if the keyway depth is added to the crack depth. Moreover, as was seen in Section 4, the stresses at the keyway are considerably higher than the areas which are remote from the keyway.

To accurately account for the effect of the keyway, other fracture mechanics models were considered for the evaluation using the stress distributions obtained in Section 5. For the larger bore flywheels of ANO-1, Palisades and St. Lucie 1 & 2, a model consisting of a longitudinal crack in a cylinder, as shown in Figure 6-1, was chosen. This model, though conservative in that it applies to infinitely long cracks, matches the t/R ratio for the

Structural Integrity Associates, Inc.

flywheels, as can be seen from Table 2-1. For the smaller bore flywheels of ANO-2, Millstone-2 and Waterford 3, which have considerably larger t/R ratios, a model consisting of a crack emanating from a hole in an infinite plate, shown in Figure 6-2, was chosen. Both of these models are featured in the **pc-CRACK** [15], computer program library and therefore were readily available for use in the evaluation.

It should be noted from Figures 6-1 and 6-2 that in order to use these models, the stress distribution in the critical keyway region has to be established. Hence, the tangential stress distributions obtained for the critical keyway regions in Figures 5-28 through 5-33 were curve-fit using **pc-CRACK** to describe the stress distribution. In curve-fitting these stress distributions, a radia distance of 2 inches from the keyway was considered in order to obtain an accurate fit, since the allowable flaw size is expected to be limited to this value for all the flywheels. The resulting stress intensity factor distribution versus crack size from the keyway for the flywheels are shown in Figures 6-3 through 6-8.

6.1.2   Shrink-fit Stresses

The same models used for the determination of stress intensity factors for the centrifugal stresses were used to determine the stress intensity factors for the shrink-fit stresses. Once again, the shrink-fit stresses determined in the previous section were curve-fit using the **pc-CRACK** software over a relatively short distance (about 2 inches) from the bore. Shrink-fit displacements have been determined to be 12.5 mils for the large-bore diameter flywheels, (ANO-1, Palisades, St. Lucie 1 & 2) and 5.2 mils for the small-bore diameters (ANO-2, Millstone, Waterford). Therefore, the stresses have been scaled accordingly. The resulting stress intensity factor distribution versus crack size are shown in Figures 6-3 through 6-8 for all the flywheels.

Structural Integrity Associates, Inc.

6.2 Fracture Toughness

The fracture toughness (K_{Ic}) values of the materials of the flywheels considered in this evaluation have been detailed extensively in References 4 through 9 and summarized in Table 6-1. These K_{Ic} values represent conservative minimum values from References 4 through 9. Some of these values were obtained at values below the normal operating temperatures of 100 - 110°F for the flywheels, and represent extreme lower bounds of the material qualification test. Therefore, considerably higher toughness values than those shown in Table 6-1 can be justified. For the purpose of this study, a minimum K_{Ic} value of 100 ksi$\sqrt{in}$ will be conservatively used.

6.3 Allowable Flaw Size Determination

Since the flywheels were all fabricated from ferritic plate material, the allowable flaw sizes can be determined using paragraph IWB-3610 of the ASME Code, Section XI [16]. The acceptance criteria can be determined based on flaw size or applied stress intensity. The acceptance criteria based on flaw size is given as: ·

$$a_f < 0.1 \, a_c$$
$$a_f < 0.5 \, a_i \tag{6-3}$$

where:

a_f = the maximum size to which the detected flaw is calculated to grow in a specified time period, which can be the next scheduled inspection of the component, or until the end of vessel design lifetime.

a_c = the minimum critical flaw size of the flaw under normal operating conditions.

a_i = the minimum critical flaw size of the flaw for initiation of non-arresting growth under postulated emergency and faulted conditions.

Structural Integrity Associates, Inc.

The acceptance criteria, based on stress intensity factor is provided separately for normal operating and emergency/faulted conditions as follows:

a) For normal conditions:

$$K_I < K_{Ia} / \sqrt{10} \qquad\qquad (6\text{-}4)$$

where:

K_I = the maximum applied stress intensity factor for normal (including upset and test) conditions for the flaw size a_f.

K_{Ia} = the available fracture toughness based on crack arrest for the corresponding crack tip temperature.

b) For emergency and faulted conditions:

$$K_I < K_{Ic} / \sqrt{2} \qquad\qquad (6\text{-}5)$$

where:

K_I = the maximum applied stress intensity factor for the flaw size a_f under emergency and faulted conditions.

K_{Ic} = the available fracture toughness based on fracture initiation for the corresponding crack tip temperature.

In this evaluation, the acceptance criteria, based on stress intensity represented by Equations 6-4 and 6-5 above are used. However, the safety margins on stress intensity factor of 3.0 and 1.4 are used for normal operating and faulted conditions, respectively, for consistency with the original Section III design margins for these loading conditions. At normal operating speed, the allowable criteria of Equation 6-4 is used while at accident speed, the criteria of Equation 6-5 is used. Accident speeds were not readily available for plants considered in this evaluation. A value of 150% of normal operating speed was selected as an upper bound (25% greater than the design overspeed). This value is generally limited by other

Structural Integrity Associates, Inc.

considerations such as the speed for electrical breaking effects of the motor which for one plant is specified as 105% of normal speed. Because the stresses and the stress intensity factors increase by the square of the speed, all the stress intensity factors determined for the normal operating conditions were factored by 2.25 to determine those for the accident condition. In addition, the critical flaw size for the most conservative LOCA overspeed case (2359 rpm at ANO-2) will be calculated and compared to the predicted balance-of-plant life flaw size to ensure that even for this severe and unlikely scenario, the flywheel integrity is maintained.

To determine the allowable flaw size, it should be noted that the maximum centrifugal stresses occur at maximum speed when the shrink-fit stresses are minimum and close to zero. The shrink-fit stresses are maximum at zero speed when the centrifugal stresses are zero. Therefore, the stress intensity distribution for the centrifugal and the shrink-fit stresses are compared separately with the allowable fracture toughness to determine the allowable flaw sizes. The minimum of the two is chosen as the allowable flaw size. The comparisons of the stress intensity factor distribution for normal operating speed with the allowable fracture toughness are shown in Figures 6-3 through 6-8 while the comparison for the accident case is shown in Figures 6-9 through 6-14. The allowable flaw size corresponds to the intersection of the stress intensity curve with the allowable fracture toughness curve. The minimum of either the centrifugal or the shrink-fit is chosen as the allowable flaw size. The allowable flaw sizes for the various flywheels are summarized in Table 6-2 for both normal and accident speeds. It can be seen from this table that for all the flywheels considered in this evaluation, the minimum allowable flaw size is 1.0 inch. It can be seen from Figures 6-3 through 6-14 that if the actual fracture toughness is considered, there is a very considerable margin before actual fracture will occur. When the most conservative LOCA overspeed case (ANO-2) is considered, the critical flaw size is about 0.8 inch, which is consistent with what was obtained in the study presented in Reference 5.

6.4 Crack Growth Evaluation

As discussed in Section 4, there are no other degradation mechanisms which will result in the propagation of existing cracks in the flywheel, other than fatigue. Hence, in this section, a fatigue crack growth evaluation is performed to determine the growth of pre-existing cracks. The flywheels are remote from the reactor coolant water and therefore the

Structural Integrity Associates, Inc.

environment is air. As such, the fatigue growth law for air environment in ASME Code Section XI Appendix A for ferritic steels is used. This law is given as,

$$\frac{da}{dN} = C_o(\Delta K)^n$$

where:

$$n \quad = \quad 3.07$$
$$C_o \quad = \quad 1.99 \times 10^{-10} \, S$$
$$S \quad = \quad 25.72 \, (2.88 \, R)^{-3.07}$$
$$R \quad = \quad K_{min}/K_{max} \quad 0 \leq R < 1$$
$$\Delta K \quad = \quad \text{range of applied stress intensity factor}$$

In performing fatigue crack growth analysis, the initial flaw size is an important input parameter. As can be seen from Tables 3-1 through 3-6, no flaw indications have been identified to date in any of the flywheels as a result of the RG 1.14 mandated inspections and, therefore, the initial flaw size was based on the maximum flaw size that could have been missed during these inspections. This, in turn, is dependent on the sensitivity and accuracy of the UT transducers used during the inspections. Discussions with several participants in this program produced varying maximum flaw sizes that could possibly have been missed during these inspections. A conservative value of 0.25 inches was used as initial flaw size in the evaluations.

The design number of startup/shutdown cycles for the RCP motor is no more than 500 for plant life. However, for this evaluation, a conservative 4000 cycles were considered to determine the crack growth. The results of the analysis are summarized in Table 6-3 and show that crack growth is very insignificant. The initial flaw size of 0.25 inches grew to, at most, 0.27 inches after 4000 cycles. This final crack size is significantly below the allowable flaw sizes calculated previously in this section. This demonstrates that fatigue crack growth is not a concern in the assessment of the structural integrity of the flywheels. Considering the maximum flaw size that could have been missed during previous inspections, the flywheels can operate for a significant number of cycles beyond plant life without concern for their structural integrity.

Structural Integrity Associates, Inc.

Table 6-1

Fracture Toughness Values

Plant Name	Flywheel Material	Minimum Fracture Toughness (K_{Ic}) ksi $\sqrt{in}$	Reference
ANO-1	ASTM-A-516 Cir. 65	109.6	4
ANO-2	ASTM-A-533 Gr. B, Cl. 1	100	5
Millstone-2	ASTM-A-516 Gr. 70	90	6
Palisades	ASTM-A-108	100	7
St. Lucie 1	ASTM-A-516, Gr. 70	90	8
St. Lucie 2	ASTM-A-543 Gr. B, Cl.	100	8
Waterford-3	ASTM-A-543 Gr. B, Cl. 1	100	9

Table 6-2

Allowable Flaw Sizes

Plant Name	Allowable Flaw Size (in)	
	Normal Operating Speed	Accident Speed
ANO-1	1.24	1.00
ANO-2	>2.00	>2.00
Millstone-2	1.64	>2.00
Palisades	>2.00	>2.00
St. Lucie 1	>2.00	>2.00
St. Lucie 2	>2.00	>2.00
Waterford-3	1.24	1.00

Structural Integrity Associates, Inc.

Table 6-3

Crack Growth Evaluation Results

Plant Name	Initial Flaw Size (in.)	Final Flaw[1] Size (in.)
ANO-1	0.25	0.2605
ANO-2	0.25	0.2557
Millstone-2	0.25	0.2535
Palisades	0.25	0.2515
St. Lucie 1	0.25	0.2519
St. Lucie 2	0.25	0.2519
Waterford-3	0.25	0.2686

Note:

1. Based on 4000 startup/shutdown cycles

Structural Integrity Associates, Inc.

$$\sigma = C_0 + C_1 X + C_2 X^2 + C_3 X^3$$

C_0: inner surface stress $(x = 0)$
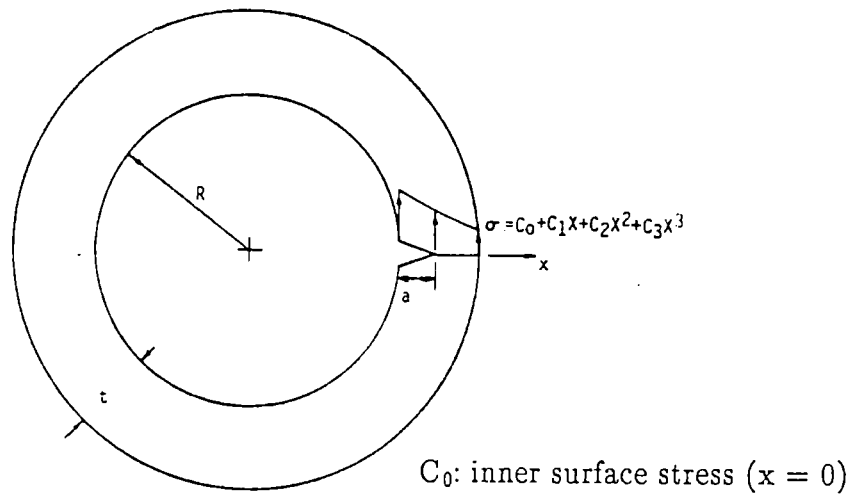
REQUIRED INPUTS:

t: wall thickness
a: crack depth $(a_{max} \leq 0.8t)$

Figure 6-1.   LEFM Crack Model H from **pc-CRACK** - Longitudinal Crack in Cylinder $(t/R = 1.2)$

Structural Integrity Associates, Inc.

$$\sigma = C_0 + C_1 X + C_2 X^2 + C_3 X^3$$
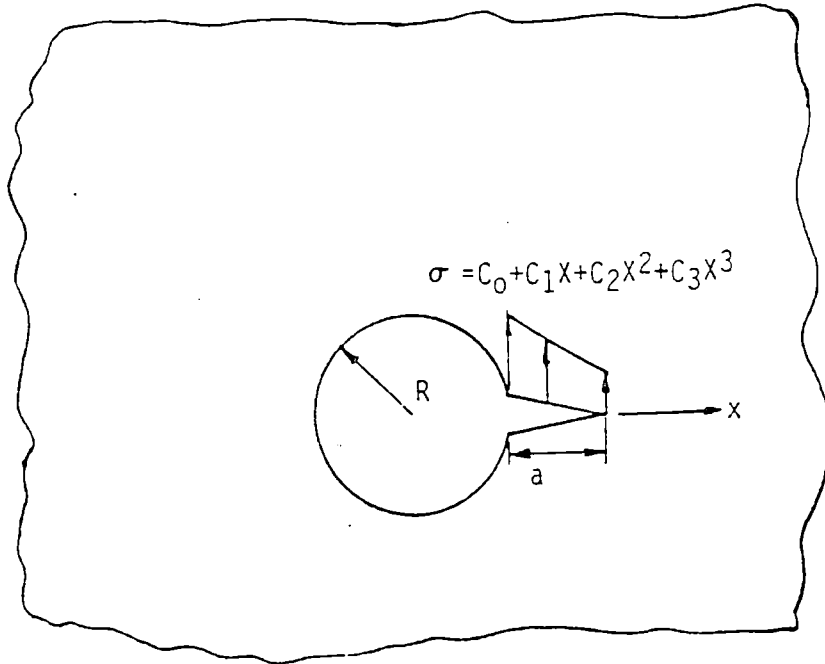
C_0: surface stress $(x = 0)$

REQUIRED INPUTS:

R: hole radius
a: crack depth $(a_{max} \leq 2.0R)$

Figure 6-2.   LEFM Crack Model I from **pc-CRACK** - Crack Emanating from Hole in an Infinite Plate

Structural Integrity Associates, Inc.

Structural Integrity Associates, Inc.
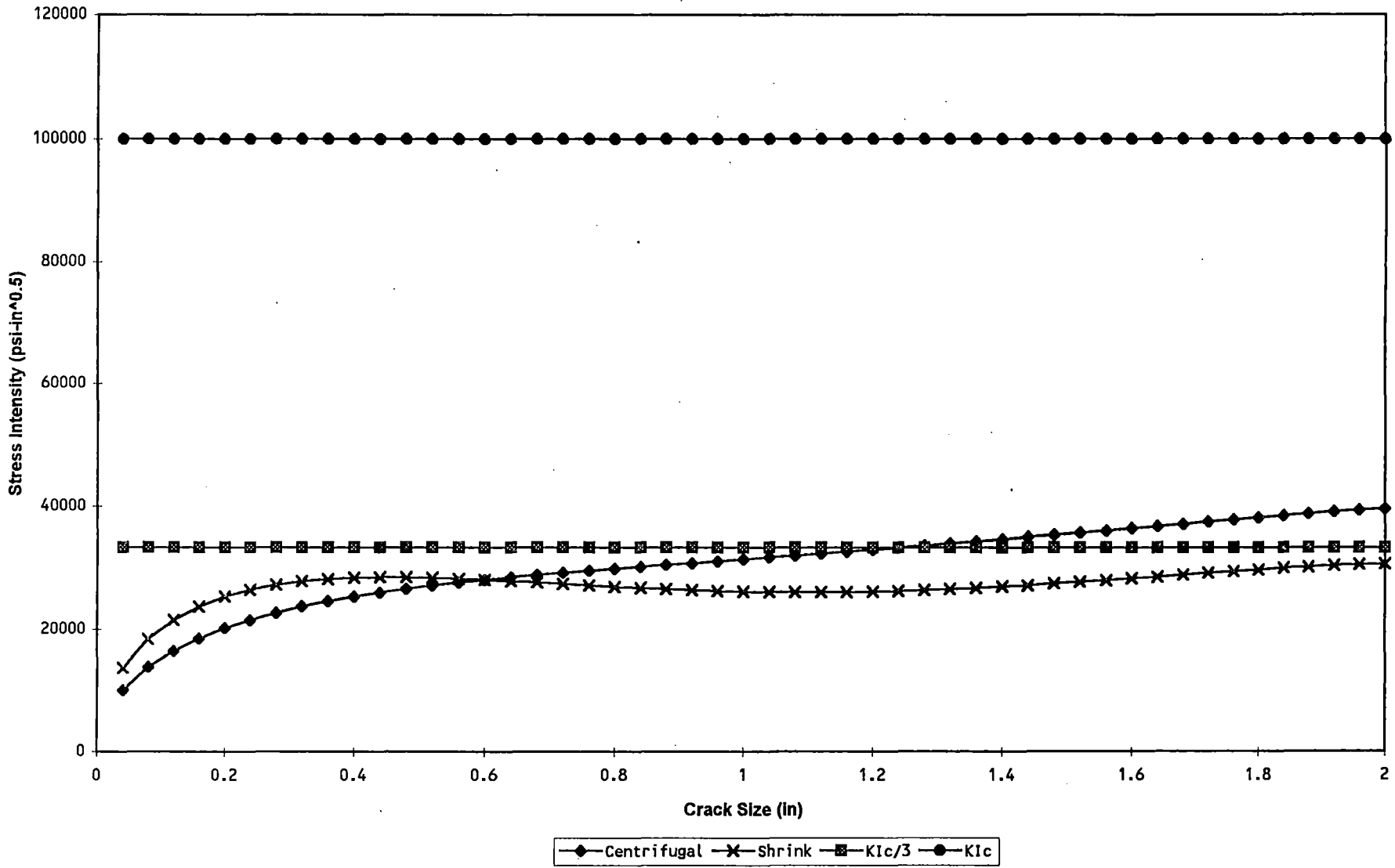
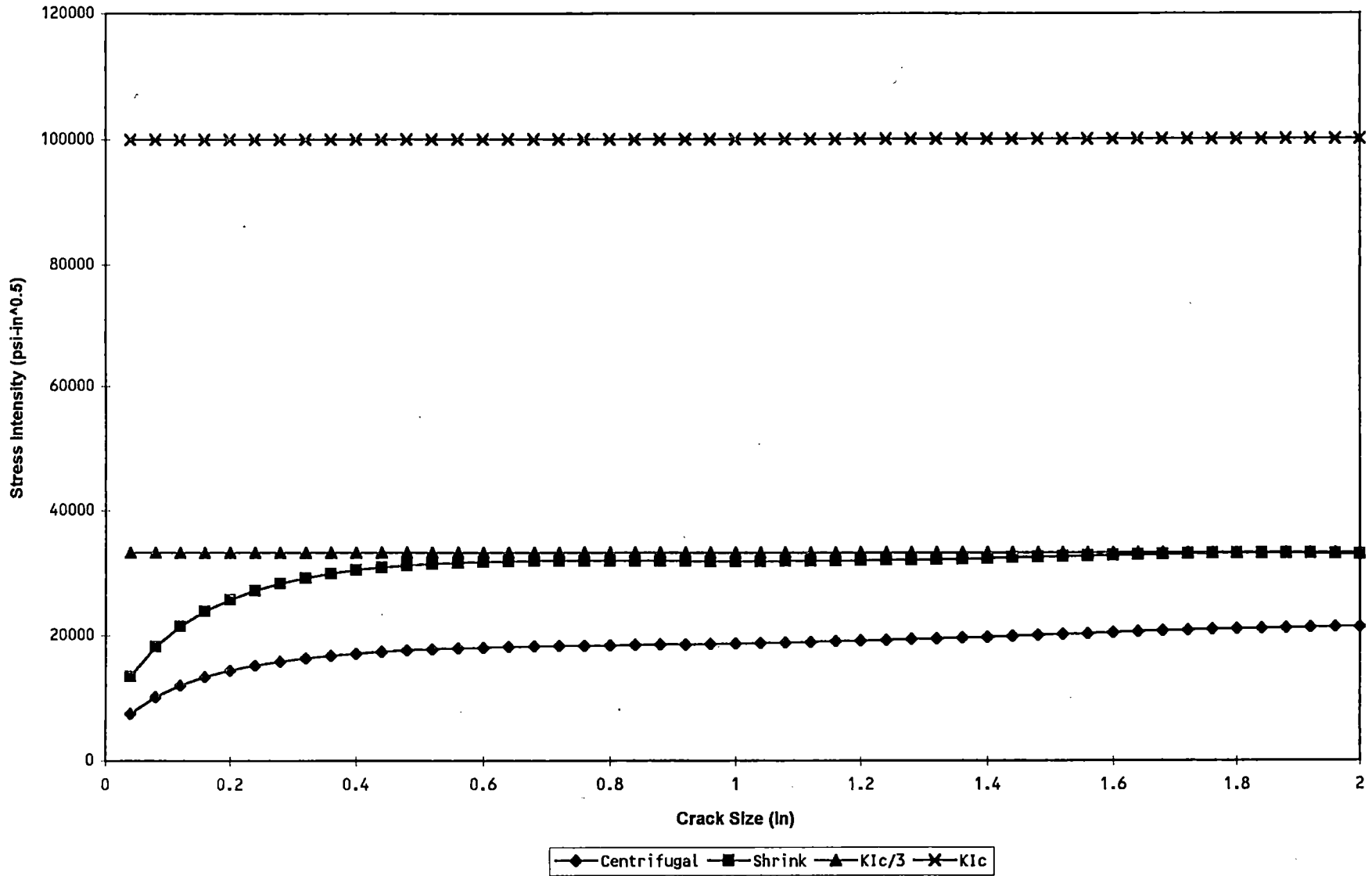Figure 6-3. Comparison of Applied Stress Intensity Factor Versus Allowable Stress Intensity Factor for Normal Operating Conditions (ANO-1)
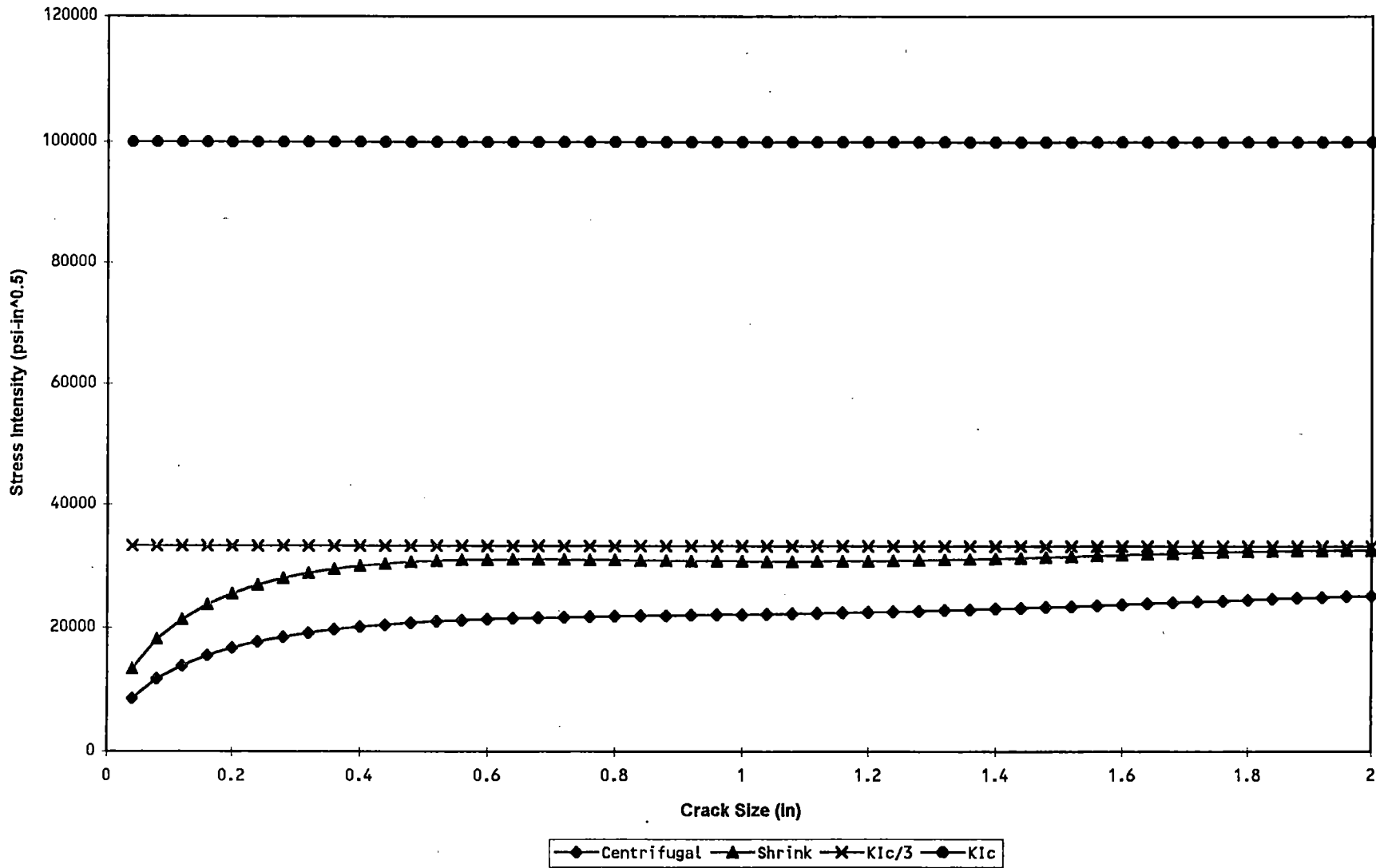
Figure 6-4.   Comparison of Applied Stress Intensity Factor Versus Allowable Stress
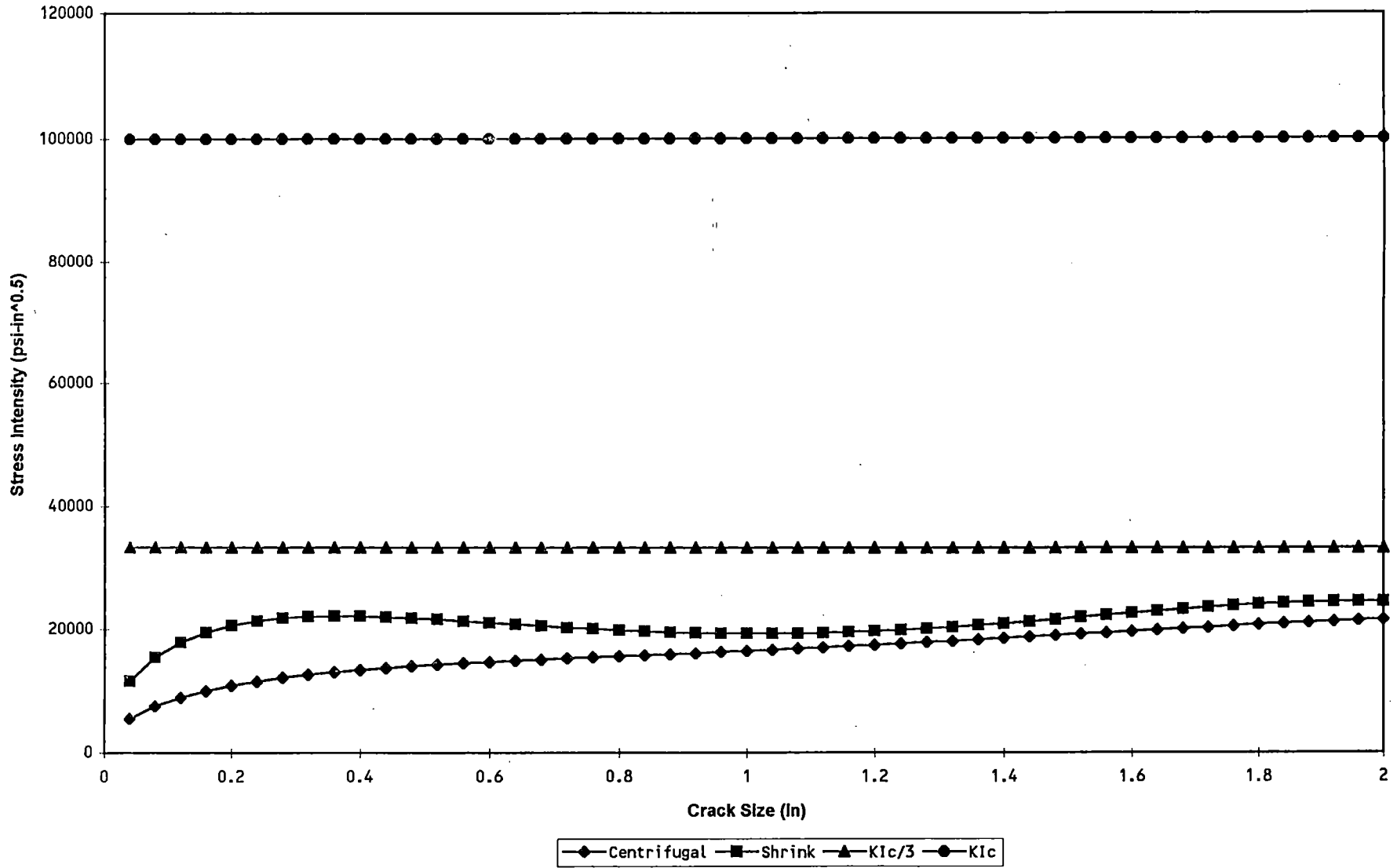Intensity Factor for Normal Operating Conditions (ANO-2)

Figure 6-5.   Comparison of Applied Stress Intensity Factor Versus Allowable Stress
Intensity Factor for Normal Operating Conditions (Millstone-2)

Figure 6-6. Comparison of Applied Stress Intensity Factor Versus Allowable Stress Intensity Factor for Normal Operating Conditions (Palisades)

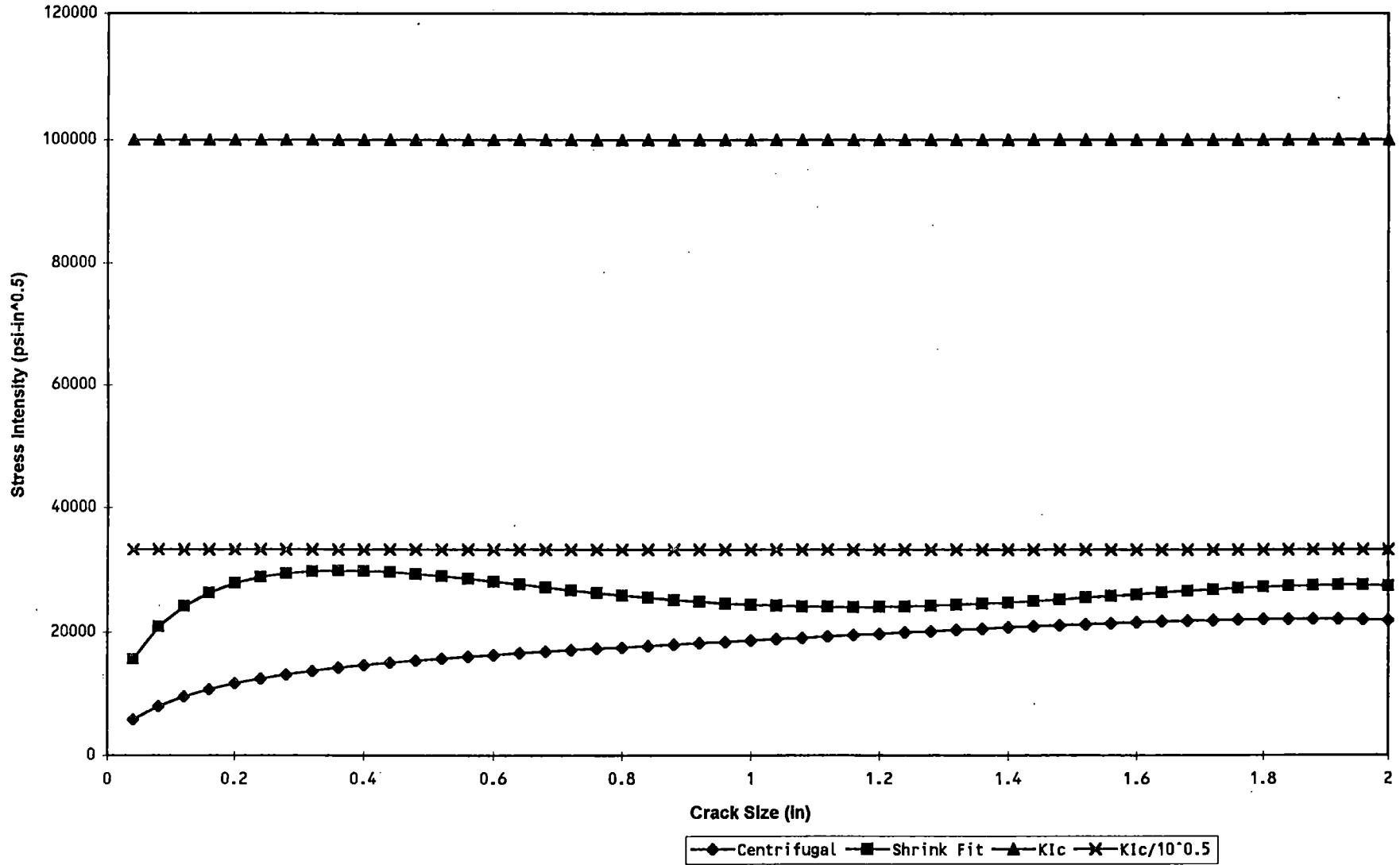**St. Lucie**
Normal Operating Conditions

Figure 6-7.   Comparison of Applied Stress Intensity Factor Versus Allowable Stress
Intensity Factor for Normal Operating Conditions (St. Lucie Units 1 and 2)
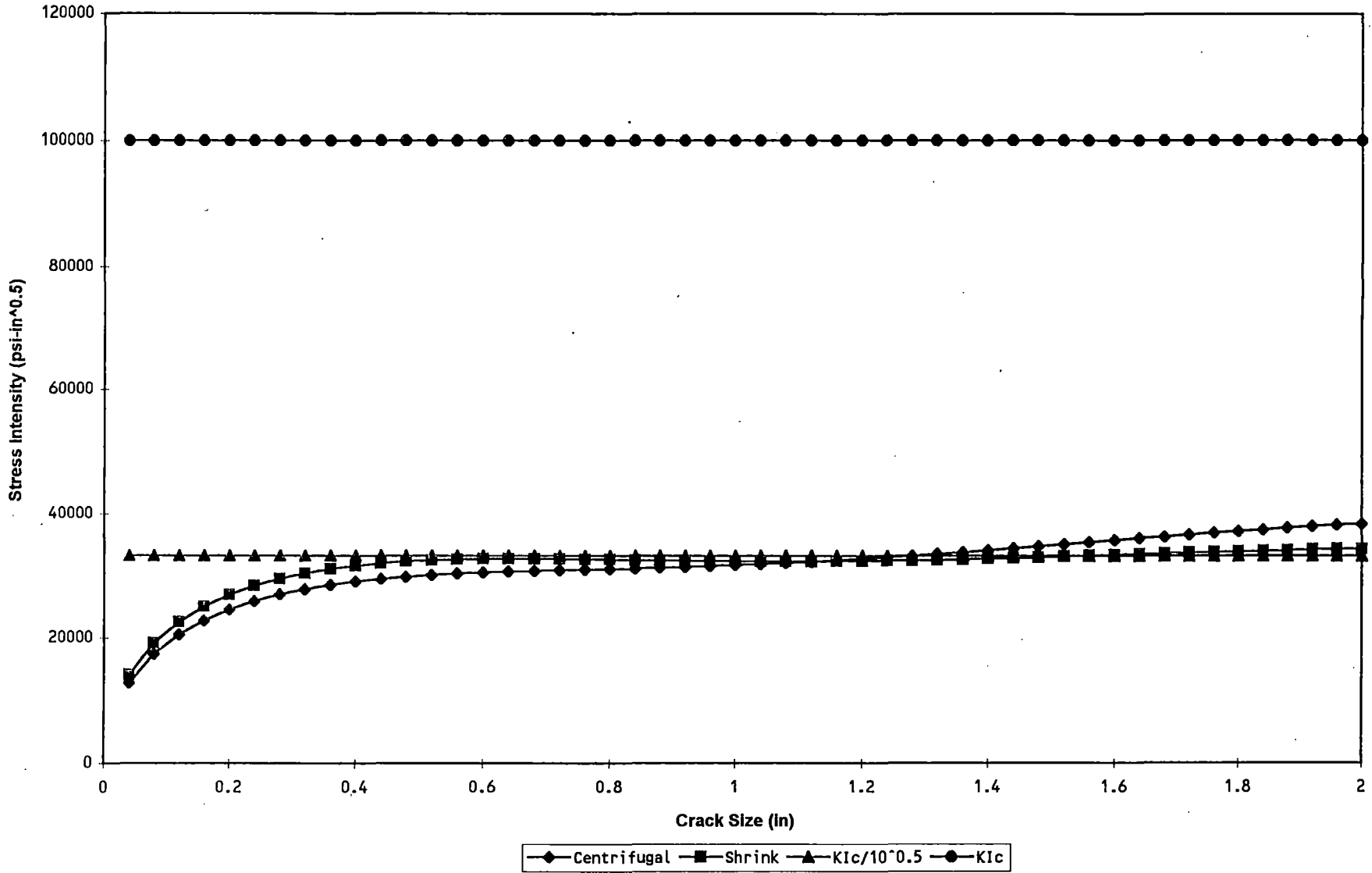
Figure 6-8.   Comparison of Applied Stress Intensity Factor Versus Allowable Stress
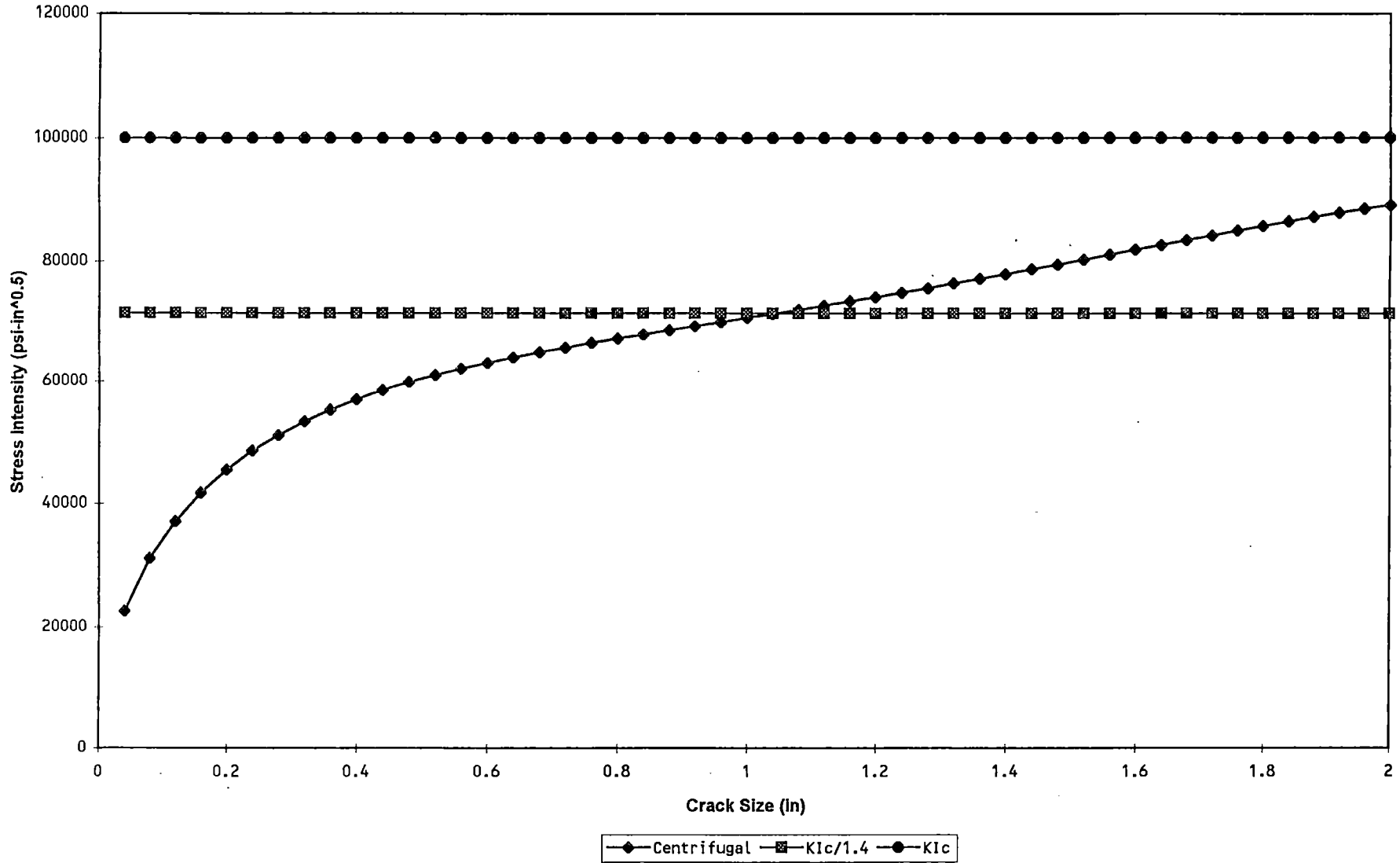Intensity Factor for Normal Operating Conditions (Waterford-3)

Figure 6-9. Comparison for Applied Stress Intensity Factor Versus Allowable Stress
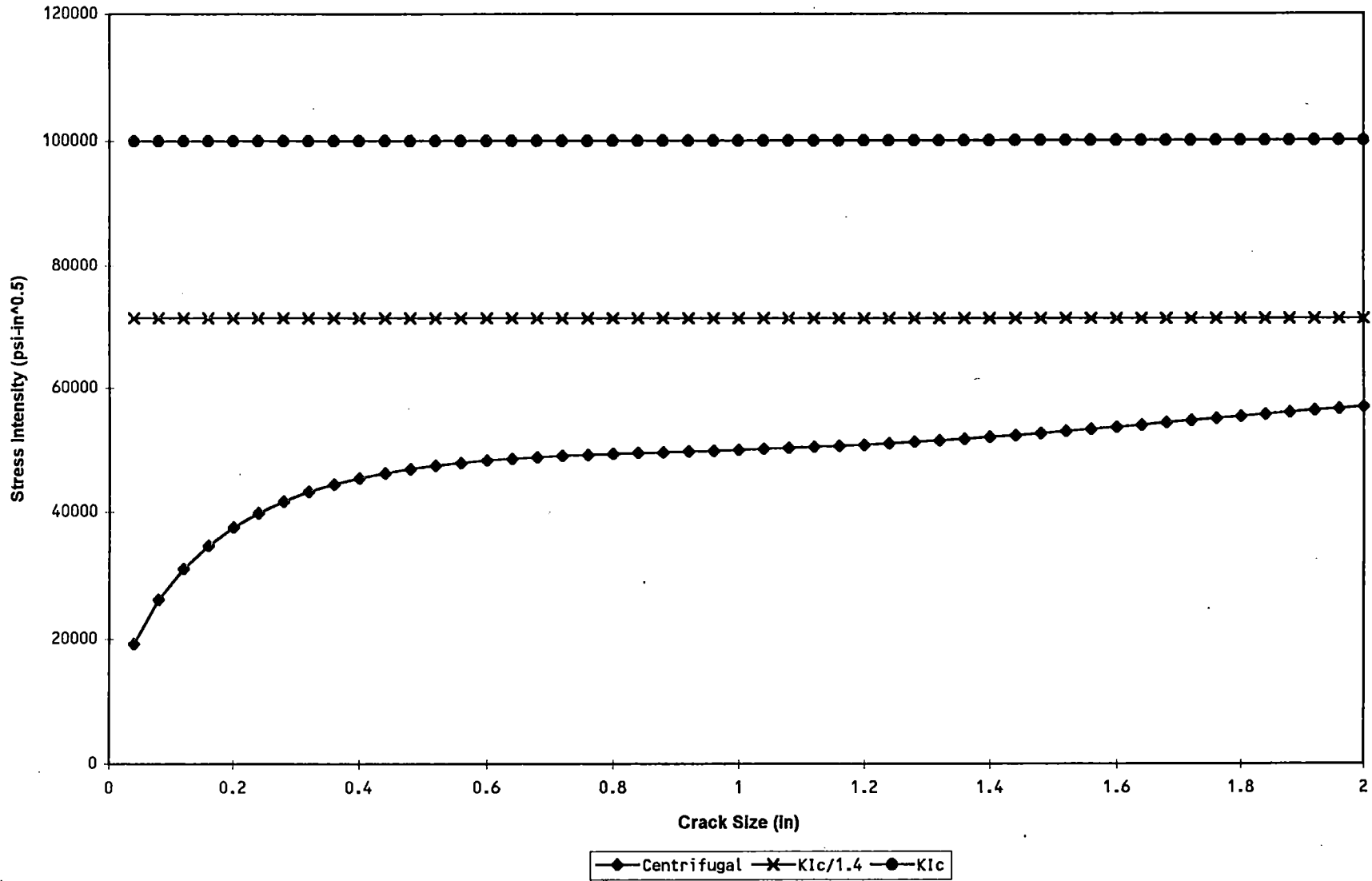Intensity Factor for Accident Conditions (ANO-1)

Figure 6-10. Comparison for Applied Stress Intensity Factor Versus Allowable Stress Intensity Factor for Accident Conditions (ANO-2)
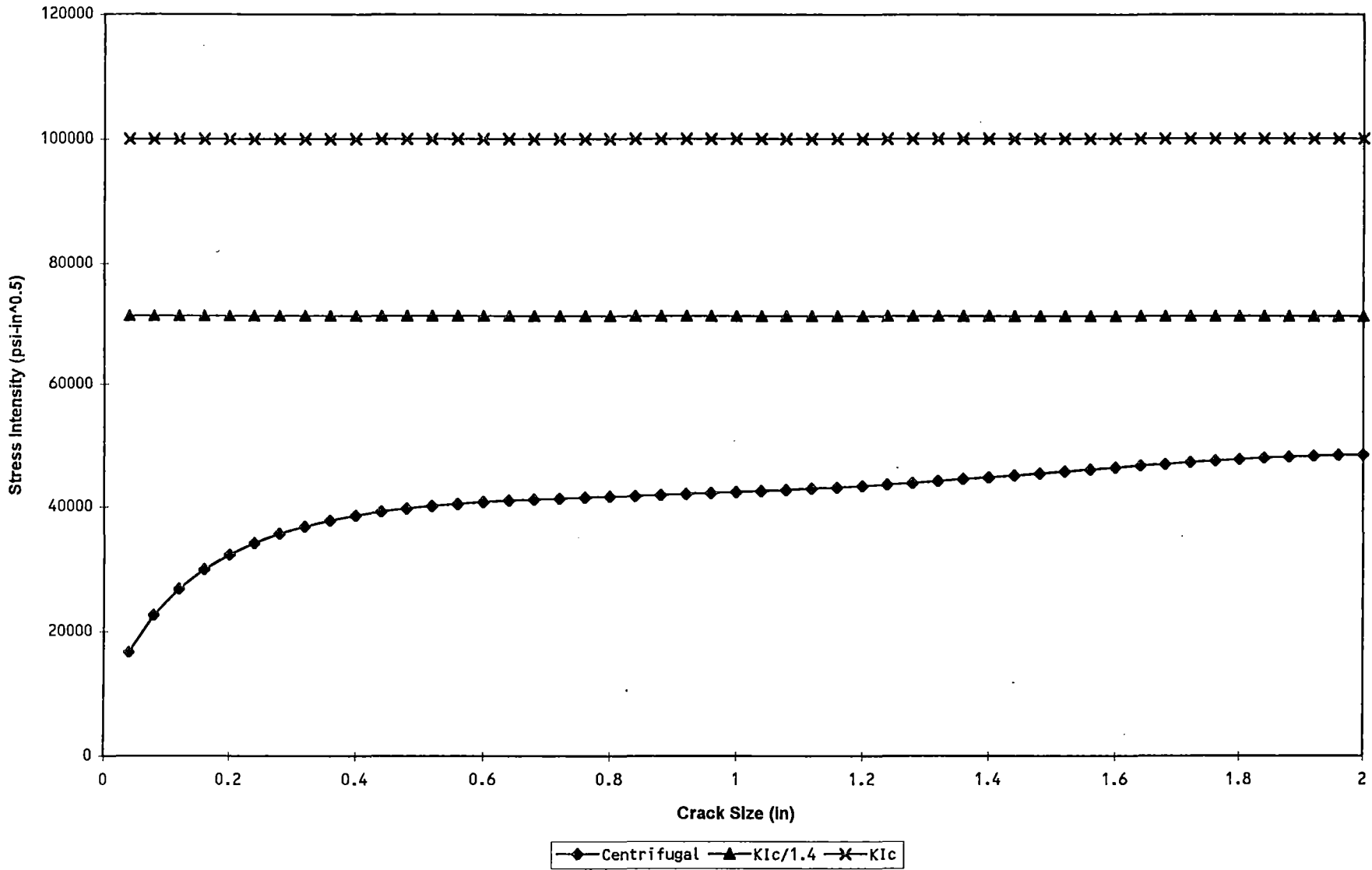
Figure 6-11. Comparison for Applied Stress Intensity Factor Versus Allowable Stress Intensity Factor for Accident Conditions (Millstone-2)
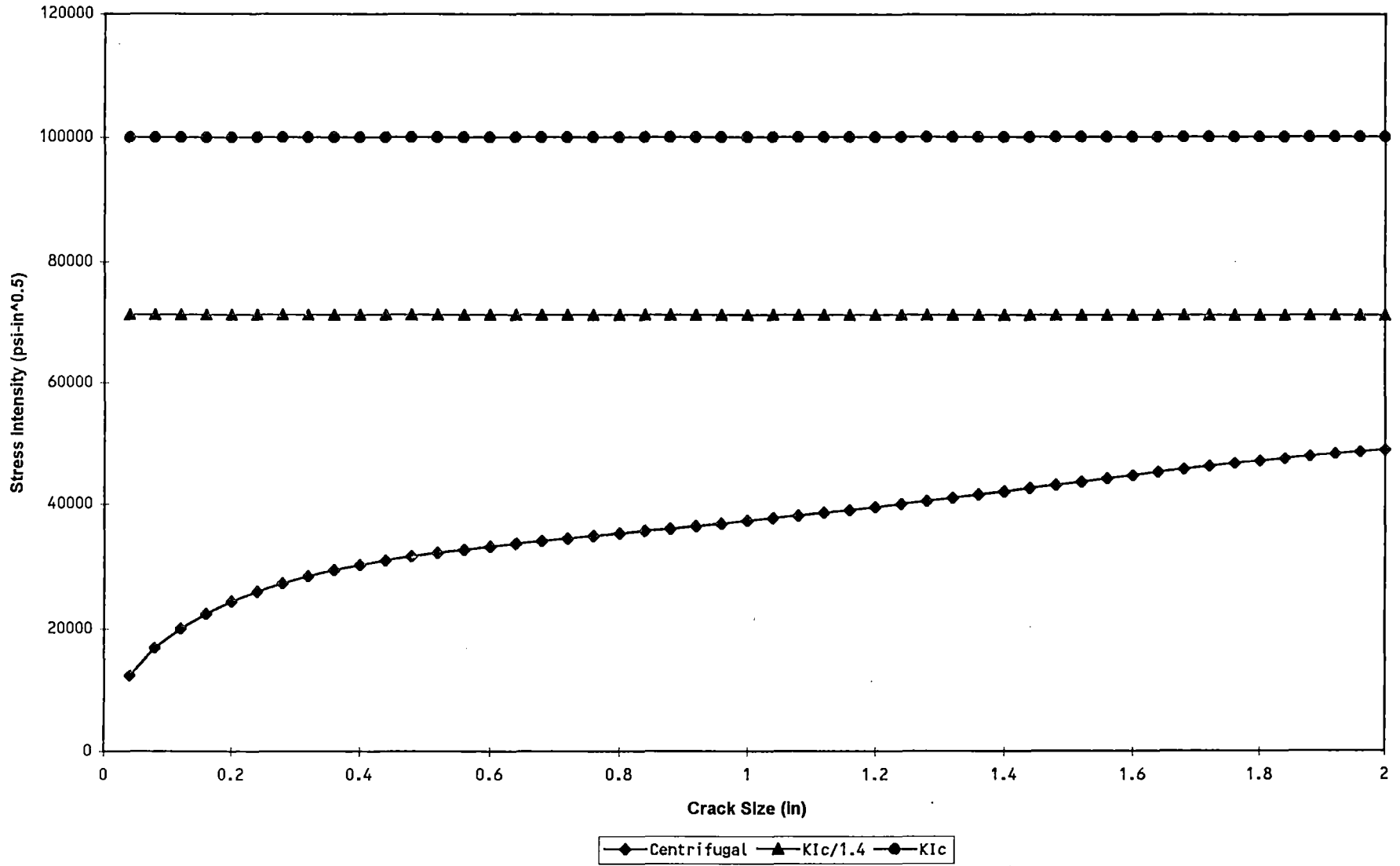
Figure 6-12. Comparison for Applied Stress Intensity Factor Versus Allowable Stress
Intensity Factor for Accident Conditions (Palisades)

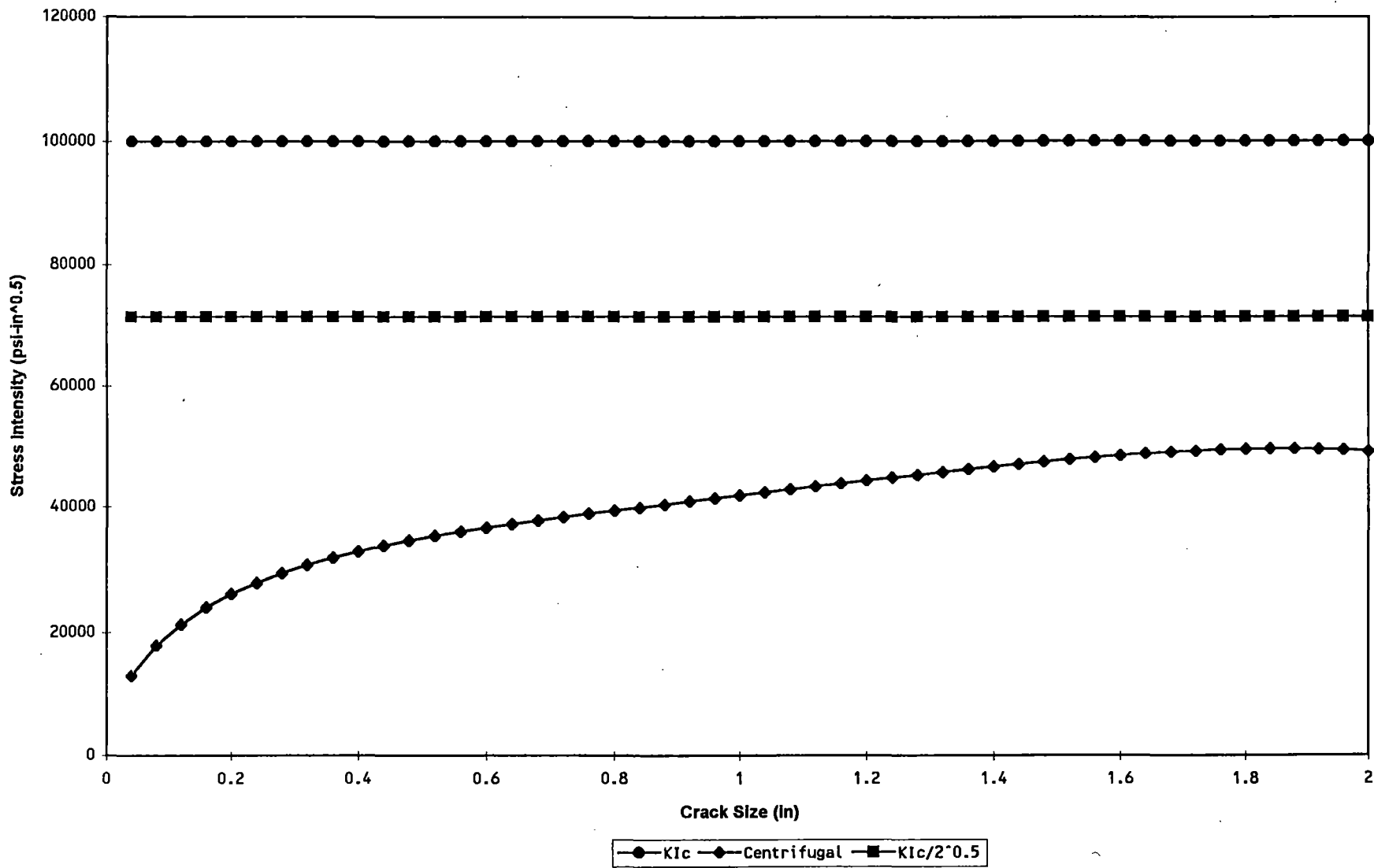Figure 12

St. Lucie
Accident Conditions

Figure 6-13. Comparison for Applied Stress Intensity Factor Versus Allowable Stress
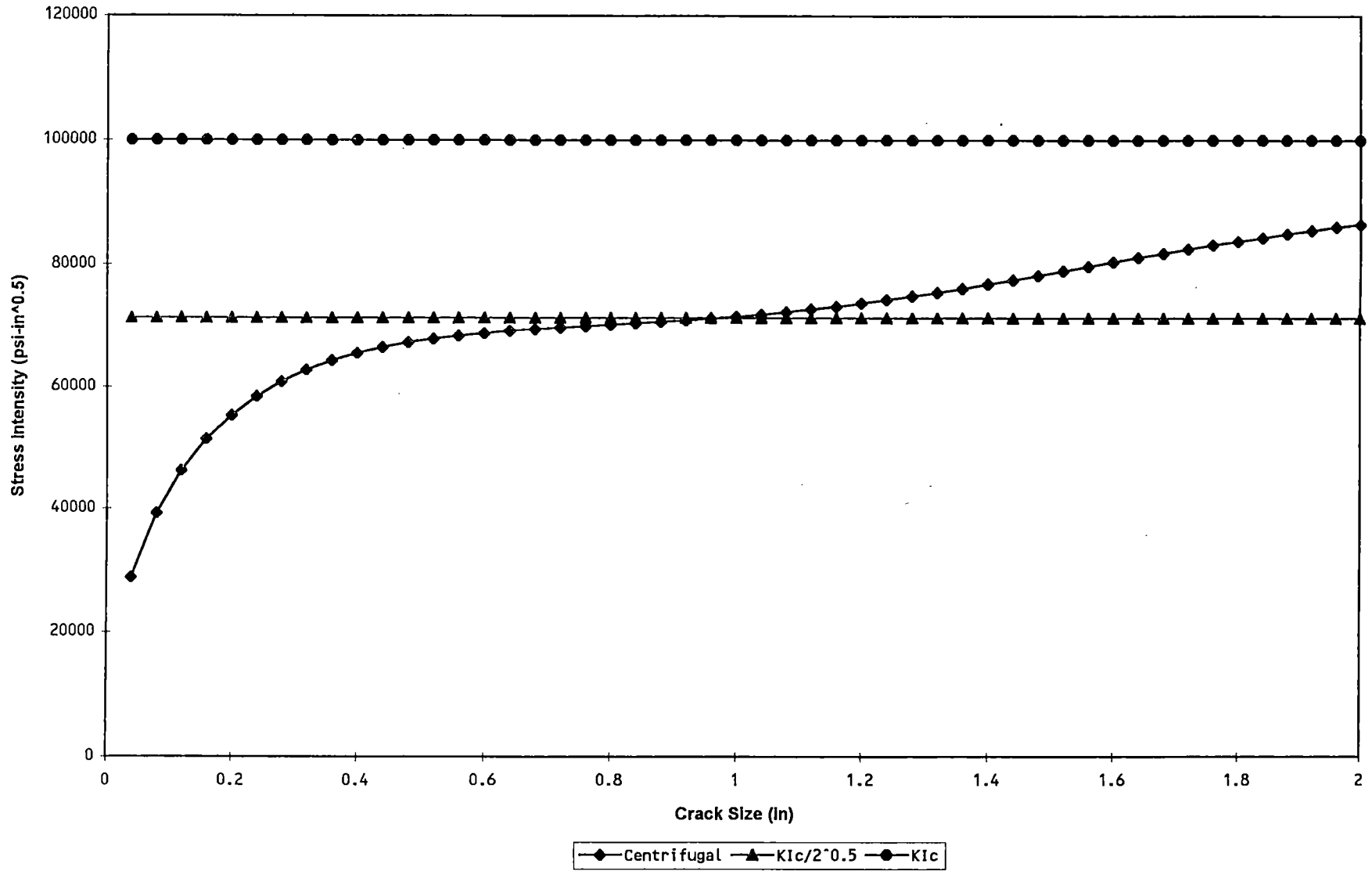Intensity Factor for Accident Conditions (St. Lucie Units 1 and 2)

Figure 6-14. Comparison for Applied Stress Intensity Factor Versus Allowable Stress Intensity Factor for Accident Conditions (Waterford-3)

7.0   SUMMARY AND CONCLUSIONS

The evaluations documented in this report have demonstrated that for the plants considered in this study, the inspection of the RCP flywheels as mandated by Regulatory Guide 1.14 and incorporated in the Plants' Technical Specifications can be eliminated without compromising safety. This conclusion is supported by several observations made during the evaluations presented in this report and summarized below.

- Inspections that have been performed to date at all seven plants have never revealed the presence of any service induced flaws. The inspections have spanned several years and have been performed using both ultrasonic and surface examinations.

- A survey of several other plants was also performed to determine if any flaws have been reported during flywheel inspections. The survey revealed that to date, no flaws have been reported in any of the plants that were contacted.

- Various mechanisms that could potentially degrade the flywheel materials during service were evaluated. It was concluded that other than fatigue crack growth, there are no other mechanisms that can affect the service performance of the flywheel. Fatigue crack growth analyses were performed to show that crack growth assuming a conservative initial flaw at the worst location is very small.

- Flaw tolerance evaluations performed using conservative linear elastic fracture mechanics principles and considering the critical location of the flywheel indicated that the flywheels do not present a safety concern for current plant life and life extension. These evaluations were performed using lower bound fracture toughness values at the most highly stressed locations. A conservative flaw size of 0.25 inch was assumed to be present, due to UT detection uncertainty. Fatigue crack growth analyses using the ASME Section XI crack growth law showed that this initial flaw propagated to less than 0.3 inch following 4000 startup/shutdown cycles (about eight

$\sum$ Structural Integrity *Associates, Inc.*

times the plant life). This final flaw size is significantly below the ASME Code allowable flaw size for any of the flywheels examined in this study.

- Economic and radiological exposure hardships are encountered during these flywheel inspections. Relaxation or elimination of the flywheel inspection requirements will reduce man-rem exposure to plant personnel and the associated cost for the inspections.

Structural Integrity Associates, Inc.

8.0 REFERENCES

1. U.S. Nuclear Regulatory Commission, Regulatory Guide 1.14, "Reactor Coolant Pump Flywheel Integrity," Revision 1, August 1975.

2. Standard Review Plan Section 5.4.1.1 - Regarding General Design Criteria 4, "Environmental Missile Design Bases," Appendix A of 10CFR50.

3. NUREG-0933, "A Prioritization of Generic Safety Issues," (Main Report and Supplements 1-12), July 1991.

4. Arkansas Nuclear One Unit 1 FSAR, Section IV, Amendment 11.

5. Combustion Engineering Interoffice Correspondence from D. F. Steinz to F. M. Stern, "Flywheel Overspeed", dated May 11, 1973, with attached document CENPD-26 and Appendices A,B,C, and D. $\triangle$ 1

6. Millstone Nuclear Power Station Unit 2 FSAR, Section 4, January 4, 1990.

7. Letter from D. M. Crutchfield (USNRC) to D.P. Hoffman (Consumers Power Company) with enclosure, "Topic III-10.B, Pump Flywheel Integrity (Palisades)," Docket No. 50-255, LS05-81-029, dated May 15, 1981.

8. St. Lucie Plants, Unit 1 FSAR, Section 5.5 and Unit 2 FSAR, Section 5.4.

9. Waterford, Unit 3 FSAR, Section 5.4.1.4, Revision 3,

10. EPRI Report No. NP-5461, "Component Life Estimation: LWR Degradation Mechanisms." September 1987, Prepared by Structural Integrity Associates, Inc..

11. Shigley, J.E., "Mechanical Engineering Design," McGraw-Hill Book Company, 1963.

12. Riccardella, P.C., Bamford, W.H., "Reactor Coolant Pump Flywheel Overspeed Evaluation," Journal of Pressure Vessel Technology, November 1974.

13. ANSYS Finite Element Program, Version 4.4a.

14. Williams J.G., and Isherwood D.P., "Calculation of the Strain Energy Release Rules of Cracked Plates by an Approximate Method," Journal of Strain Analysis, Volume 3, No. 1, 1968, pp. 17-22.

15. pc-CRACK Fracture Mechanics Software, Version 2.1, Structural Integrity Associates, Inc.

16. ASME Boiler & Pressure Vessel Code, Section XI 1989 Edition.

Structural Integrity Associates, Inc.

ATTACHMENT 5

CONSUMERS POWER COMPANY
PALISADES PLANT
DOCKET 50-255

TECHNICAL SPECIFICATIONS CHANGE REQUEST
LICENSE DPR-20
PRIMARY COOLANT PUMP FLYWHEEL INSPECTIONS

CBLA Justification

1 Page

TECHNICAL SPECIFICATIONS CHANGE REQUEST
LICENSE DPR-20
PRIMARY COOLANT PUMP FLYWHEEL INSPECTIONS

CBLA Justification

Performance of Primary Coolant Pump Flywheel Inspections in accordance with Technical Specification 4.3 and Table 4.3.2 requires funding which could be more appropriately directed to items of greater safety significance. The costs associated with these inspections are based on costs incurred during the Palisades 1995 refueling outage. These costs include actual NDE costs, an estimate of plant costs, and estimated costs for radiation exposure received. These costs and their basis are summarized in the following sections.

NDE Costs

These costs for the 1995 refueling outage inspections were billed at $ 24,733.00.

Plant Costs/ Refueling

Plant costs for the 1995 refueling outage inspections include two (2) electrical maintenance workers and one (1) engineer for twenty four (24) hours per individual.

$$[(2 \times \$30.00) + (1 \times \$44.00)] \times 24 = \$2496.00$$

Radiation Costs/ Refueling

The cost of radiation dose has been determined based on $7000.00 per R. Inspection radiation dose per refueling outage has historically been 0.5 R.

$$0.5\ R \times \$7000.00/R = \$3500.00$$

Total Cost per Refueling

Total Cost/ Refueling = $24,733.00 + $2496.00 + $3500.00

Total Cost/ Refueling = $30,729.00

Palisades operating license expires in 2007. Based on this, Palisades has seven remaining refueling outages. Total cost savings for this Technical Specification Change Request is $215,103.00